NEGATIVE MAGNETORESISTANCE IN INDIUM ANTIMONIDE

A Thesis submitted for the Degree of Ph.D. in the University of London, Bedford College, by

by Terry Ellis, M.Sc.

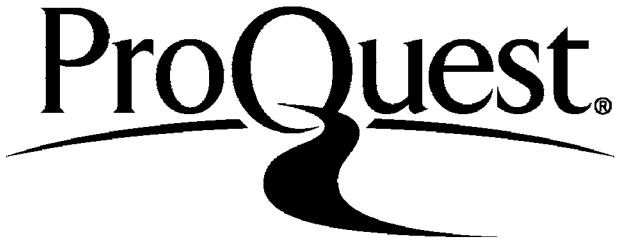

ABSTRACT

Negative longitudinal magnetoresistance in indium antimonide subject to a quantizing magnetic field [$\hbar\omega_c > kT$ and $\omega_c \tau >> 1$ where ω_c is the cyclotron frequency] has been investigated under ohmic and non-ohmic conditions. Conduction band electron concentrations ranged from 1×10^{14} cm $^{-3}$ up to 2.23×10^{15} cm^{-3}. Under ohmic conditions the negative magnetoresistance was studied at various stabilized temperatures between 4.2^{o}K and 130^{o}K. Non-ohmic results were taken at 4.2^{o}K, using pulsed electric fields up to 10 V cm^{-1} (5A) to induce free carrier heating. Using an "electron temperature model" to represent the energy distribution of the electron system, the ohmic and non-ohmic behaviour are compared. The comparison yields some idea of the validity of this model in the presence of large magnetic and electric fields. The mechanism proposed for the observed negative magneto-resistance is the magnetic field reduction of the small-angle scattering from collisions with the ionized impurities, as originally proposed theoretically by Argyres and Adams (1956) and extended by Dubinskaya (1969). A computer programme is formulated for the extreme quantum limit [$\hbar\omega_c >> kT$ and E_F] where only the ground state Landau level is occupied. As well as incorporating arbitrary degeneracy the calculations include the effect of drift momentum relaxation by small angle forward scattering events. These contribute to momentum relaxation because of the energy uncertainty of an electron associated with finite collision times. The role of higher Landau energy levels is also considered. The inclusion of the forward scattering events results in a fairly good quantitative agreement with experiment. Various theoretical approximations and the effects of sample inhomogeneity

--

are discussed as limitations on the agreement. An experimental and theoretical review of the phenomenon of negative magnetoresistance in semiconductors, associated with a variety of mechanisms, is also given.

CONTENTS

CHAPTER 1.

INTRODUCTION.

The present work is an experimental investigation of the negative magnetoresistance in indium antimonide. Although in Chapter 3 we review various kinds of negative magnetoresistance, both theoretically and experimentally, in a variety of substances, the present investigation is concerned with the negative magnetoresistance in indium antimonide arising from the Landau quantization of the electron energy spectrum.

If we solve the one electron Hamiltonian for an electron in a magnetic field, we find the electron spectrum goes from

$$\varepsilon = \frac{\hbar^2 k^2}{2m^*} \quad \text{the standard quasi-continuum equation}$$

$$\text{to} \quad \varepsilon = (n + \tfrac{1}{2})\hbar\,\omega_c + \frac{\hbar^2 k_z^2}{2m^*}$$

for an electron in a strong magnetic field such that $\omega_c \tau >> 1$, where $\omega_c = \left(\frac{eH}{m^* c}\right)$ is the cyclotron frequency and τ is the collision time of the electron. If this inequality is valid the Landau energy levels $(n + \frac{1}{2})\hbar\,\omega_c$, where n is the Landau subband number, are well defined. In this solution the magnetic field is in the z direction and so the z component of the motion remains unchanged.

The changed electron spectrum is also exhibited in the changed density of states behaviour. In Fig. 1a we see the normal band $\varepsilon^{\frac{1}{2}}$ form of the density of states. Fig. 1b shows how this is changed by the presence of a quantizing magnetic field as defined above. The discontinuities occur at each Landau energy level. It is this form of the state density which is used in the present analysis. In actual fact Fig. 1b is a somewhat idealized picture of the state density and there are various broadening effects which round of the discontinuities, e.g. the

FIG.(1).

Density of States in a Quantizing Magnetic Field.

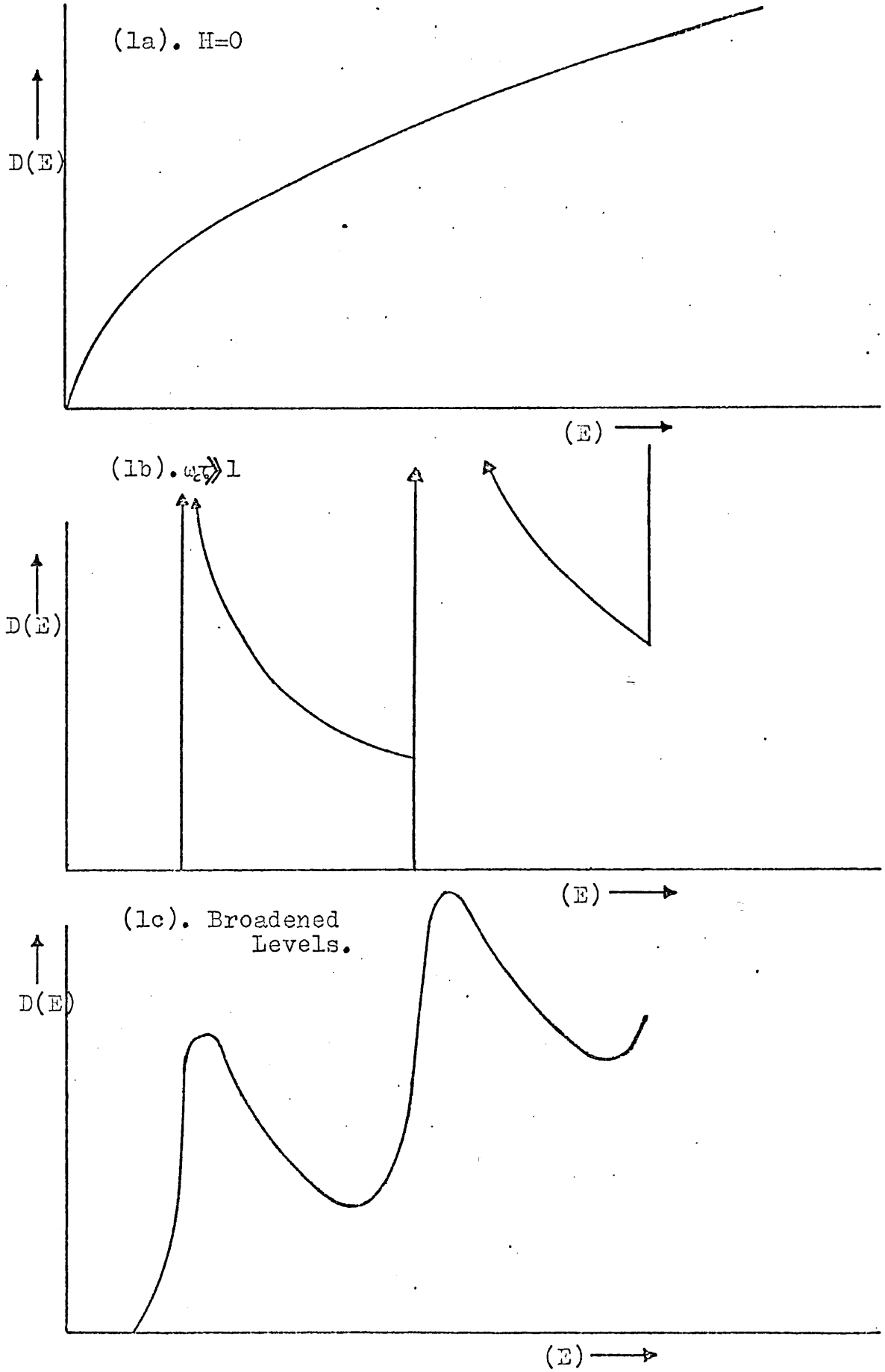

various collision processes and the fluctuating impurity potential. A modified [broadened] diagram is shown in Fig. 1c.

The condition $\omega_c \tau >> 1$ means that substances with small effective mass having comparatively large ω_c values, most readily display the Landau quantization and also give the largest Landau energy spacings $\hbar \omega_c$.

The effect of conduction band quantization displays a wide range of new phenomena when the condition $\hbar \omega_c > k_B T$ is approached. If the substance is degenerate $[E_F >> \hbar \omega_c]$ then many Landau levels are occupied and various phenomena such as the de-Haas, Van Alphen and Shubnikov, de-Haas effects are observed. These are oscillatory changes in the magnetic susceptibility and resistivity respectively, which occur in relationship to an increasing magnetic field as successive Landau levels pass through the Fermi level and are emptied. If we have a non-degenerate material $[E_F << \hbar \omega_c]$ then only the first few Landau levels are occupied and the above oscillatory phenomena are not observed. However, the quantization is still apparent in the transport behaviour. Various other oscillatory phenomena appear, such as the magnetophonon resonance which occurs when a Landau level passes some resonant scattering energy, such as the optical phonon energy $\hbar \omega op$.

We also find that the magnetoresistive behaviour displays new characteristics and becomes sensitive to the relative electric and magnetic field configuration as well as the type of electron scattering mechanism present.

One particular manifestation [the one investigated in this work] is the appearance of a strong negative magnetoresistance of up to - 90%. This only occurs for a longitudinal configuration [E parallel to H]. We give a detailed study of this particular aspect of the Landau quantization and investigate it quantitatively for the condition $\hbar \omega_c >> k_B T$,

the so-called "extreme quantum limit" where all the electrons are in the ground state Landau level.

Experimentally the extreme quantum limit requires high magnetic fields and, preferably, low effective mass, if it is to be readily achievable over a wide range of temperatures. The present study measures the transport in this region up to 130°K with a fairly limited field of 40,000 Gauss. This means that a material with a low effective mass is a necessity. Therefore, indium antimonide, with $m^* = 0.013\ m_e$ is particularly appropriate.

Because of its small effective mass and the present availability of pure crystal samples with low levels of impurity, the mobility at low temperatures is high. The purest sample used has a mobility of 640,000 $cm^2\ V^{-1}\ sec^{-1}$ at 77°K. The strong negative magnetoresistance increases this mobility up to a value of $5 \times 10^6\ cm^2\ V^{-1}sec^{-1}$ (this is under non-ohmic conditions for this particular case). It is possible to obtain samples of even greater purity than this.

The problem of transport in the quantum and extreme quantum limits is by no means a completely solved problem on the theoretical side. Attempts using a quantum mechanical formulation have been made in various approximations, but the complexity of the problem is rather involved in any full-scale treatment.

For the analysis of the results in Chapter 4 the early theory of Argyres and Adams (1956) together with some additional theory by Dubinskaya (1969) is used. The combination of these is sufficient to explain the essential features of extreme quantum limit behaviour under ohmic conditions.

The non-ohmic comparison which follows is based upon the electron temperature model. This is a fairly simple model, especially when compared with certain other more involved derivations, which

nevertheless is sufficient to show that the basic mechanism for the ohmic and non-ohmic effects is the same. In fact, the electron temperature model often produces a rather good quantitative analysis, especially for the impure samples.

CHAPTER 2.

EXPERIMENTAL PROCEDURE.

2.1 Apparatus: 2.2 Cryomagnetic System: 2.3 Sample Holder Design: 2.4 Experimental Technique.

2.1 Apparatus.

A block diagram of the experimental apparatus is shown in Fig. 2.1. Central to the arrangement is the liquid helium cryostat, containing the sample holder and super-conducting magnet system. These features are described later. The superconducting magnet is supplied from a source having a current range of 0 → 40 amps. (With the particular Oxford Instrument magnet used 32 amps. is specified as the recommended largest operating current, giving a central magnetic field of 40 kilogauss.) Automatic current trip-out operates in event of a critical voltage appearing across the terminals, so protecting the magnet from damaging power dissipation. A reversing switch enables the magnetic field to be applied in either direction. A separate D.C. source, giving a current of 40 mA, operates the superconducting switch, allowing operation in the persistent or variable modes.

A two way selector switch connects the current leads of the sample to either a D.C. supply or the pulse generator. Both of these have a reversing switch for changing the direction of the sample current. The D.C. current is read from a Keithley digital multimeter (Type 168). A large series resistor is included in the D.C. supply line to give a constant current source for all ohmic measurements. For the pulsed readings standard resistances are used to measure the current

FIG.I.

EXPERIMENTAL APPARATUS.

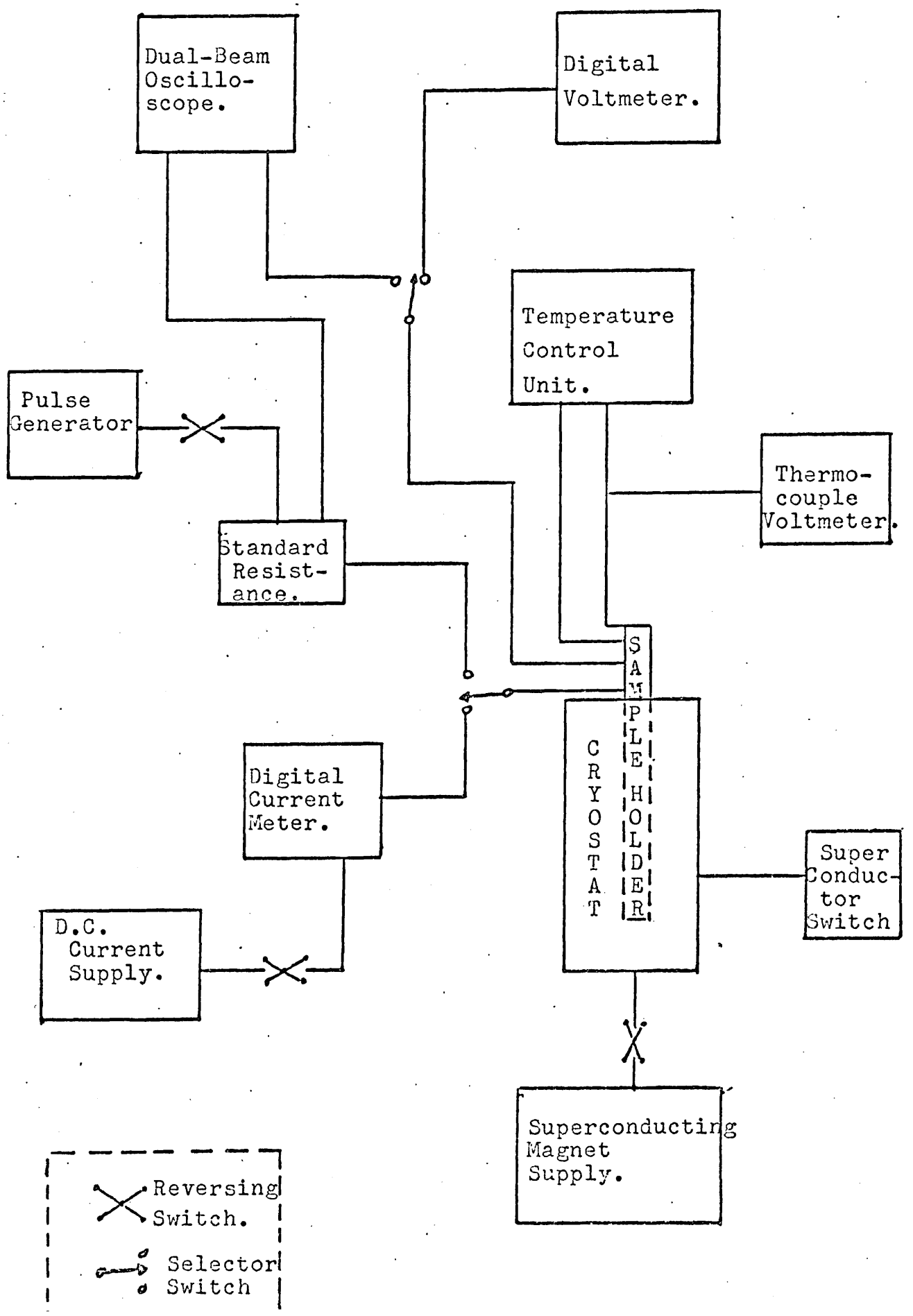

pulses, by way of the oscilloscope display.

Both supplies give a floating output. This is necessary because one end of the sample is electrically earthed by way of the cryostat body, which serves as a common earthed lead. The pulse generator was specifically built for the high electric field negative magnetoresistance measurements (A.K. Betts, Physics Department, Bedford College). It provides a floating output and can give current pulses from 0 to 15 Amps. at voltages up to 100 V. Pulse length is adjustable around 5μ sec. and repetition rate down to 1 per sec. A repetition rate of around 5 per sec. was used in the experiments.

A second selector switch connects either a digital voltmeter (Keithley Type 168), for D.C. measurements, or the oscilloscope, for pulsed readings, to the sample voltage probes. These probes must also remain floating. To achieve this the oscilloscope input is a differential amplifier, having a sufficiently large resistive isolation from earth. The current and voltage pulses can be simultaneously displayed on the oscilloscope.

Temperature adjustment and stabilization is accomplished by an Oxford Instrument - Precision Temperature Control Unit. This is used, in combination with a helium exchange gas system, to obtain temperatures between $4.2^{o}K$ and $150^{o}K$. The unit has a gold/iron versus chromel thermocouple as a temperature sensor, with reference junctions attached to the $4.2^{o}K$ helium heat sink. The control unit supplies power to the sample heater until the set temperature is achieved. The unit stabilizes to the set temperature, to better than $0.1^{o}K$. Response of the controller, as well as maximum heater output voltage can be adjusted to give optimum performance for the particular cryogenic system. A separate direct reading of the thermocouple voltage is obtained from a Keithly micro-voltmeter (Model 155).

2.2 Cryomagnetic System.

The cryomagnetic system is shown in Fig. 2.2. Basically, it consists of two silvered glass dewars (the inner for liquid helium, and the outer for liquid nitrogen) with the sample holder and superconducting magnet being supported from stainless steel flanges attached to the top of the taller inner dewar by means of a rubber collar. The flange arrangement, with the helium vessel inlet and outlet tubes and superconducting magnet/switch terminals, is itself supported by the larger framework containing the whole system. The rubber collar, connecting the stainless steel flanges and the inner helium dewar, is secured by two O-rings clasped between metal rings. The grip is secured by screwing the rings, on each O-ring, closer together.

The sample holder was designed to fit the central column, and the lower (sample) end fits snugly into the 2 cms diameter bore at the centre of the super-conducting coil. The sample holder position is adjusted and secured so that the sample lies exactly at the longitudinal centre of the magnet. This is necessary to ensure the homogeneity and correct calibration of the magnetic field. Graph 2.1 shows how the field strength decreases with distance from the centre of the coil on a longitudinal axis. (The coil is a fairly short one (4 cms), so that a marked drop off in calibration is to be expected.) The calibration of the magnet at its centre point is 1250 gauss/amp.

The superconducting magnet is composed of niobium titanium superconducting wire with a transition temperature around $11^{o}K$. It is important in sample holder design to ensure that there is no strong thermal link between the sample heater and any section of the superconducting coil. If even a small part is heated sufficiently to "go normal" the magnet supply must cut out, if permanent damage to the

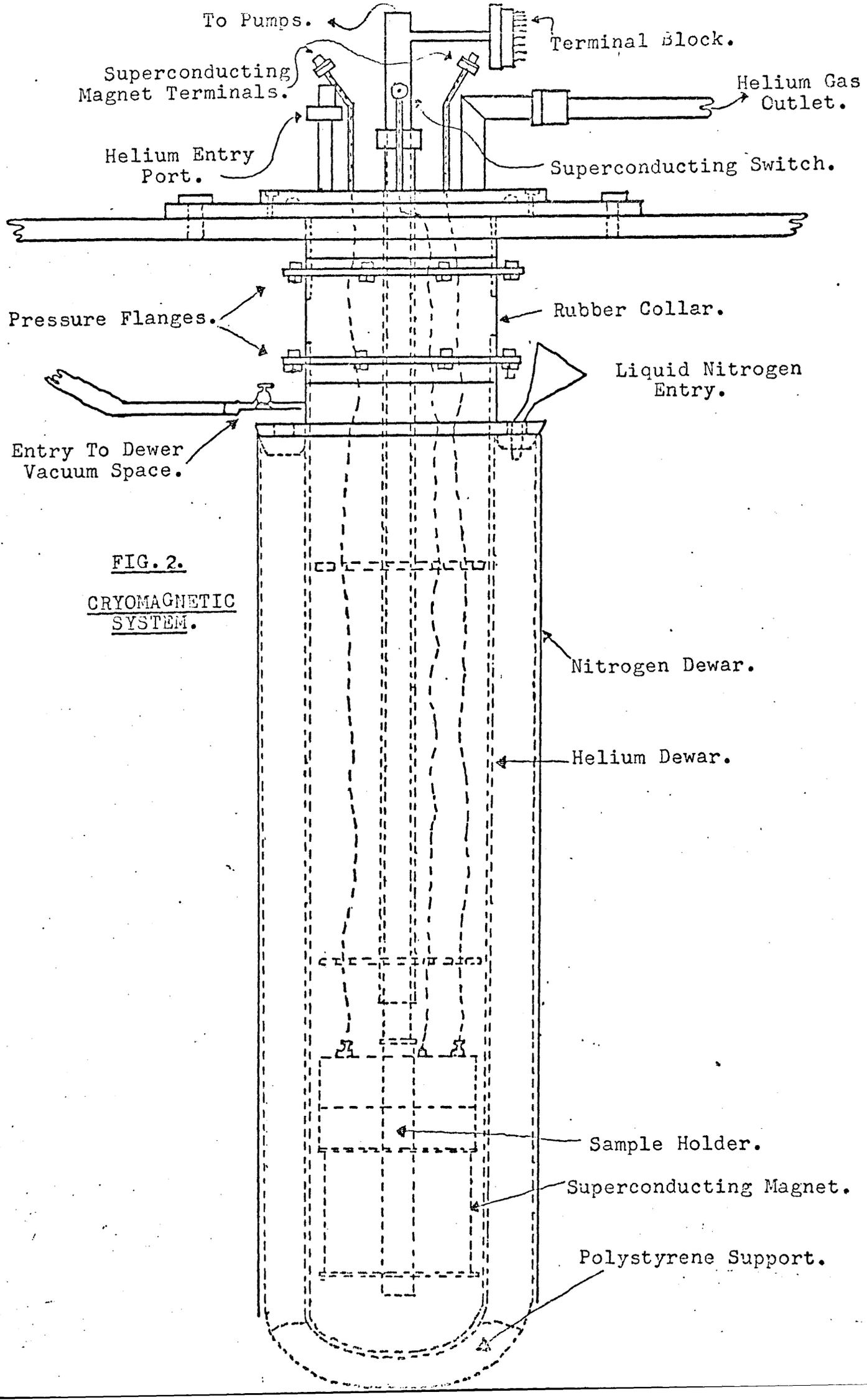

FIG. 2.

CRYOMAGNETIC SYSTEM.

Graph.(2.1)

Magnetic Coil Calibration.

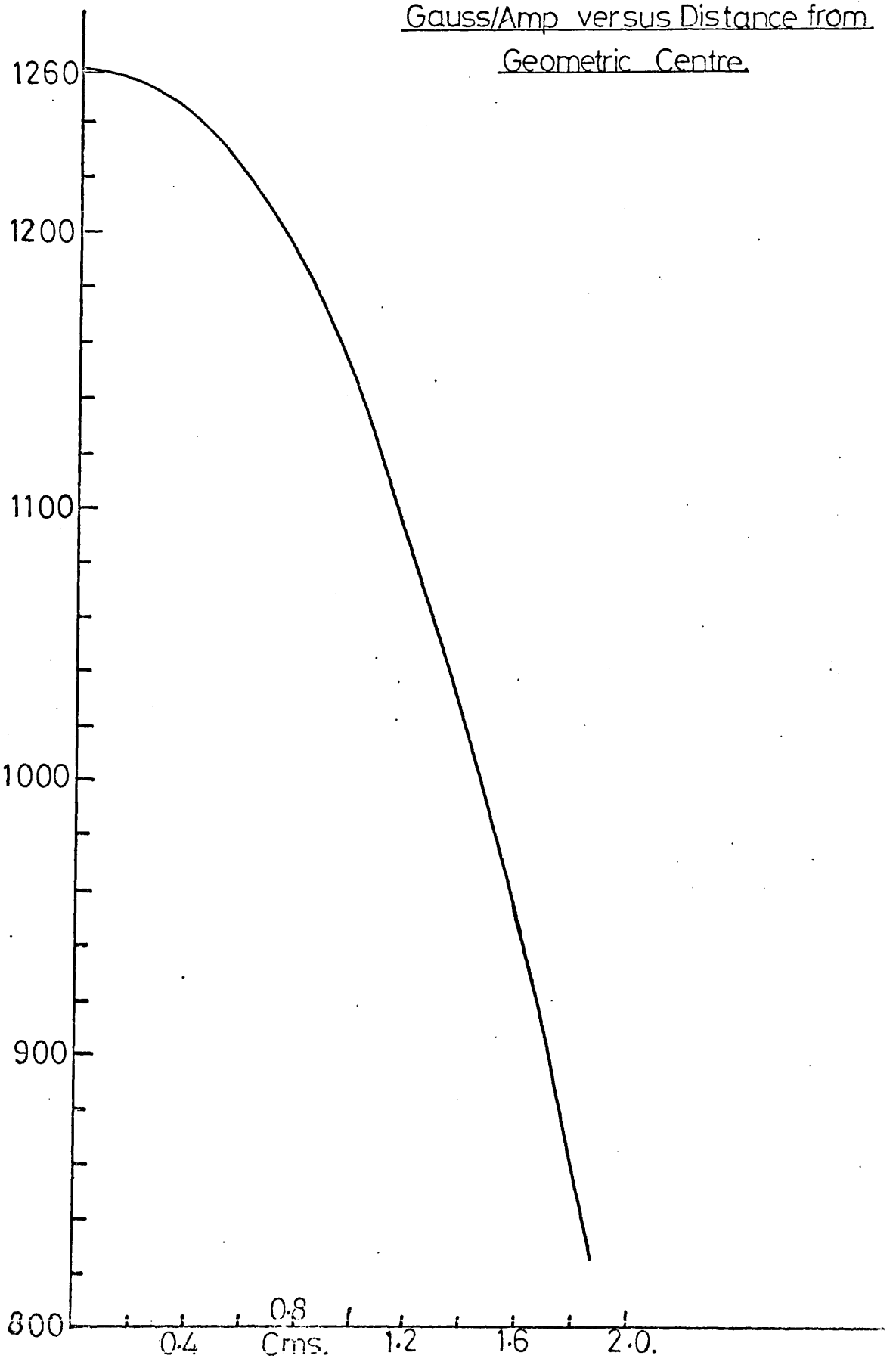

resulting high resistance section is to be avoided. In the present design the main heat path flows into the copper shoulder (shown in Fig. 2.2) well away from the main body of the magnet.

The main heat input into the helium bath, besides the sample heater, comes from the superconducting switch, when it is open (switch current on). Therefore, where possible, it is desirable to work in the permanent field mode. Other heat sources are conduction down the stainless steel tubing and the large gauge copper feed wires to the superconducting magnet. The large superconducting supply current in these wires also generates appreciable heating. The 5 litres of helium in the inner dewar is sufficient for about 7 hours.

The sample holder tube and helium dewar vacuum insulation are connected to the exchange gas and vacuum pump systems. (The vacuum space is initially pumped out before being sealed off.)

The confined nature of the superconducting coil bore and the design of the sample holder permit only a longitudinal magnetic field configuration for the sample. A separate liquid nitrogen system was used to make Hall measurements at $77^{o}K$. These were necessary to find the free electron concentrations present in the samples. The transverse magnetic field was sufficiently strong ($\omega_c \tau >> 1$) to make the Hall factor $r = 1$. Therefore, at this temperature and field $1/R_H ec = n$ (concentration of free electrons) $= N_D - N_A$ (the difference between donor and acceptor concentrations).

2.3 Sample Holder Design.

The sample holder is drawn in Fig. 2.3. The principal materials used are non-magnetic stainless steel and high purity (99.999% pure) copper. The stainless steel tubing is used because of its low thermal conductivity. The high purity copper is used for the opposite reason, in that it has a very large thermal conductivity, especially around

liquid helium temperatures. (The low temperature thermal conductivity of pure copper is more than an order of magnitude higher than the room temperature thermal conductivity of either pure copper or the various other coppers.)

The sample platform and heater area is machined from the high purity copper. Between the sample and the copper platform is a very thin layer of mica, for electrical insulation. The mica is attached to the copper and the bottom of the sample by a thin smearing of special low temperature n- type vacuum grease. One end of the sample is indium soldered to a small copper end plate, which is greased and then screwed onto the main body of copper, to ensure good thermal contact. In this way one end of the sample is earthed both electrically and thermally to the whole sample holder and cryostat. Because the bottom of the sample also has fairly good thermal contact, temperature gradients down the sample should be minimised.

The electrical terminals are formed from small cylindrical blocks of P.T.F.E. (< 2 mm. diameter) with a hole drilled through the axis and the inside section of a small co-axial cable glued into position to act as a copper terminal. The P.T.F.E. is glued onto a shouldered hole drilled through the copper platform. The copper leads are soldered to the ends of the terminals beneath the platform. Fine gauge platinum wire, 0.1 mm. diameter, is used to make the connection from the terminal platform end, onto the sample. The wire for the current contact is indium soldered to the end of the sample.

The two platinum wire voltage probes are resistance welded onto the sample by capacitor discharge. A 100 μF capacitor is charged to about 20 Volts and discharged through each wire in turn. The platinum wires are sprung onto the required part of the sample, with an initial contact resistance between 20 and 100 ohms. The high instantaneous

FIG.3.

(1). COMPLETE SAMPLE HOLDER.
(Sample Jacket In Position.)

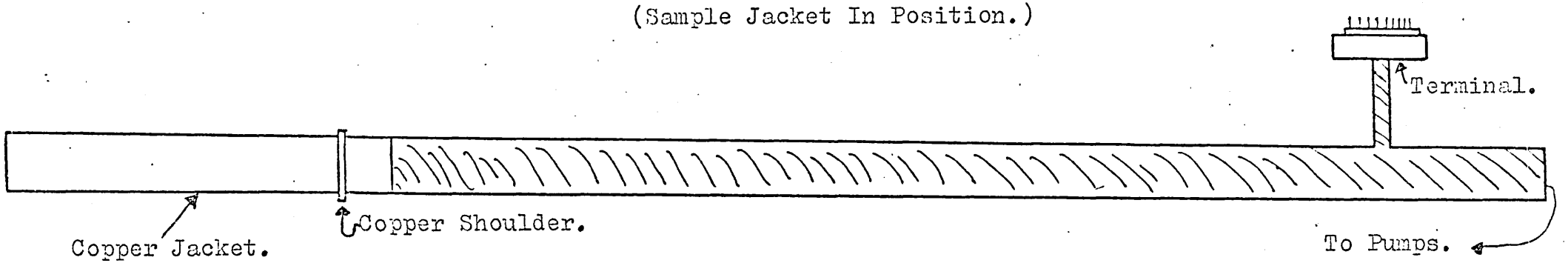

(2). SAMPLE END OF HOLDER.
(Without Jacket.)

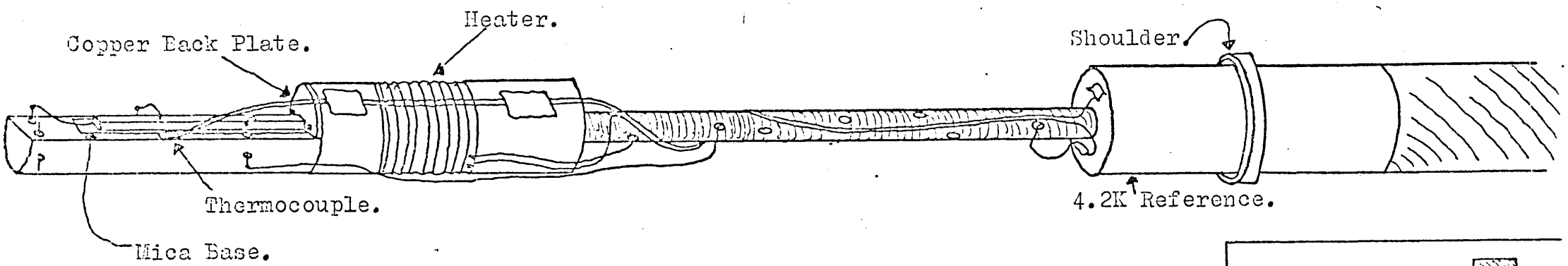

(Not To Scale)

capacitor current flowing through the contact resistance is sufficient to weld the wire to the sample. The contacts produced by this method are mechanically weak and can easily break away when the system is cryogenically cooled. However, the great advantage is that the weld area is small and covers only a tiny portion of the sample width. This is especially important for magnetoresistance measurements, particularly on high mobility samples, such as indium antimonide. The probes can disturb the current flow and thereby lead to misleading, non bulk effect, magnetoresistance.

The heater is situated immediately behind the sample area and is wound from 40 Gauge, cotton insulated Manganin wire, and glued into position.

The hot junction of the thermocouple is glued to the copper platform beside the sample. The junction is electrically insulated from the copper and fixed with low temperature G.E.7031 varnish. A smearing of n-type grease is also applied. The gold/copper and chromel/copper junctions are both attached to the 4.2^{o}K copper base, as reference points. The gold wire is soldered directly onto the copper base, so that this junction is electrically earthed. (The copper base is joined to an external wire which leads to the measuring apparatus.) The copper/chromel junction is glued to, but electrically insulated from the copper base in a similar way to the sample junction. The thermocouple was tested with the hot junction at room temperature and the reference at 77^{o}K. The output agreed reasonably well with published values. Gold/iron thermocouple tables given by Rosenbaum (1968) were used for temperature measurements. The calibration is shown graphically in Graph 2.2.

Stainless steel $\frac{1}{4}$" tubing joins the sample platform/heater to the copper base so as to minimize the heat blow into the helium bath.

Graph(2.2) Thermocouple Calibration.

Couple Output
Versus
Temperature.

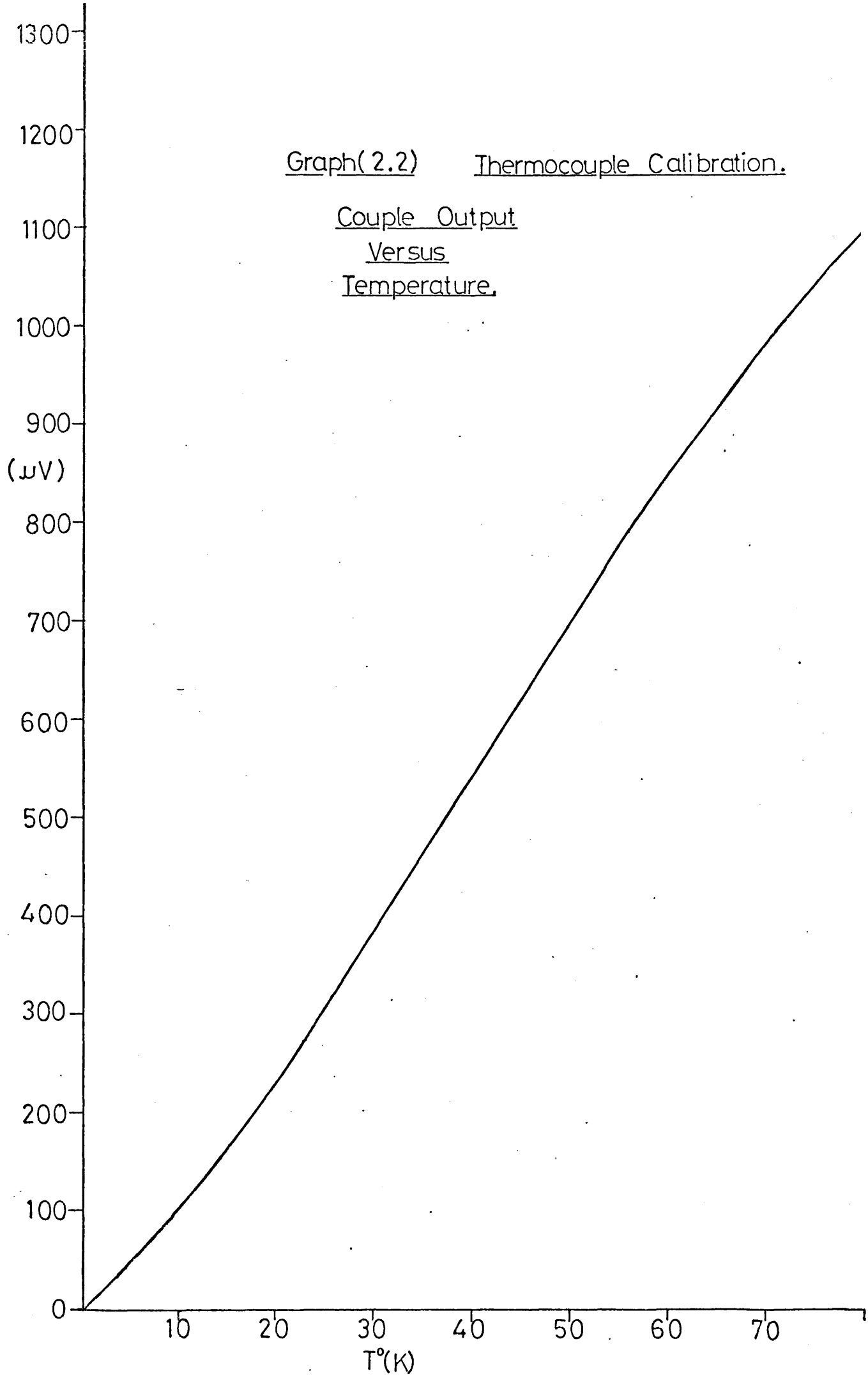

Holes drilled into the side of the tube give entrance to the main stainless steel ½" tubing. The electrical leads are passed through these holes, to the main terminal block at the top of the holder. They also allow the sample space to be pumped out when the copper jacket has been soldered into position.

The jacket is machined to fit over the copper base and rest against the base shoulder. It is important that the jacket does not touch any other part of the sample holder, as it is in direct contact with the helium bath and would provide a strong thermal short. The jacket is vacuum sealed with Woods Metal Alloy low melting point solder.

The top outlet of the main ½" tubing is left open, for attachment to the vacuum system. A side connection from the ½" tubing leads to the glass insulated 9 pin base terminal, which makes all the electrical connections between the sample holder and external apparatus.

2.4 Experimental Technique.

After the liquid nitrogen precool and helium transfer stages, initial checks were made for vacuum leaks and electrical or thermal shorts in the system. Preliminary readings were taken of the sample and voltage probe resistances. Cooling strains can (and did) result in the probes breaking away, or the current contacts cracking, as a result of differential contraction processes.

With no exchange gas present the sample platform slowly cooled to around $20^{o}K$ before reaching equilibrium. Therefore, to begin with, sets of measurements were taken at temperatures above this value. Only when all the required readings in excess of $20^{o}K$ had been taken was helium exchange gas admitted. With the exchange gas present the temperature immediately dropped to $4.2^{o}K$. (The remaining output from the thermocouples was spurious and not indicative of any actual

temperature difference. As such it was allowed for - deducted - from the higher temperature measurements.) Most of the exchange gas was pumped out, until the temperature began to rise, and the pumping was stopped a few degrees before the desired temperature was reached. The control unit was then used to heat the sample the remaining few degrees. This method was the most convenient, economical and stable way of achieving the required temperature.

For the ohmic results a set of voltage versus magnetic field readings were taken at each stabilized temperature. The current was set at a constant value. It was therefore possible to view directly the resistivity dependence on magnetic field. Voltage readings were taken at steps of 5 kilogauss, for both directions of magnetic field and sample current. Changing the magnetic field direction gave a substantial reading difference, which was largely independent of sample current direction. This results from a slight misalignment of the potential probes and sample orientation from the desired longitudinal configuration, with a resulting additional Hall field contribution to the measured voltage. The conditions of observation with $\mu H >> |$ (μ is the mobility and H the magnetic field) means that the Hall field is much greater than the resistive field, for a transverse configuration. This in turn means that even a slight misalignment in the longitudinal configuration, giving a small net transverse component of H, may result in a significant Hall voltage. This is particularly relevant for the negative magnetoresistance measurements, where mobilities higher than 2×10^6 cm^2 $V^{-1}sec^{-1}$ mean that $\mu H \sim 1$ ($\mu H/10^8$ in mixed units) for magnetic fields (transverse component) as low as 50 gauss. The voltage independence of current direction indicates that there were no, or at least very small, temperature gradients. The four voltage readings for each magnetic field were averaged to eliminate the above contributions.

Sets of results were taken typically at 4.2°K, 10°K, 15°K, 20°K, 25°K, 35°K, 45°K, 55°K, 77°K, 100°K and 130°K. Regular checks were made that the measurements were taken in the ohmic region, i.e. I-V have a linear relationship.

With exchange gas admitted the non-ohmic results were taken at 4.2°K, and the sample switched to the pulse system. The results were taken with the magnetic field in the permanent mode, typically at 0, 10 kilogauss, 20 kilogauss, 30 kilogauss and 40 kilogauss, a set of current and voltage pulse measurements being made for each magnetic field setting. From these the required resistivity versus electric field values could be calculated. Fields up to 10 V/cms were found sufficient to cover the whole non-ohmic negative magnetoresistance range. Pulse measurements were made down to low (mA) current ranges, so that a check could be made that they married up to the D.C. ohmic measurements taken at 4.2°K. Readings were taken for both magnetic field directions and current directions, with a similar treatment to the ohmic case.

Because of the large currents involved it was necessary to keep the pulse repetition rate at a very low level, even though the pulse length was less than 5μ sec. Typically at 10V with a current of 10 amps and a pulse rate of 5 there is still a sample power of 2.5 milliwatts. Higher repetition rates quickly resulted in a thermal heating of the sample. Observation of the voltage pulse and comparison with the current pulse ensured that no significant thermal heating took place in the duration of the pulse and, on the other hand, that the pulse was significantly longer than the energy relaxation time, such that the electron system could reach an equilibrium state. The current and voltage pulses compared favourably.

The relative errors in the system were small, being about 1% for

the ohmic measurements. For the pulse measurements the readings were taken from an oscilloscope display with an error of 5% or more. The non-ohmic measurements, therefore, have a greater inaccuracy.

Measurements were repeated during the run, ensuring reproducibility and to check that there were no hysteresis effects with current, voltage or magnetic field sweep.

Sample dimensions and probe spacings were measured before and after each run with a travelling microscope.

CHAPTER 3.

NEGATIVE MAGNETORESISTANCE AND HOT ELECTRONS IN SEMICONDUCTORS. (A REVIEW)

3.1 Introduction: 3.2 Negative Magnetoresistance - Review of Theory: 3.3 Negative Magnetoresistance - Experimental Review: 3.4 Hot Electrons.

3.1 Introduction.

Section 3.2 reviews the various mechanisms which have been proposed to explain the negative magnetoresistance observed in semiconductors. Broadly speaking there are two different types of negative effect: (i) comparatively small effects (generally < - 10%) seen at very low temperatures and associated with the detailed structure and interactions around the impurity levels and the bottom of the conduction band; (ii) larger effects (up to -90%) taking place in the conduction band, and arising from the energy quantization of the conduction band electrons caused by high magnetic fields. The quantization imposes strong limitations on the effective scattering cross-section.

Most emphasis is given to the second of these effects, being the most relevant to the present investigation. In particular, attention is given to the interaction of conduction band electrons with ionized impurities when subject to high (quantizing) magnetic fields.

In section 3.3 we review the experimental work on negative magnetoresistance in semiconductors. Examples are given over a wide range of semiconductors, temperatures and magnetic fields. Various models, as expounded in section 3.2, are used by the authors to explain the experimental results. The agreement is by no means unanimous, especially in the type (i) effects studied. Sample inhomogeneity and shape are also shown to complicate the investigations.

Finally section 3.4 looks at the phenomenon of "hot" electrons in semiconductors, i.e. when the electron system is not in thermal equilibrium with the lattice. In particular, the behaviour of hot electron systems under high magnetic fields is explored both theoretically and experimentally. The magnetic field can result in strong deviations from the normal equilibrium formof the distribution, with the possiblity of various non-linear and "runaway" effects.

3.2 Negative Magnetoresistance - Review of Theory.

Standard solutions of the Boltzmann equation, for a parabolic conduction band, give the magnetoresistance as being proportional to H^2 for the transverse configuration and zero for the longitudinal configuration. This is derived for low magnetic fields, such that $\omega_c \tau << 1$ (ω_c is the cyclotron frequency and τ the electron collision time). For high magnetic fields, where $\omega_c \tau >> 1$, the simple theory predicts a transverse saturation magnetoresistance and still a zero longitudinal magnetoresistance.

Experimentally this behaviour is seldom found, especially at low temperatures and for the high magnetic field condition $\omega_c \tau >> 1$. More refined approaches must take into account the effect of a magnetic field on the relaxation time of the electron. (It is also necessary to note how the concentration of conduction band electrons may depend on the magnetic field, as this can exert a substantial effect on the magnetoresistance.)

Early experimental observations of negative effects were generally explained as resulting from contacts, or sample inhomogeneity. See Frederikse and Hosler (1957) or Bate et al (1961). Indeed, sample shape, contacts and inhomogeneity were sometimes deemed sufficient to explain all magnetoresistance, positive or negative, Weiss (1961).

However, two main approaches to negative magnetoresistance as a bulk effect emerged: (i) Toyozawa (1962) with the local spin model, and (ii) Argyres and Adams (1956) who showed the importance of the Landau energy quantization of the conduction band. We will look at these two approaches in turn, along with their extension and/or alternative theories.

- - - - -

(i) The Toyozawa model treats the interaction of the electrons in the impurity band with a localized spin system. The theory was adapted from Yosida (1957) who interpreted low temperature resistance anomalies in noble metals containing magnetic impurities using a Kondo type system of s - d exchange interaction between free electrons and the magnetic impurities. This interaction leads to the well-known Kondo minimum, seen in metals at low temperatures, where the resistance increases with decreasing temperature. Normal first order perturbation treatment is insufficient and higher orders must be used to reproduce this behaviour. (The mathematics of the Kondo problem can become very involved in a fuller treatment:Nozières (1975).)

However, in non-magnetic semiconductors it is not readily seen how local magnetic moments exist in the first place. Toyozawa shows that by introducing electron correlation energy into a network of random impurities, localized electron spin systems can exist around relatively isolated centres. Provided that these centres are not too isolated they can scatter the remaining "conducting" electrons in the impurity band. Using second order perturbation calculations the resistivity is found to increase logarithmically with decreasing temperature. Applying a magnetic field removes the dynamical and spatial randomness of the magnetic moments, effectively reducing the scattering cross-section and hence giving a negative magnetoresistance.

Both the spin scattering and the magnitude of the negative magnetoresistance should increase with decreasing temperature.

From the theory the magnetoresistance ratio $(-\Delta\rho/\rho o) \propto M^2$, where M is the magnetization of the moments.

So that for low magnetic fields,

$$(-\Delta\rho/\rho o) \propto \chi^2 H^2$$

where χ, the magnetic susceptibility, should follow the standard Curie-Weiss type law,

$$\chi = \frac{C}{T + \theta}$$

θ being the Curie or Néel temperature of the spin system. More generally, for arbitrary magnetic fields where χ becomes a function of magnetic field, the resistivity ratio should vary as the Brillouin function.

The partial localization of electrons within the impurity band is not the only way that the magnetic scattering centres are taken to arise. Other uses of the Toyozawa type system assume localization on isolated "single" impurity sites, fluctuating wells in the bottom of the conduction band or the formation of impurity aggregates. The last of these is taken to be a possible situation in heavily doped semiconductors, the precipitation of impurities being discussed by Andrianov (1975) for the case of Gallium Arsenide. Examples of the other systems are given in section 3.3.

Experimentally the local spin model has not been clearly established and the data is rather conflicting. The H^2 behaviour is rarely found and it may be necessary to extend the calculations past the second order; Alexander (1969). Alternatively, the magnetic moments themselves may depend on H and T in a complicated way, Andrianov (1975), giving strong divergence from the simple theory.

There has also been theoretical criticism of the spin model, with alternative mechanism for the negative magneto resistance being proposed. Mott (1974) states that the localized spins probably do not exist. He suggests that the dependence of the Fermi energy on magnetic field could result in a negative magnetoresistance. The conductivity in the impurity band is proportional to the density of states squared at the Fermi level. If the magnetic field dependent Fermi energy moves to a higher state density a negative magnetoresistance results. (This, of course, would not explain any negativity observed in the conduction band at higher temperatures.)

Another explanation of the low temperature results is based upon a two-band model proposed by Hedgcock (1970). In this model the impurity and conduction bands overlap, but with a fairly well defined mobility edge. A magnetic field causing spin alignment (as in Pauli Paramagnetism) with the corresponding energy changes - spin up or spin down energies - redistributes the electrons between the impurity and conduction bands. A simple calculation shows that there can be a net transfer of electrons across the mobility edge and so an increased conductivity.

Hedgcock fits a curve of the form,

$$\frac{\Delta\rho}{\rho o} = aH^c + bH^2 \quad \text{(a is a negative number)}$$

to the experimental results. (The bH^2 term is the "normal" positive magnetoresistance given by simple theory.) He obtains a fit with a value of $c = 1$, which is close to the value calculated on the two band model. The Toyozawa theory gives $c = 2$.

So far we have viewed electron interactions around the impurity energy levels. We now look at electronic conduction processes in the conduction band, and how the interaction with the standard scattering

mechanisms is modified by a large magnetic field.

- - - - -

(ii) The theory of Argyres and Adams (1956) is concerned with scattering processes in the conduction band, resulting from the standard phonon and ionized impurity interactions. The Hamiltonian for a free (conducting) electron in a magnetic field is used to evaluate the electronic wavefunctions and energy eigenvalues of the system. The wavefunctions are then used to calculate the scattering matrix elements for both acoustic phonons and screened ionized impurity interactions. (Optical phonon interactions or the piezo-electric component of the acoustical phonon interaction are not considered in the theory.) The matrix elements are used to calculate the relaxation times. The theory is done for the "Extreme Quantum Limit" condition given by $\hbar \omega_c >> kT$ and $>> E_F$, such that all the electrons are in the ground state Landau level. The expressions for conductivity are calculated from the standard type of relationship, for the limits of degenerate and non-degenerate statistics. The theory is only applied to the longitudinal (H parallel to E) configuration.

For the case of non-degenerate statistics and scattering from ionized impurities a negative magnetoresistive effect is predicted. The explanation of this result can best be given with reference to Fig. 3.1. For the "Extreme Quantum Limit" all electrons are confined to the lowest Landau level and the energy of any electron is given by,

$$\tfrac{1}{2} \hbar \omega_c + \frac{\hbar^2 k_z^2}{2m^*},$$

where $\frac{1}{2}\hbar \omega_c$ is the ground state level. (The magnetic and electric fields are in the z direction.) Scattering off ionized impurities is elastic, which means that the magnitude of k_z must remain unchanged if energy is to be conserved. Therefore $+k_z$ can only go to $-k_z$ and vice

FIG.(3.1)

E(k). relationship for z direction.

(showing two Landau levels.)

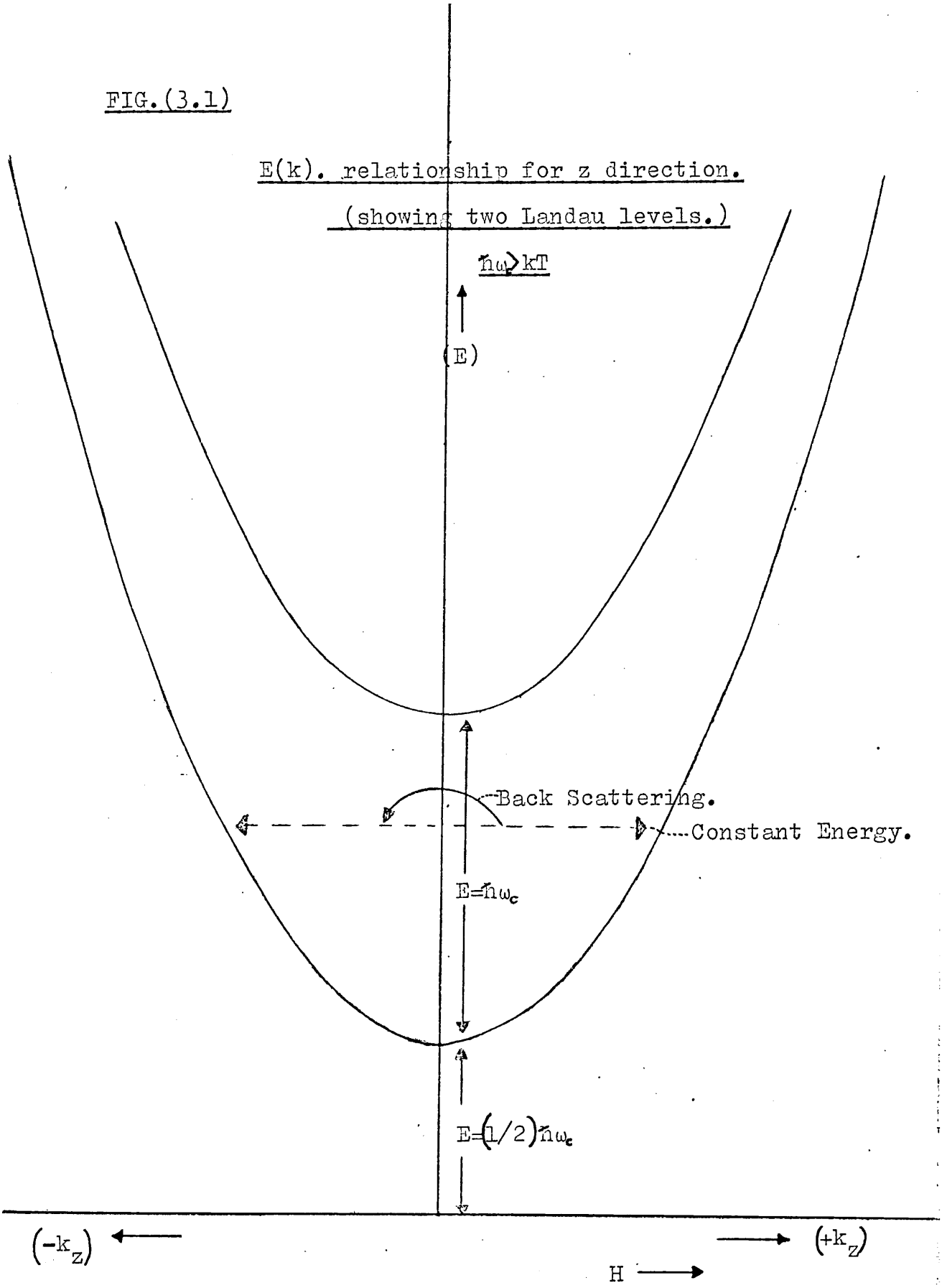

versa, i.e. momentum reversal of the electron. See Fig.3.1. There are many scattering events where kz remains unchanged - forward scattering - but these do not relax drift momentum and therefore do not contribute to the resistance. Because the scattering from ionized impurities is predominantly small angle scattering, the 180 degree momentum reversal has only a small effective cross-section. Therefore, the relaxation efficiency is strongly curtailed.

The strength of the negative magnetoresistance depends on the magnitude of (kR), where k is the mean electron momentum and R the screening radius of an ionized impurity. For $kR \gg 1$ small angle scattering is predominant and occurs down to a minimum angle of $\theta \sim 1/(kR)$, without the presence of a magnetic field. If the parameter $kR<1$, which occurs for low temperature and/or strong screening, then the scattering becomes much more isotropic and small angle processes do not predominate (momentum reversal has a larger effective cross-section). Therefore, the net effect from the magnetic field cutting of small angle scattering is reduced.

More generally, when more than just the ground state Landau level are occupied, the scattering restrictions are not so stringent. This is the case for $\hbar\omega_c \sim kT$ or E_F. When the condition $kT \gg \hbar\omega_c$ applies the electrons are spread over a number of levels and the normal quasi-continuum of states applies. Ionized impurity scattering, in the non-degenerate limit, when more than one level is occupied is treated by Dubinskaya (1969). For more than one level the mathematics becomes rather tedious and it becomes necessary to solve sets of simultaneous equations, an additional equation being needed for each Landau level. Numerical calculations for two Landau levels are given by Dubinskaya.

Dubinskaya also gives an additional approximate treatment for

effects due to collision broadening of the allowed states. The effect allowed for is a certain amount of small-angle scattering resulting from the finite time between collisions and the associated uncertainty energy spread.

From the uncertainty principle $\Delta E \sim \frac{h}{\tau c}$

(where τc is the collision time).

This in turn gives an uncertainty in kz, given by:

$$\Delta k_z \sim \left(\frac{2m^*}{h\tau}\right)^{\frac{1}{2}}$$

This gives the possibility of collision processes with small kz changes (small angle). The uncertainty Δkz is generally rather small, but the effect on the negative magnetoresistance can be substantial because the forward scattering events have a high probability.

The correction can be included in the "extreme quantum limit" by introducing a relaxation time τf associated with the forward scattering collisions. This can be combined with the relaxation time from the backward scattering events in the standard relationship, to yield a total transport relaxation time, so that:-

$$\frac{1}{\tau \text{ transport}} = \frac{1}{\tau \text{ Back}} + \frac{1}{\tau \text{ forward}}$$

The main result is to uniformly reduce the magnitude of the negative magnetoresistance, as shown by Dubinskaya for different degrees of a forward scattering contribution. (The inclusion of a forward scattering would also appear to change the qualitative behaviour for low values of the quantum parameter ($\hbar \omega_c / k_B T$), as discussed in Chapter 4.)

A further possible correction comes from the non-parabolicity of the conduction band, which is fairly strong for the case of indium antimonide with its low effective mass and strong band interaction. See Phadke (1975) and Agaeva (1974). The non-parabolicity results in a magnetic field dependent effective mass. As the magnetic field

technique, which is shown to converge rapidly, enables a solution to be derived for multiple Landau level occupancy. The main concern of Magnusson was the magnetophonon resonance phenomenon, but his calculations also show a strong negative magnetoresistance associated with the optical phonons. The magnetoresistance from this source remains negative up to the highest magnetic fields. Addition of acoustic scattering, in the high field region, quickly pushes the calculations into the positive region.

A negative magnetoresistance should also result from electon-hole scattering. The mass of the hole is much greater than the electron and so the scattering anisotropy is similar to the ionized impurity case. However, the author is not aware of any investigation, theoretical or experimental concerning this mechanism. The experimental situation would probably be difficult to realize, as the electron-hole scattering only predominates at high temperatures (above $400^{o}K$ for indium antimonide).

A different kind of negative magnetoresistance can exist in many valley semiconductors such as Germanium and Silicon. Miller (1965) shows how an electric field can redistribute the electrons amongst the more mobile valleys. The associated negative effect is fairly small and strongly anisotropic.

The quantum limit with degenerate statistics and multiple Landau occupancy has been investigated theoretically by Serre (1974). Ionized impurities are taken as the only scattering mechanism. A substantial negative magnetoresistance is shown to result from the quantization effects. In the extreme quantum limit, if the statistics remain degenerate, the magnetoresistance starts to go positive, unlike the non-degenerate case where the negative magnetoresistance saturates to a constant negative value. Serre incorporates a density of state broadening factor Γ, which arises from the fluctuation of the bottom of

the conduction band caused by the potential from the random distribution of charged impurities. See Dyakonov, Ebros and Mitchell (1969) or Keldysh (1964). This broadening can result in the second Landau level being occupied even for the condition $\hbar\omega_c > E_F$, and is calculated as exerting a fairly strong effect on the magnitude of the magnetoresistance. The broadening effect besides changing the negative magnetoresistance may decrease or totally remove the de-Haas Shubnikov oscillations normally associated with the degenerate multiple-occupancy case.

The negative magnetoresistance in the degenerate case, with more than one Landau level, has also been covered by Gerhardts and Hajdu (1971). Ionized impurity scattering is used, but no additional corrections are used. They state that a more complete approach using a generalized Born approximation and allowing for Landau broadening, would be desirable.

In fact Gerhardts gives a formally more complete approach to the quantum limit transport problem (Gerhardts (1971)) but using the physically unrealistic point impurity scattering mechanism. Four different approximations are investigated: (i) the lowest Born approximation; (ii) the T-matrix method; (iii) the generalised Born approach; (iv) the self-consistent T matrix. The calculations are done for the degenerate case in the quantum and extreme quantum limits. The calculations, especially in the extreme quantum limit, are found to be sensitive to the approximation used and the treatment of the Landau broadening.

A rigorous quantum mechanical formulation using the ionized impurity scattering mechanism has not been attempted and would involve fairly formidable evaluation techniques. Most treatments use the standard Born approximation, which is discussed further in Chapter 4. The treatment of the Landau broadening may be important, as shown by

Serre. The broadening can arise from collision effects, as well as the random impurity potential as used by Serre. Barker (1972) gives a treatment of the possible broadenings of the Landau states, in reference to the damping of magnetophonon resonances. The effect is to curtail the sharp singularities that exist in the undamped state structure. At low temperatures we also have the possibility of multiple scattering events that occur when an electron interacts with two or more sites simultaneously. Multiple scattering events, for the zero-magnetic field scattering from ionized impurities, have been calculated by Moore (1969) as a correction to the standard Brooks-Herring mobility equation.

3.3 Negative Magnetoresistance - Experimental Review.

Most of the published experimental work is concerned with spin/impurity mechanisms of negative magnetoresistance. Although Argyres predicted the negative conduction band effect in 1956, it is only more recently that it has been investigated experimentally.

Negative magnetoresistance has been observed in a wide range of substances, both metallic and semiconducting, crystalline and non-crystalline. We will not cover the metallic work, although the metallic alloys with their low temperature resistance anomaly were the first subjects of the Kondo spin-interaction theory.

Various magnetic semiconductors display, quite strongly, the spin scattering mechanism and the associated negative magnetoresistance. See Shapira (1971) for work on Eu.Te. or a review of magnetic semiconductors by Gurevich (1975). The scattering is within the conduction band and is associated with the net magnetic moment of the impurity atoms and not any hypothesized correlation effects between electrons and impurity centres. The scattering and associated negative magneto-resistance is found to increase as the temperature is lowered, reaching

a maximum value when a phase transition to ferromagnetic or anti-ferromagnetic ordering is taking place. At this critical temperature the magnetic order fluctuations are at a maximum. All transport coefficients, not only conductivity, display anomalies in this region.

Mell (1970) has investigated negative magnetoresistance for a range of amorphous semiconductors (Ge, Si, In Sb and Ge Te) and reports that nearly all show a negative effect, which varies as H^n where $0.5 < n < 1$. This occurs in the hopping conduction region and quickly vanishes at higher temperatures.

Various negative magnetoresistance results have also been associated with heating effects other than the case of using an electric field to merely raise the electron temperature. For non-parabolic semiconductors, with multi-valley structure, an electric field can redistribute the carriers into more mobile valleys. This was mentioned in the previous theory review section (Miller). Kotkus (1972) obtains a 2% negativity at $77^{o}K$ in germanium resulting from this effect.

Newhouse (1969) has observed a transverse negative magneto-resistance in germanium at $4.2^{o}K$. This was attributed to impact ionization of the impurity levels, caused by the increasing Hall field as the magnetic field was raised.

A resistive drop with magnetic field can be observed in the pinch effect, seen in semiconductors at sufficiently high electric fields to excite an electron-hole plasma. See Glicksman (1959). The pinch, which results from the currents own magnetic field, narrows the effective cross-sectional area of the current and gives a higher resistance. An applied longitudinal magnetic field destroys this self-containment and thereby decreases the resistance.

Investigations have also been made on carbon in its various

forms. See Delhaes (1972); Yazama (1969); Delhaes (1974); Fujita (1968). The negative magnetoresistance has been attributed to a variety of causes. Proposed mechanisms are: magnetic field reduction of diffuse scattering at crystalline boundaries; changes in the free electron concentration with magnetic field; Toyozawa spin scattering effects. The effects would seem to depend on the detailed structure of the material used and its degree of graphitization.

Negative magnetoresistance resulting from spin scattering has been investigated fairly extensively, although not conclusively. A number of authors have used the Toyozawa theory, and extensions of it, to interpret their results. See Delhaes (1972) on pyrocarbon; Larsen (1973) on sulpho-spinels; Zotova (1963) on indium arsenide; Zavaritskaya (1973) on gallium arsenide; Sasaki (1961) and (1961) on germanium; Khosla (1970) on cadmium sulphide; and Matveenko (1971) on gallium antimonide.

Takita (1973) reports a negative magnetoresistance of -5% in p-type tellurium at 1.2^{o}K and below. At the higher levels of doping used there is no separate impurity band and the dominant carriers are in the conduction band. He states, however, that the existence of localized spins is somewhat questionable and the Toyozawa type model is found to be inapplicable, especially as there is only a small g-factor associated with the band.

Iwai (1974) reports a small negative magnetoresistance <1% in Cd In_2 S_4, which is observed up to a temperature of 130^{o}K. As no Toyozawa H^2 dependence is observed Iwai used the Hedgcock mobility edge model to interpret the results.

The negative magnetoresistance observed in gallium arsenide exceeds -35% and appears to be the largest effect, in a non-magnetic semiconductor, attributed to a spin system. An H^2 dependence is seen at

low magnitude fields and $(\Delta\rho/\rho_o)^{\frac{1}{2}}$ fits a Curie-Weiss susceptibility law, being proportioned to $1/(T - \Delta)$. Experimentally Δ is found to be a negative value, indicating anti-ferromagnetic coupling between the spins. A g factor of 25 is necessary to explain the results. (A high g factor is characteristic of all the experimental work on non-magnetic semiconductors.)

As stated in section 3.2 the spin systems are not only limited to the original Toyozawa impurity bonding regime. Garyagdyer (listed above) used the fluctuating bottom of the conduction bond as a mechanism for localization of the electron spin system. (The fluctuation arises from the random impurity distribution as used by Serre (see section 3.2) to account for Landau level broadening.) Gayagdyer uses a root mean squared fluctuating potential of 30 meV for indium arsenide. This value has a strong dependence on the degree of compensation. The local magnetic moments required by theory to fit the data rise to 200 Bohr magnetons. (A rather high value!) Although results show a general qualitative agreement with the Toyozawa theory, the calculated magnitude of the moments does not follow the Toyozawa dependence on magnetic field or temperature.

This seems to be the case for a variety of investigations. Even where the spin systems are assumed to exist the agreement with theory is often of a somewhat ambiguous nature. Results on cadmium sulphide, which gives an unsaturated magnetoresistance up to 140 kG, do not give the expected H^2 fit even at very low fields. Susceptibility measurements have also been found to give ambiguous results. Andrianov (1975) points out that the susceptibility seems to be independent of any heat treatment, whereas the negative magnetoresistance seems to show a strong sensitivity to such treatment.

As stated in the theoretical review it might be necessary to

extend the calculations past the second order of perturbation in order to account for these discrepancies. The Toyozawa magnetic moment system comes from a many-body interaction and is therefore a complicated group excitation, in the way a plasma oscillation is. It is therefore possible that the normal magnetic susceptibility functions are inapplicable.

Polyanskaya (1975) reported that for low magnetic fields a deviation from the expected (Toyozawa) H^2 dependence may result from contacts disturbing the current flow. When a double cross sample was substituted the H^2 dependence was obtained. At higher magnetic fields the behaviour was found to be independent of sample shape and contacts.

Katayama (listed previously) attributes a very low temperature negative magnetoresistance in indium antimonide to the establishment of a Toyozawa spin system at the bottom of the conduction band. In indium antimonide the resistivity can be observed to go through a minimum and saturate at very low temperatures. This behaviour is greatly amplified by a strong magnetic field, Sladek (1958), resulting from the freeze out of conduction electrons into the impurity band. However, Katayama measured the Hall coefficient with a very small magnetic field to show that there is no freeze out with temperature alone, down to $0{\cdot}1^{\circ}K$. A negative magnetoresistance of -10% was measured using magnetic fields less than 1.5 kG. A g factor of 200 is necessary to explain the results. Above 1.5 kG magnetic freeze out and Landau quantization predominate over the negative effect, to give a strong positive magnetoresistance.

The condition for the extreme quantum limit, $\hbar\omega_c >> kT$ or E_F and $\omega_c \tau >> 1$ means that this regime can most readily be achieved in semiconductors with low effective mass. Elements such as germanium and silicon require very high magnetic fields to reach the extreme quantum limit. Therefore, most experimentation has been on III-V and some

II-VI compounds with low effective masses.

Experiments by Amikhanov (1967) on indium arsenide and Aliev (1975) on $Ga_x\ In_{1-x}\ As$ solid solutions, have shown negative magnetoresistance arising from the Argyres mechanism of reduction in cross-section of ionized impurity scatterers. Temperatures ranged from 77^oK to 300^oK, and the negative magnetoresistance reached -30% for the lower temperatures. Aliev studied the result of changing the mixture (adjusting the x parameter) for a constant electron concentration $n = 1.2 \times 10^{17}\ cms^{-3}$, where the samples are degenerate. The postion of the negative maximum depended on the degree of degeneracy and the value of x. Changing the composition factor x tended to increase the effective mass, reducing $\hbar\omega_c$, so that the maximum shifts to higher magnetic fields. However, for all the samples the maximum occurred around $h\omega_c/E_F = 1.5$, which corresponds with the value given by Gerhardt's degenerate theory.

Berchenko (1974) investigated $Cd_x\ Hg_{(1-x)}\ Te$ solid solutions, in the quantum limit. The statistics are non-degenerate and so the Dubinskaya theory was used. A negative effect of -60% was found. The effect of varying the x parameter was also investigated. The x parameter changes the effective mass and a corresponding shift in the maximum position (maximum negativity), similar to the Aliev case, resulted. However, the turning value when plotted against the quantum parameter $\beta\left(\frac{\hbar\ \omega_c}{kT}\right)$ was approximately 9, for all the samples. The Dubinskaya theory gives a turning point around $\beta \sim 4\text{-}5$. No detailed analysis of the results was attempted.

Dubinskaya tested her theory on tellurium, which gave a fairly small effect, and found a qualitative agreement with the theory. Bastard (1974) also investigated tellurium at temperatures between 1.6^oK and 4.2^oK with impurity dopings from $10^{14}\ cms^{-3}$ up to $5 \times 10^{16}\ cms^{-3}$. The investigation was done just for the extreme quantum limit with the

Argyres theory being extended to include the double valley structure. The negative behaviour was not observed for low dopings, but occurred with impurity banding concentrations. This work would appear to be the only application of "normal" scattering mechanisms for the explanation of negative magnetoresistance the impurity banding regime, i.e. not spin scattering or redistribution amongst states behaviour.

Negative magnetoresistance in indium antimonide has been investigated by Ilin (1973) and Tokumoto (1974). Various papers on the hot electron behaviour in the quantum limit also deal with negative magnetoresistance and these are dealt with in the next section.

Ilin investigated the longitudinal magnetoresistance at a temperature of $30^{o}K$ for electron concentrations ranging from 0.72 to 5×10^{14} cms^{-3}. The results were interpretted on the Dubinskaya theory, but no quantitative analysis was attempted. The turning points, with regard to β seemed to be in rough agreement with theory, as well as the fact that the magnitude of the negativity increased with increasing sample purity. However, there was a very much stronger dependence on impurities than predicted by theory, as well as a smaller magnitude than given by theory. Indeed, for the more impure specimens of 3 to 5×10^{14} cms^{-3} concentration (although still rather pure) no negative magnetoresistance was observed at all.

The Tokumoto results also display a wide range of magnitude for samples of apparently similar levels of impurity. Also, the results taken at $77^{o}K$ seem to display an overall independence on impurity concentrations, which range from 10^{14} up to 10^{16} cms^{-3}, although individual samples show a negativity anywhere between 0 and -60%. (This would appear to be in contradiction of the Ilin paper and expectations of the Dubinskaya theory.) This range of results and discrepancies would seem to result from the effect of sample inhomogeneities. It is clearly

important to have as homogeneous a sample as possible, if there is to be as little masking of the negative magnetoresistance as possible.

Other Tokumoto results, taken up to room temperature, sometimes show a maximum negative effect at temperatures in excess of $100^{o}K$, often showing a magnitude >60%. These results are for a 7×10^{13} cms^{-3} sample (high purity) where the zero magnetic field resistivity resulting from ionized impurity scattering is far less than 60% at these high temperatures. The conclusion is that other scattering mechanisms must give rise to the observed negative magnetoresistance, the most likely source being polar optical phonons. Indeed, the Magnusson paper, previously outlined, predicts a strong negative effect from this source. No detailed investigation appears to have been made at higher temperatures.

3.4 Hot Electrons

The term "hot electron" was first used by Shockley to denote the increase of electron energy in semiconductors in excess of the lattice energy when a strong electric field was applied. Considerable work, both theoretical and experimental, has been undertaken since. Detailed reviews have been given by Conwell (1967) and Putley (1964). With the addition of a magnetic field to a hot electron system a wide range of different phenomena may be observed. These effects will be reviewed briefly, with reference to more detailed discussions.

The plasma pinch effect has already been mentioned. This occurs for an electrically excited electron-hole plasma. With the addition of a magnetic field microwave radiation is found to occur. The sample acts as a microwave aerial. Buchsbaum (1965) reports a microwave emission from indium antimonide placed in a longitudinal magnetic field with electric fields as low as 12 $V.cm^{-1}$. The experiments were performed at $77^{o}K$. At such low fields and lattice temperatures no excitation of holes occurs, so that no electron-hole plasma should exist. However, Ancher

Johnson (1969) showed that soldered current contacts, composed of indium, injected holes into the sample even at comparatively low electric fields. In this way an electron-hole plasma may exist along a section of the sample and result in the observed microwave emission. A variety of such instabilities are reviewed by Putley (1964) and Bowers (1964).

Instabilities associated with high magnetic fields may arise from the magnetically induced freeze out of the free carriers, or the Landau quantization effects. Under such conditions critical electric fields may result in the avalanche ionization of the frozen out electrons, or a transition between the $\hbar\omega_c >> kT_e$ and $\hbar\omega_c << kT_e$ regimes with their different magnetic field dependency of the resistivity. This second case has been investigated theoretically by Kazarinov and Skobov (1962) using a transverse magnetic field configuration. In the transition region from $\hbar\omega_c >> T_e$ to $\hbar\omega_c << T_e$ (where T_e is the electron temperature) the ρ_{xx} component of the resistivity decreases as the cube of the current density. Zlobin (1972) gives a review of hot electron effects in a quantizing magnetic field and shows how S and N type I/V characteristics, with accompanying instabilities, may arise when quantization is destroyed as given above in the Kazarinov transition region. The particular behaviour depends largely on the important scattering mechanisms present.

The formation of electric field domains or filamentary current regions have been associated with these transition regions and their associated instabilities. The instability of the domains give rise to electrical oscillations which are dependent upon the external circuitry (see Ridley (1963)).

For the case of electron excitation from impurity sites, Mansfield (1970), we find an avalanche effect at critical electric fields. An S shaped characteristic can arise under such circumstances,

from the changing screening of the impurities by the electrons excited into the conduction band, as discussed by Zaĭtser, Zvezdin et al (1971). The change of resistivity can extend over several orders of magnitude.

A particularly relevant effect with regard to the Landau quantization is the reduction in the effective electron-electron collisions as the extreme quantum limit is approached. In fact, the electron-electron collision frequency in the extreme quantum limit is given by $\Theta_{ee} \propto \exp\left(\frac{-\hbar\,\omega_c}{kT}\right)$. The mutual electron interactions are therefore rapidly supressed by the magnetic field. Normally the electron collisions serve to establish the form of the distribution function in both energy and momentum space. When they lose effectiveness (when electron-electron interactions become much less frequent than other electron collisions) strong deviations from the standard Boltzmann statistics may result, with the possibility of electron energy runaway phenomena, in the presence of strong "heating" electric fields.

The reason why the collisions become inefficient in energy and momentum redistribution may be understood quite simply. When two electrons collide their total energy and momentum must be conserved (it can only be redistributed between them) but because of the basic one dimensional nature of the extreme quantum limit transport they can only exchange positions in phase space, leaving the distribution form of the electron system unchanged.

A general solution of the Boltzmann equation for the exact distribution function, with arbitrary electric field and/or magnetic field, cannot be derived analytically. Various procedures and approximations have been used to estimate it. Price (1970) has given a theoretical account of these various approaches when strong electric fields are present.

The simplest approach is the "electron temperature" model. The

electron temperature model, introduced by Frohlich (1947), assumes that the heating of an electron system can be represented by a shifted equilibrium (Boltzmann) distribution, with an effective electron temperature T_e to replace the thermal lattice temperature T_L. This can only be the case when electron-electron collisions exceed all other collision processes to establish such a distribution. Clearly, with quantum limit transport this model should be inapplicable. Even in the absence of quantizing magnetic fields the model is generally only justified when the electric field is not too strong - "warm" electrons. The warm electron condition is often defined as $T_e - T_L << T_L$.

The electron temperature is evaluated from the energy balance equation:- Rate of energy gain from electric field ($ne\mu E^2$) = Rate of loss of energy to relaxing mechanism. n is electron concentration, μ the mobility and E the electric field. Where the energy loss rate is derived theoretically as some function of electron temperature, so that

$$n\ e\ \mu\ E^2 = f(T_e).$$

See Hughes and Tree (1970).

Expressions for $f(T_e)$ have been calculated for various scattering mechanisms which relax energy. Frohlich (1947) for acoustic phonons and Stratton (1957) for polar optical phonons.

The wide availability of computation facilities has made possible various Monte Carlo numerical calculations of the distribution function. The standard ensemble average in phase space $f(\underline{k})$, is replaced by a time averaged functional representation. This is calculated by following the motion of one electron in phase space and scattering it by use of a random numbers system. The distribution function is constructed from the length of time the electron spends in each section of phase space. Detailed explanations of the method have been given by Kurosawa (1966) and Fawcett (1970).

Other techniques for calculating the distribution function involve the use of truncated Legendre polynomial expansions, iteration of trial functions or variational type procedures.

The addition of a strong magnetic field to the hot electron system results in stronger deviations of the distribution from the equilibrium form. This may be especially true with the above mentioned runaway effects. A theoretical method devised by Kurosawa (1965) and used in a number of experimental investigations, replaces the Boltzmann equation by a Brownian type diffusion motion in energy space, with an associated diffusion equation. The electric field and collision processes are viewed as producing small Brownian type changes in the energy of the electron $\Delta\varepsilon$, between each interaction. This means that the electric field and energy relaxation processes must not be over strong. This assumption is a fair one as far as acoustic phonon interactions are concerned. For optical phonons Kurosawa uses an energy continuity equation. This describes the acceleration of electrons by an electric field to the point at which they reach the optical phonon energy $\hbar\omega_{op.}$, whereupon they spontaneously emit a phonon and return to the ground state energy. The process can then be repeated.

This model only allows for the calculation of $f_o(\varepsilon)$, i.e. the symmetrical part of the distribution function. This is a strong drawback if the true distribution has a significant streaming property. In fact for a low temperature regime, $T_L << \hbar\omega_{op.}$, where only polar interactions are significant (this is seldom the case however) the distribution is likely to assume a needlelike shape under high electric field conditions. See Vosilius (1966).

Hot electron transport in the quantum limit has also been treated by Magnusson (1972). The theory is for arbitrary electron degeneracy and a longitudinal magnetic field configuration. Scattering

from ionized impurities, acoustic phonons and polar optical phonons are all incorporated. The distribution is calculated analytically for the extreme quantum limit, with just the ground state Landau level occupied and by an iterative technique for more than one Landau level being occupied. The parameters of indium antimonide are used to give an example of the calculated distribution function (although the theory is valid for any parabolic polar semiconductor) and compared with the drifted Maxwell approach, to show how widely they differ, i.e. how wrong the "electron temperature" distribution is.

Although the various simpler models frequently give a very misleading picture of the electron distribution, it is mostly true that the values of the required transport parameters, performed as averages, are not very sensitive to the exact form it may take. It is quite often the case, although not always so, that using the correct function, or a better approximation, gives only a quantitative change in transport behaviour with the essential characteristics remaining largely unchanged.

There have been several experimental papers using the Kurosawa method in the quantum limit regime. See Kotera et al (1968); Kotera et al (1971); Komatsubara et al (1969). These investigations looked at the transverse and the longitudinal conductivity, as well as the microwave absorption properties, with strong electric and magnetic fields. The experiments were all on pure samples of indium antimonide. The theory was used to calculate $f_o(\varepsilon)$ for electric fields up to 10 $V.cm^{-1}$ and magnetic fields up to 20 kG. The calculated distribution showed strong deviations from the Boltzmann distribution with sharp discontinuities appearing at the Landau levels. The distribution is also strongly attenuated beyond the optical phonon energy as might be expected. The calculations are done for a lattice temperature of $4{\cdot}2^{o}K$, but from these

calculations the higher Landau levels are still occupied because of the heating electric field and the possibility of thermal runaway. The I/V characteristics calculated from these distributions showed strong non-linear behaviour and were compared with experimental results. The comparison is complicated by the magnetic freeze out of conduction electrons, which leads to a further addition to the non-linear behaviour. Scattering included ionized impurities, acoustic and polar optical phonons. Electron-electron scattering was not taken into account, but these interactions are probably not very important owing to the low carrier concentrations and quantizing magnetic fields.

Results for the longitudinal configuration are particularly relevant. The distribution shows a strong tendency to maximize around each Landau sub-band. This results from the runaway effect, which occurs in each sub-band at a critical electron energy, where the electron energy increases rapidly until the point where electrons are scattered to a higher Landau energy level, or emit an optical phonon, whereupon they return to the ground state. The Kotera paper gives a typical longitudinal configuration I/V plot, which shows a negative magneto-resistance effect for electric fields in excess of 1 V/cms. i.e. the I/V characteristics cross-over as this region is entered. Similar behaviour was found experimentally. However, those researchers do not investigate the negative magnetoresistance and attribute the crossing of the characteristics to the hot electron magnetophonon effect, where a Landau level crosses the optical phonon energy leading to resonance scattering.

Yamada (1973) deals mainly with the hot electron magnetophonon effect and how its behaviour depends upon the distortion of the distribution function. The increase of the mobility with magnetic field (negative magnetoresistance) is explained as resulting from

mobility limiting transitions. The electrons in a sub-band rise in energy, being heated by the electric field, until they reach the next sub-band (Landau level) and are scattered into it. As the sub-bands spread apart with increasing magnetic field this transition energy increases, so that electrons can gain a greater mobility before reaching the higher Landau level. None of these hot electron papers interpret the negative magnetoresistance explicitly as arising from a magnetic field reduction of the effective scattering cross-section.

The various energy relaxing mechanisms are clearly of central importance in the interpretation of hot electron data. In indium antimonide these have been widely investigated for both degenerate and non-degenerate statistics. See Kinch (1967); Szymánska and Maneval (1970); Sladek (1960); Gershenzon et al (1973); Kahlert and Bauer (1973). These investigations are mainly concerned with the relaxing processes at, or around liquid helium temperatures.

For comparatively small heating, where Te < 16^{o}K, the results are generally analysed using just acoustic phonon interactions via the deformation potential and piezo-electric modes. The relative importance of these modes depends on sample temperature and concentration of free electrons. The degree of degeneracy is also an important factor. See Bauer. For greater heating levels, polar optical phonons soon become the dominant energy relaxing mechanism. Solution of the Boltzmann equation and experimental results show that the polar optical phonon processes are the only important ones when Te > 18^{o}K. At slightly lower temperatures, around 16^{o}K, a two phonon process may be important over a small temperature range. See Stradling and Wood (1970). This interaction involves two transverse acoustical phonons of high energy (generally taken to be at the Brillouin zone edge)

being simultaneously emitted in opposite directions. Although only a second order process, the relaxation efficiency is high because a large value of energy can be emitted in each event.

Additional corrections to these basic mechanisms, such as electron-electron interactions and screening effects can also be included in the analysis, as well as corrections from band non-parabolicity. The last correction mentioned results in a p-type function admixture to the standard S-type wavefunction of the electrons, in additions to the changing effective mass value. The treatment of the inter-electron behaviour and the screening parameters is rather complex and is therefore frequently ignored or simplified. A full quantum mechanical treatment has not been attempted.

Gershenzon looked at the hot electron behaviour in indium antimonide at low temperatures ($4.2^{o}K$), without a magnetic field and explained, qualitatively, the resistive behaviour with increasing electric field. He points out three regions of different interactions as the field is increased.

Firstly, a fairly rapid decrease in resistivity as the electrons are heated efficiently by the electric field (or possibly excited into the conduction band, if they are frozen out) and can lose energy only to the comparatively few inefficient acoustic phonons present at $4{\cdot}2^{o}K$. Secondly, a quasi-ohmic region where the resistivity is almost independent of electric field. In this region the electrons have sufficient energy to begin spontaneously emitting polar phonons and are cooled very efficiently, so that the net energy of the electron system only increases slowly with electric field. In both of these regions the mobility is still determined by the elastic scattering on ionized impurities. Finally, in the third region the resistivity increases with the electric field. This happens when the polar phonons begin to

limit the mobility, as well as relaxing the energy.

Il'in et al (1974) extend this work by applying a strong longitudinal magnetic field to this system. The three regions are still in evidence, but in a modified form.

For low electric fields (the first region) carrier freeze out becomes very important with large magnetic fields and the breakdown at critical electric fields can be drastic. (This region is not shown in in the Il'in reference.) The second region shows a very strong negative magnetoresistance, as in the Kurosawa calculations and experiments. The energy is still relaxed by polar optical phonons and the mobility determined by ionized impurity scattering events, as in the zero magnetic field case. The reduction in scattering cross-section by the quantizing magnetic field (Argyres) explains the negative effect.

The authors also point out how the electron-electron scattering reduction by the high magnetic fields may lead to a qualitative difference in the observed behaviour. This concerns the behaviour in the second region. For weak electron-electron scattering the quasi-ohmic region is independent of electric field, whereas for strong electron-electron scattering it shows a weak increase with electric field. Therefore, if the electron-electron scattering is initially important with no magnetic field, a noticeable change in behaviour occurs as the magnetic field is increased.

In the third, optical phonon region, there is a rather small positive magnetoresistance which saturates very quickly. Consequently, all the resistances for various magnetic fields converge to a single characteristic.

CHAPTER 4.

ANALYSIS AND DISCUSSION.

4.1 Introduction: 4.2 Results and Errors: 4.3 Ohmic Analysis: 4.4 Non-ohmic Analysis: 4.5 Discussion.

4.1 Introduction.

Results are given for a range of samples and temperatures, with both ohmic and non-ohmic investigation of the negative magnetoresistance. Most emphasis is given to the ohmic results and a full quantitative analysis is attempted only for this case. The ohmic analysis uses the Argyres and Adams theory of the magnetic field dependent scattering cross-section from ionized impurities. Additional allowance is made for small angle forward scattering (Dubinskaya) resulting from finite collision times and the uncertainty principle. The equations are generalized for arbitrary degeneracy and evaluated with a computer programme. A comparison is made between ohmic and non-ohmic effects, using the simple electron temperature model to interpret the non-ohmic data. The theoretical analysis, its approximations and correspondence with experiment is discussed in detail.

4.2 Results and Errors.

Considerable initial research was conducted on a variety of samples with different dimensions. These experiments were performed using a different sample holder to the one previously described. The samples were immersed directly in liquid helium, so that only non-ohmic $4.2^{o}K$ measurements could be made. Results on samples with small cross-section tended to display greater anomalies in the magnitude of the negative magnetoresistance. For this reason all the measurements reported

here were made on large samples.

The samples used are shown below in Table 1. Samples were purchased from either Malvern or M.C.P. Electron concentrations ranged from 1.1×10^{14} cms^{-3} up to 2.23×10^{15} cms^{-3} and mobilities from 640,000 $cm^2\ V^{-1}\ sec^{-1}$ down to 270,000 $cm^2\ V^{-1}\ sec^{-1}$. All the samples had the same dimensions of $1 \times 2 \times 20\ mm^3$.

TABLE 1.

Sample	Origin	n (77^oK)	μ(77^oK)
S_1	MALVERN	1.1×10^{14}	6.4×10^5 $cm^2\ V^{-1}\ s^{-1}$
S_2	M.C.P.	2.7×10^{14}	3.1×10^5
S_3	M.C.P.	5.6×10^{14}	5×10^5
S_4	M.C.P.	8.0×10^{14}	4×10^5
S_5	MALVERN	2.23×10^{15}	2.7×10^5

The S_2 sample displayed somewhat anomalous results - the negative magnetoresistance was curtailed and was positive for $T < 15^oK$. This probably resulted from inhomogeneities or imperfections in the crystal (the dislocation density was high).

An experiment was also undertaken to increase the donor concentration N_D by placing a sample in a nuclear reactor to undergo thermal neutron bombardment. Indium has a very high neutron capture cross-section and the element rapidly transmutes, by beta decay, to tin. Therefore, valency is increased by one and the original indium site becomes a donor. This method should provide a controlled means of increasing the donor concentration in one sample, over a series of experiments. These results are not presented here, and the method has not been fully investigated. The residual radioactivity and the possibility of fast neutron damage are problems

encountered. However, use of a moderating medium and precautions in handling may enable this to be a useful tool.

The ohmic and non-ohmic results of the remaining specimens are presented in Graphs 1. The ohmic results give a plot of the resistivity ratio $\Delta\rho/\rho_o = \left\{ \frac{\rho_H - \rho_o}{\rho_o} \right\}$ versus $\beta\left(\frac{\hbar\omega_c}{kT}\right)$. This is the most appropriate plot to show the magnetoresistivity behaviour for the quantum ($\beta \sim 1$), and extreme quantum limit ($\beta >> 1$), assuming the statistics are non-degenerate. (In the extreme quantum limit the statistics of all the samples become non-degenerate, even though the higher doped specimens may be strongly degenerate for low or zero magnetic field.) The non-ohmic results are shown graphically, with ρ versus the electric field E, the lattice temperature being held at a constant $4.2^{o}K$. For clarity only the negative magnetoresistance region is shown. At lower electric fields strong magnetic freeze out effects give a high positive magnetoresistance, with a sudden breakdown at critical electric fields. The end of the breakdown region can be seen in the graphs.

The electron concentration (n) and the mobility (μ) quoted in Table 1, are both calculated from the Hall and conductivity measurements at $77^{o}K$.

The greatest source of error in the results is probably the effects of inhomogeneities. Some samples were tested for reproducibility, the voltage probes being shifted to different points on the surface. Although, the relative errors are probably only 1% or so (or 5% for non-ohmic) the absolute error is more, probably around 10% for the samples analysed.

GRAPHS.(1).

(1). 1.1 . 10^{14}	$\frac{\Delta\rho}{\rho_0}$ versus β
(2). 5.6 . 10^{14}	" " "
(3). 8.0 . 10^{14}	" " "
(4). 2.23 . 10^{15}	" " "
(5). 1.1 . 10^{14}	Magnetophonon Resonance.
(6). 1.1 . 10^{14}	ρ versus E
(7). 5.6 . 10^{14}	" " "
(8). 2.23 . 10^{15}	" " "

GRAPHS (1)

No.(1) 1.1×10^{14}

Experimental Data.

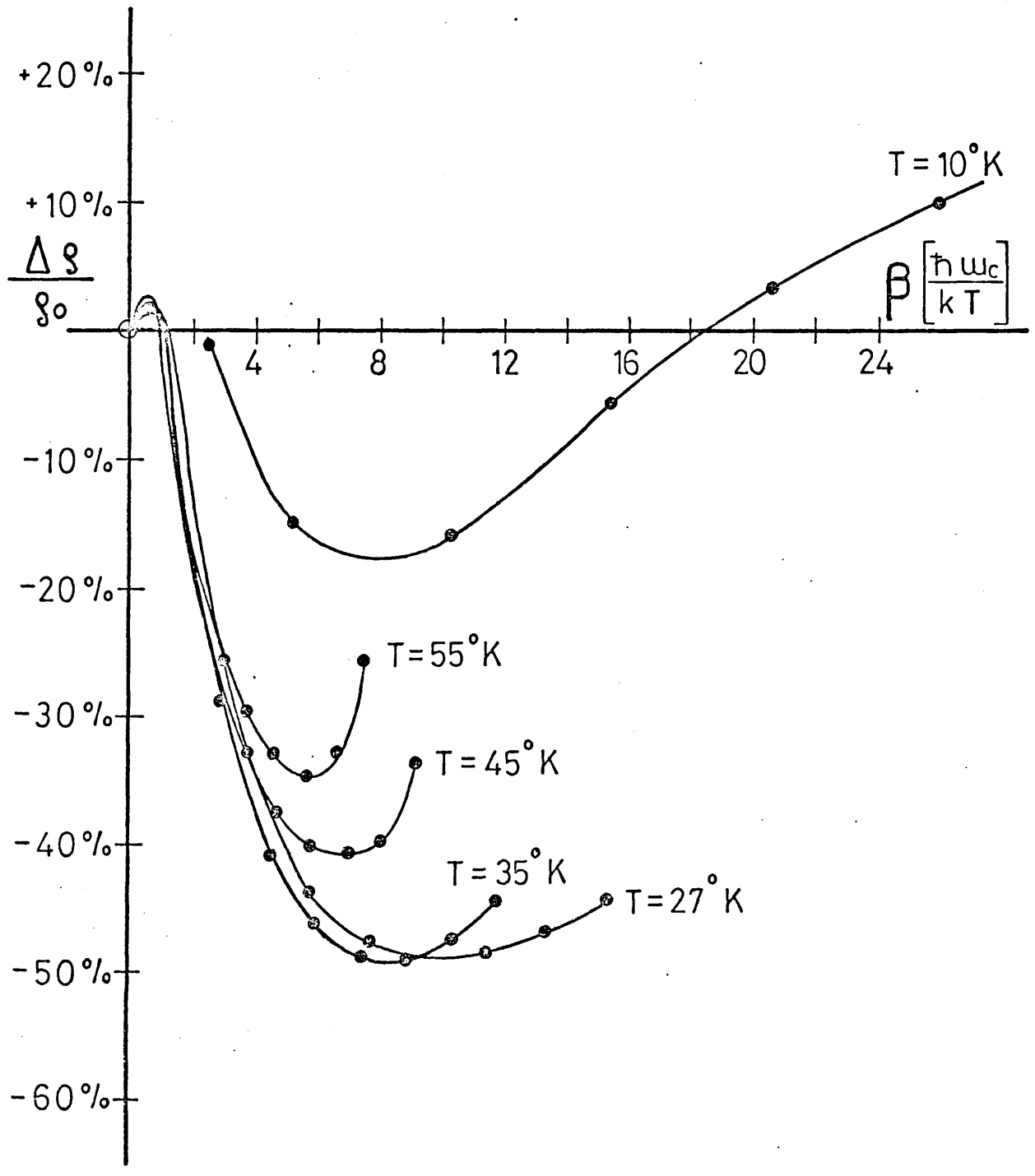

GRAPHS (1).

No.(2) 5.6×10^{14}

Experimental Data.

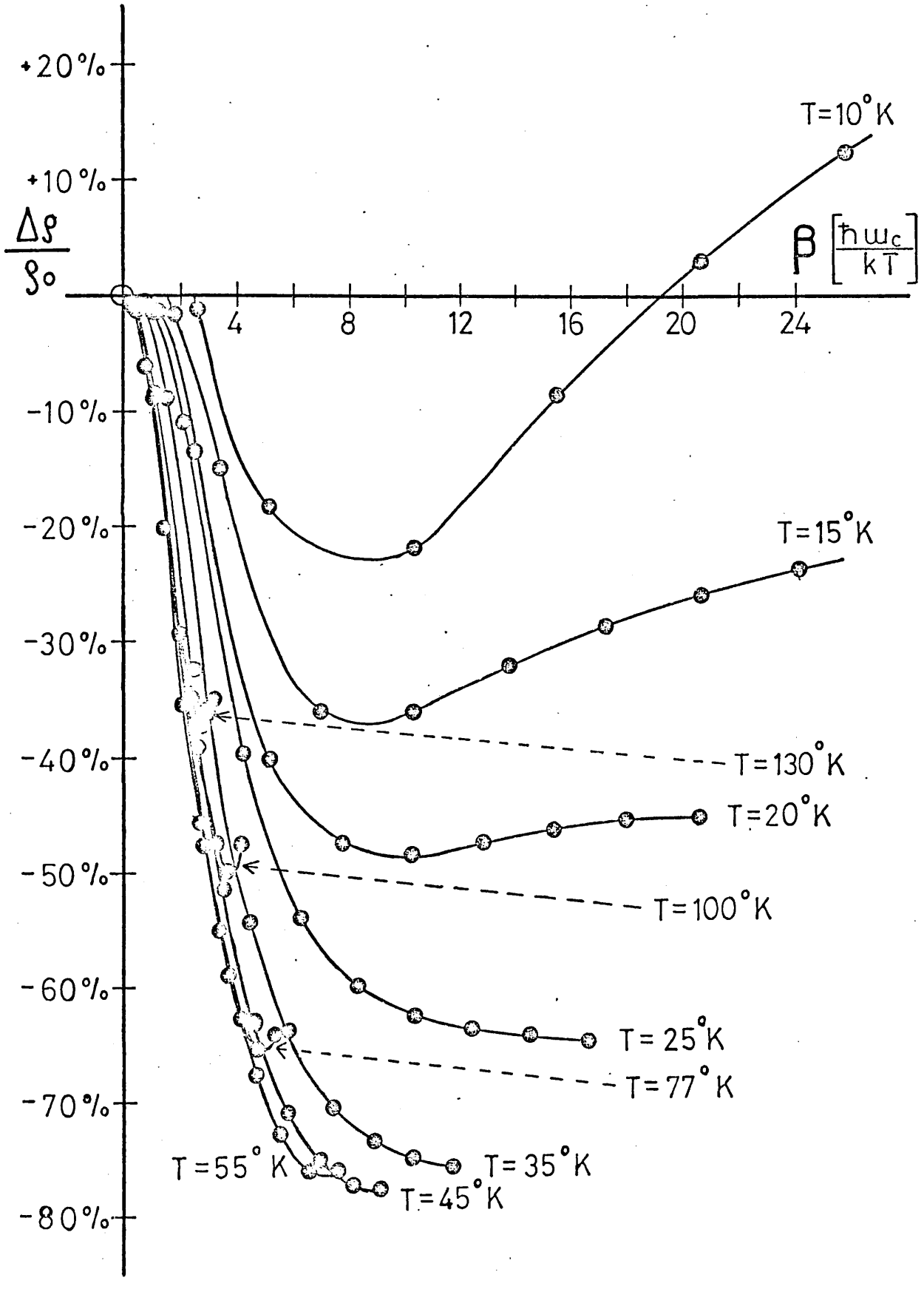

GRAPHS (1).

No.(3) 8.0×10^{14}

Experimental Data.

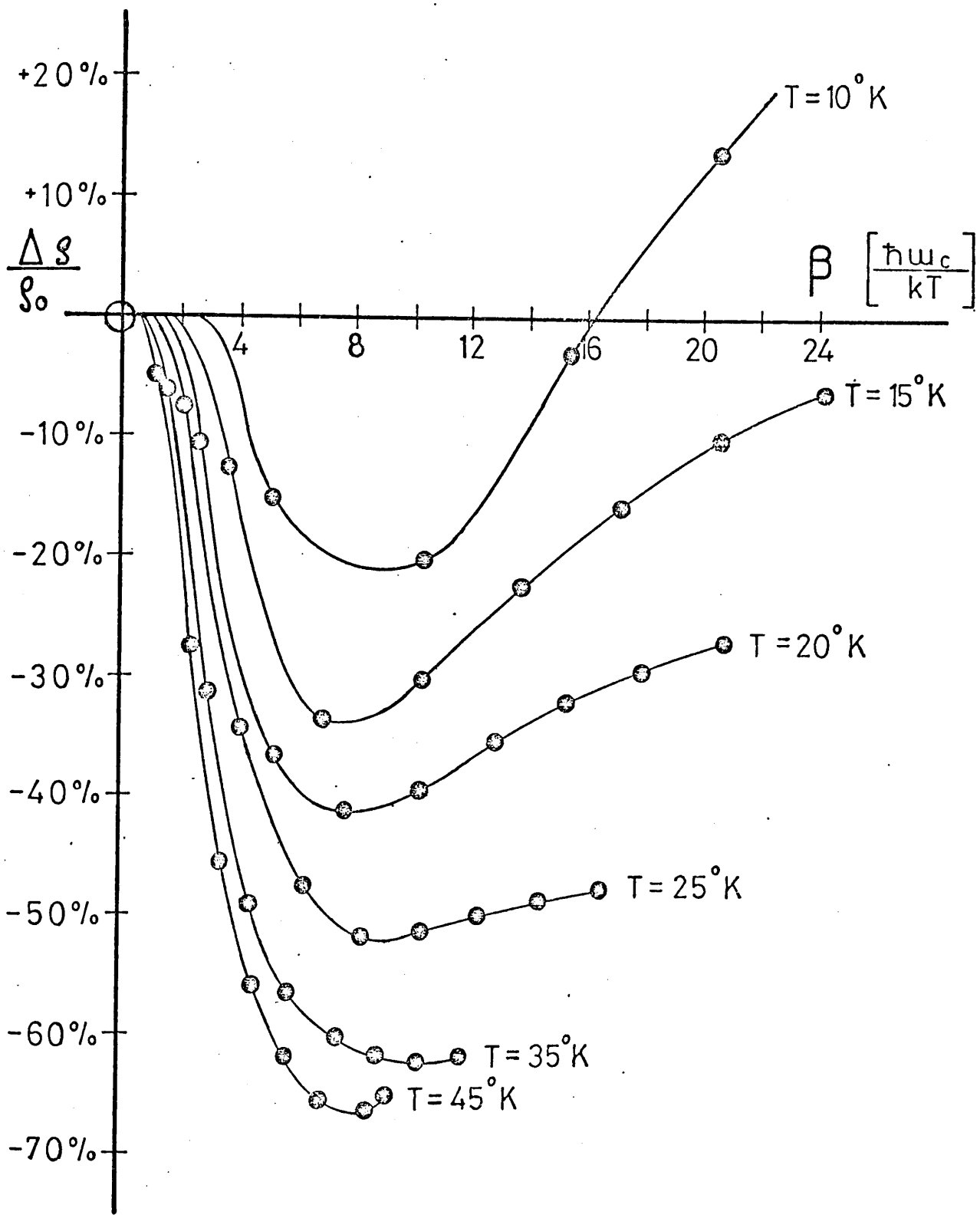

GRAPHS (1).

No.(4) 2.23×10^{15}

Experimental Data.

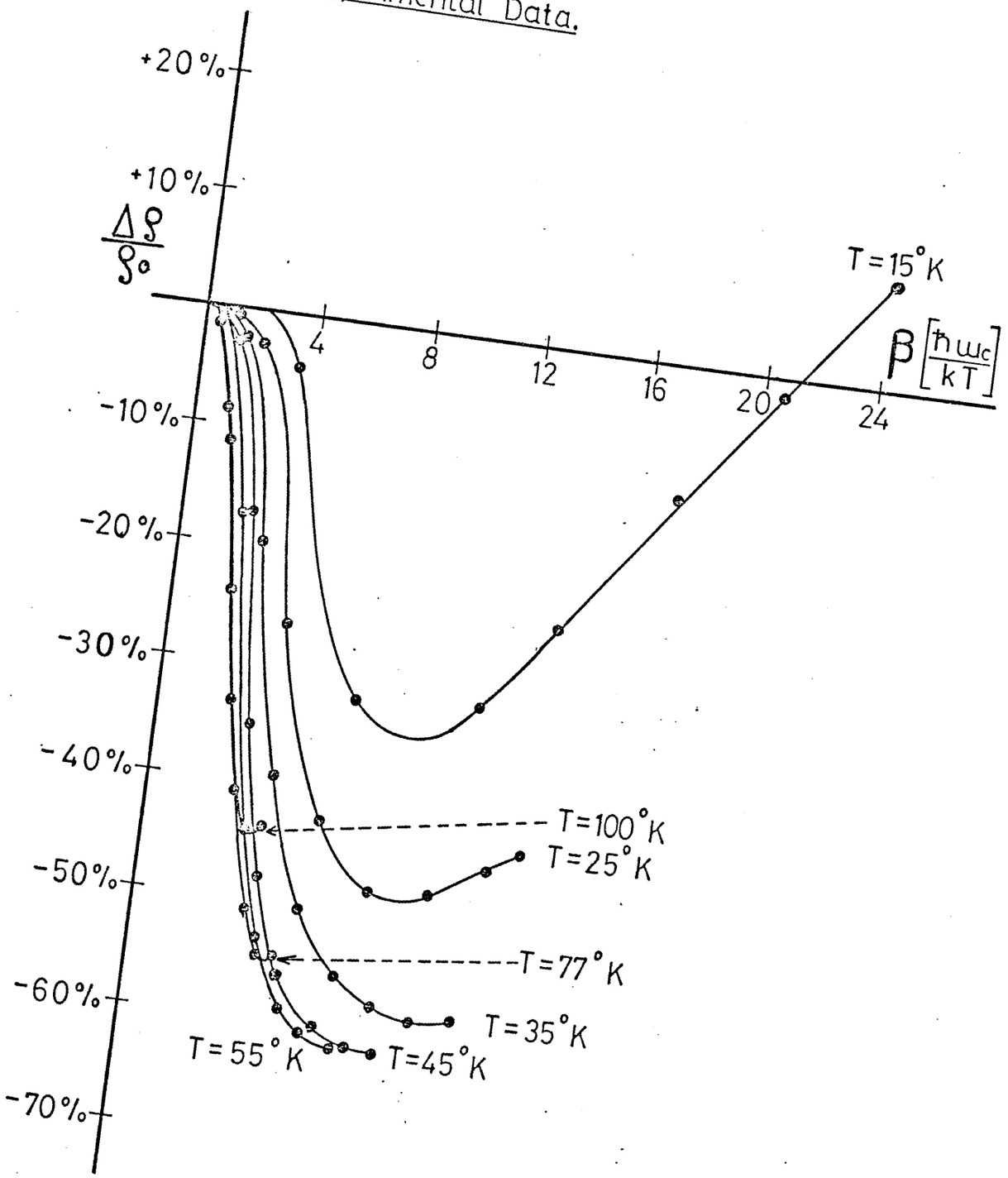

GRAPHS (1).

No.(5) 1.1×10^{14}

Magnetophonon Resonance.
at High Temperatures.

(Expanded section of No.(1))

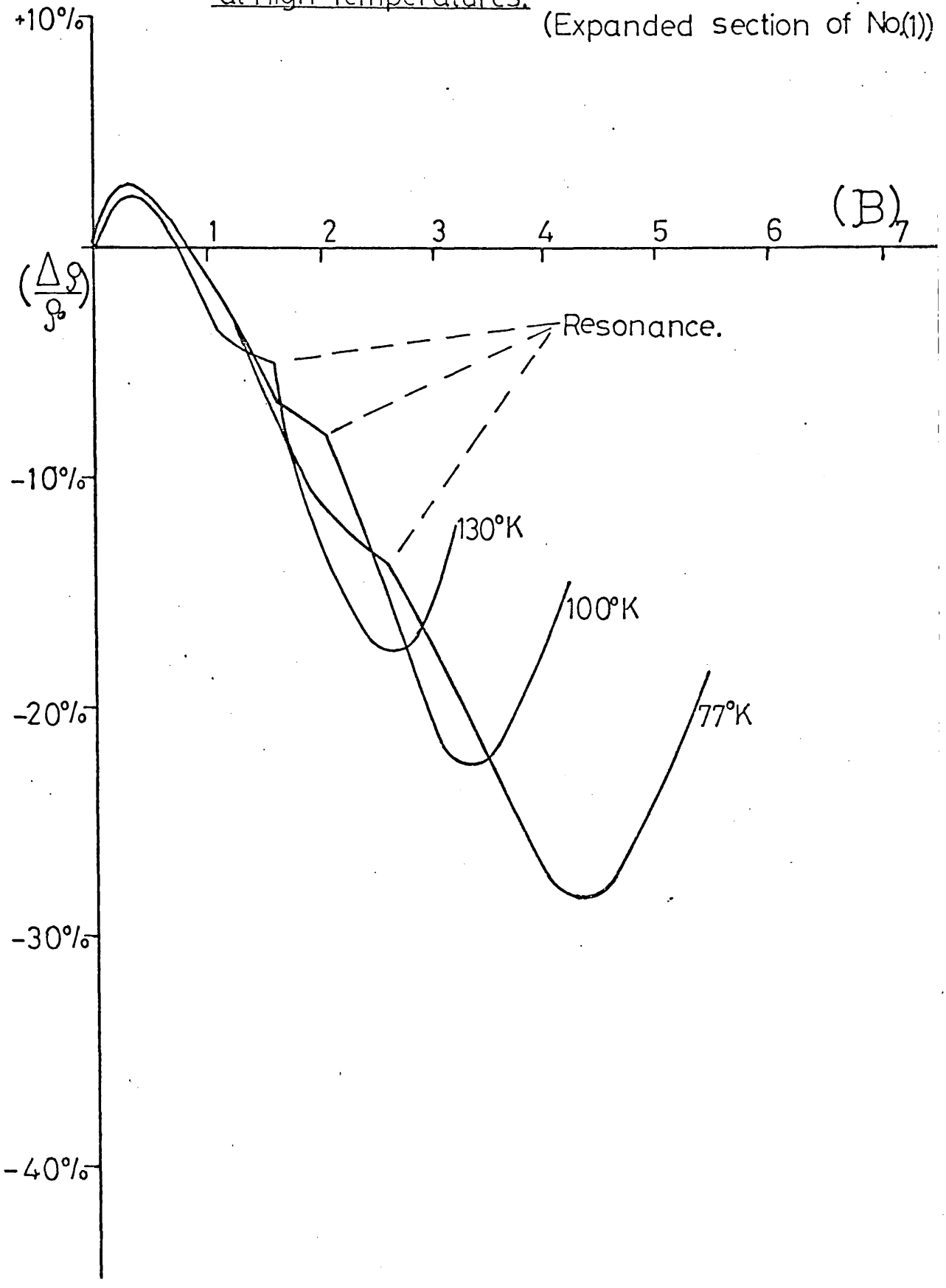

GRAPHS (1)

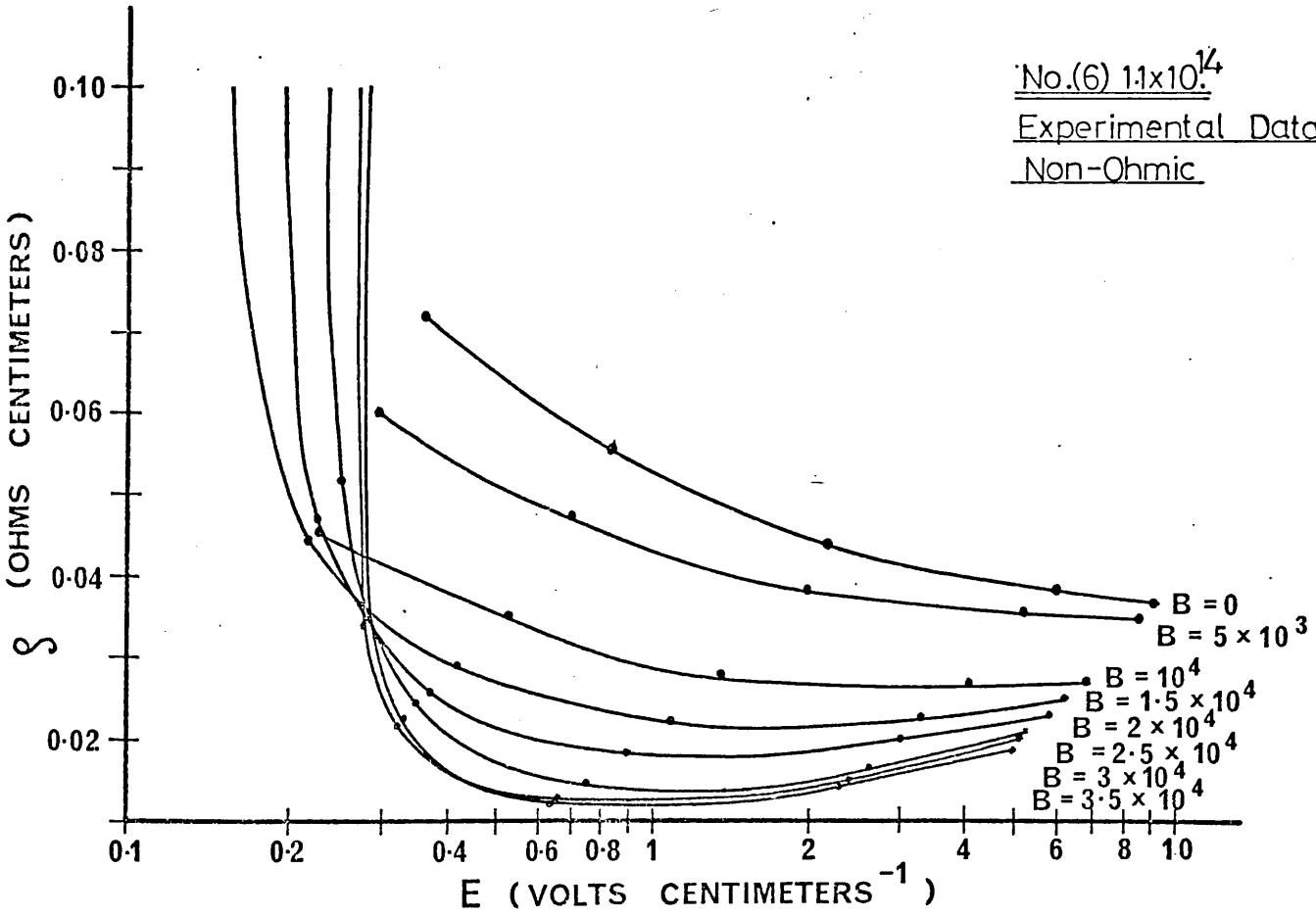
No.(6) 1.1x10^14
Experimental Data.
Non-Ohmic
0·10
0·08
0·06
0·04
0·02
ρ (OHMS CENTIMETERS)
B = 0
B = 5 x 10^3
B = 10^4
B = 1·5 x 10^4
B = 2 x 10^4
B = 2·5 x 10^4
B = 3 x 10^4
B = 3·5 x 10^4
0·1
0·2
0·4
0·6
0·8
1
2
4
6
8
10
E (VOLTS CENTIMETERS^-1)

GRAPHS (1)

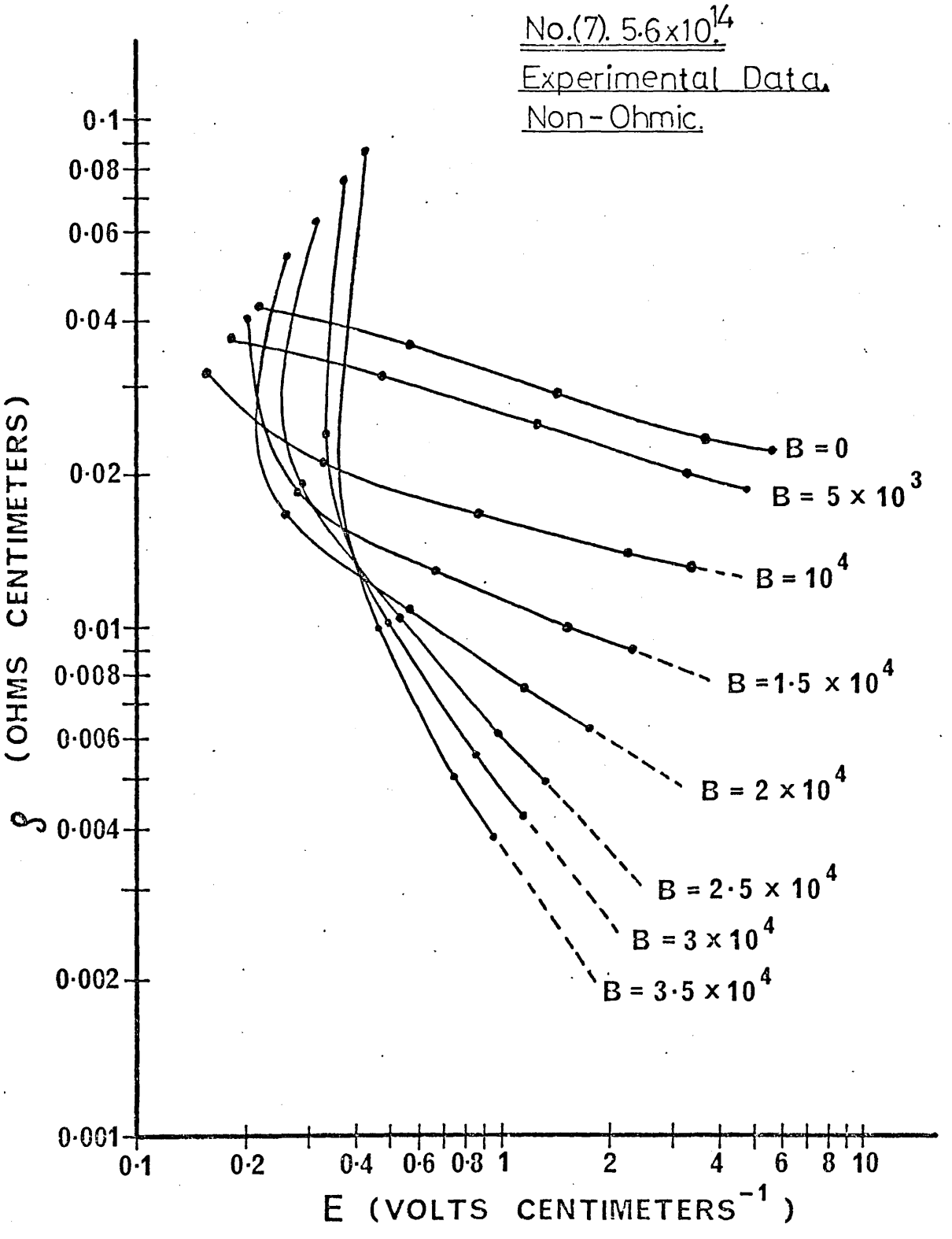
No.(7). 5·6x10^14
Experimental Data.
Non-Ohmic.
0·1
0·08
0·06
0·04
0·02
0·01
0·008
0·006
0·004
0·002
0·001
ρ (OHMS CENTIMETERS)
B = 0
B = 5 x 10^3
B = 10^4
B = 1·5 x 10^4
B = 2 x 10^4
B = 2·5 x 10^4
B = 3 x 10^4
B = 3·5 x 10^4
0·1
0·2
0·4
0·6
0·8
1
2
4
6
8
10
E (VOLTS CENTIMETERS^-1)

GRAPHS (1).

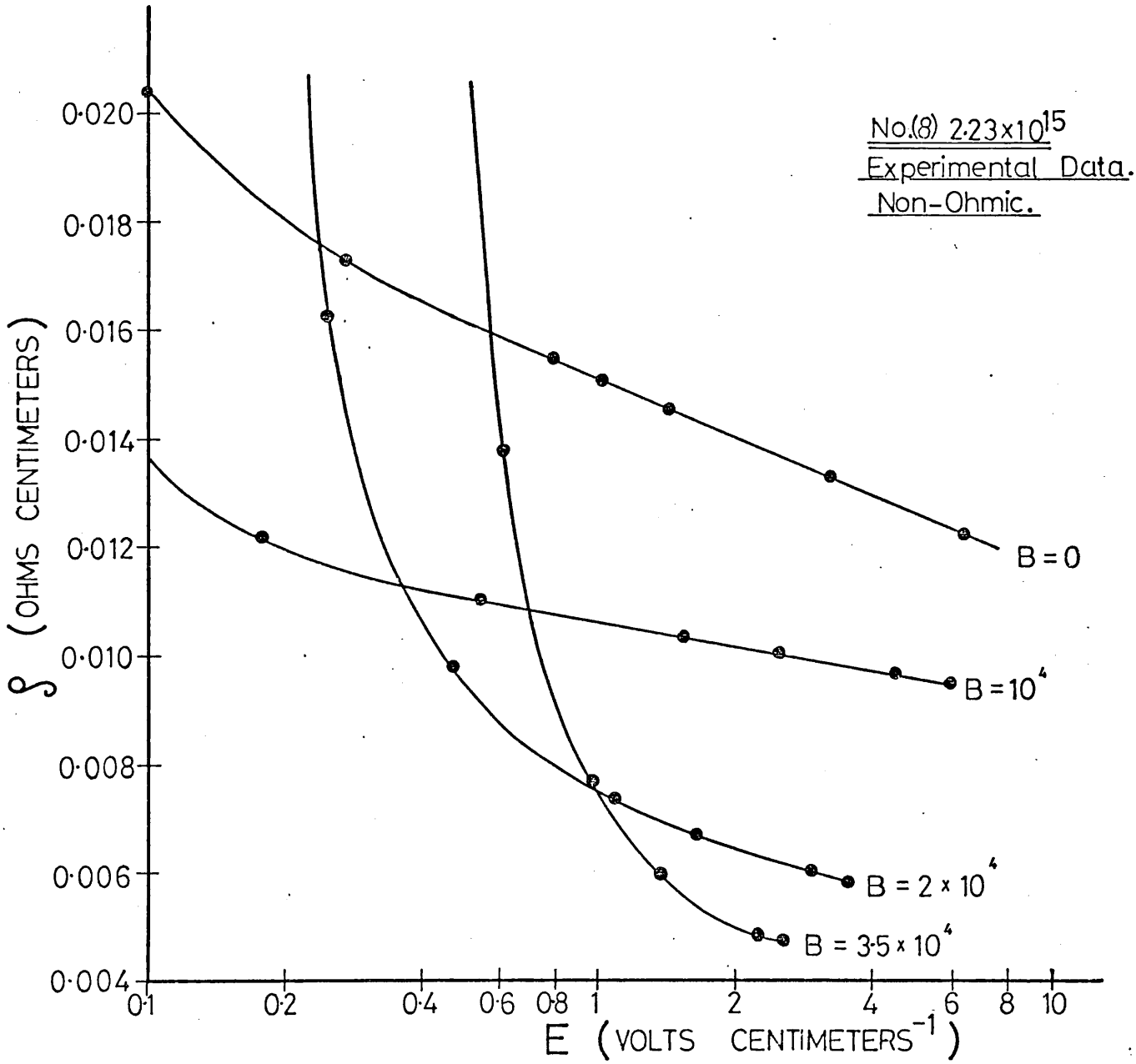
No.(8) 2·23×10^15
Experimental Data.
Non-Ohmic.
ρ (OHMS CENTIMETERS)
0·020
0·018
0·016
0·014
0·012
0·010
0·008
0·006
0·004
B = 0
B = 10^4
B = 2 × 10^4
B = 3·5 × 10^4
0·1
0·2
0·4
0·6
0·8
1
2
4
6
8
10
E (VOLTS CENTIMETERS^-1)

4.3 Ohmic Analysis.

Following the theory of Argyres and Adams for electron transport in the extreme quantum limit and longitudinal configuration, we have

$$\sigma_H = \frac{-2\,e^2}{m^*} \frac{1}{(2\pi)^2} \left(\frac{2m}{\hbar^2}\right)^{3/2} \hbar\omega_c \int_0^{\hbar\omega_c} \varepsilon_z^{\frac{1}{2}}\, \tau_H(\varepsilon_z) \frac{df_o}{d\varepsilon_z}\, d\varepsilon_z \qquad (1)$$

and without a magnetic field, the standard expression

$$\sigma_o = \frac{-2\,e^2}{3m^*} \frac{2}{(2\pi)^2} \left(\frac{2m^*}{\hbar^2}\right)^{3/2} \int_0^{\infty} \varepsilon^{3/2}\, \tau_o(\varepsilon) \frac{df_o}{d\varepsilon}\, d\varepsilon \qquad (2)$$

Where the essential difference between the two equations (besides the different τ expressions) arises from the changed density of states behaviour:-

$$D_o(\varepsilon) = \frac{2}{(2\pi)^2} \left(\frac{2m^*}{\hbar^2}\right)^{3/2} \varepsilon^{\frac{1}{2}} \qquad (3)$$

$$D_H(\varepsilon) = \frac{1}{(2\pi)^2} \left(\frac{2m^*}{\hbar^2}\right)^{3/2} \hbar\,\omega_c\, \varepsilon_z^{-\frac{1}{2}} \qquad (4)$$

(Note the dependence on just the z component in the magnetic field expressions, indicative of the one dimensional character of the extreme quantum limit transport.)

The expression for the zero field relaxation time for scattering from ionized impurities is given by the standard Brooks-Herring relationship,

$$\frac{1}{\tau_o} = \frac{\pi e^4 N_I}{K^2 (2m^*)^{\frac{1}{2}}} \varepsilon^{-3/2} \left(\ell n(1+x) - \frac{x}{(1+x)}\right) \qquad (5)$$

where $x = (2k\,R_s)^2 = \frac{4\varepsilon}{\varepsilon^o_s}$ where $\varepsilon^o_s = \frac{\hbar^2}{2m^*} \frac{1}{R_s^2}$

K is the dielectric constant.

k is the electron wave vector.

R_s is the impurity screening length.

N_I is the ionized impurity concentration.

In a high magnetic field the free electron wavefunctions are given by:-

$$\psi(N, k_y, k_z) = Q_N (x + \lambda^2 k_y) e^{i k_y y} e^{i k_z z} L_y^{-\frac{1}{2}} L_z^{-\frac{1}{2}} \qquad (6)$$

N, k_y and k_z are the three quantum numbers of the electrons.

λ is the magnetic length $\left(\frac{c\hbar}{eH}\right)^{\frac{1}{2}}$ i.e. measure of orbit radius.

L_y and L_z are just the normalization parameters associated with the y and z directions.

$Q_N (x + \lambda^2 k_y)$ is the wavefunction of a harmonic oscillator of frequency ω_c in its Nth excited state

The potential of the ionized impurities is given by

$$v(r) = \pm\left(\frac{e^2}{K}\right)\left(\frac{e^{(-r/R_s)}}{r}\right) \qquad (7)$$

where R_s is the screening length (derived in the appendix).

The scattering rate from ionized impurities in the extreme quantum limit is calculated from the matrix element of the interaction, i.e.

$$W_{Scatt} = \frac{2\pi}{\hbar} \sum_R |\langle 0, k_y', k_z'| v(\underline{r} - \underline{R}) |0, k_y, k_z\rangle|^2 \delta|\varepsilon_z' - \varepsilon_z) \qquad (8)$$

where equations (6) and (7) are used as the wavefunctions and perturbing (scattering) potential respectively. N = 0 in both the initial and final wavefunctions, so that the electron remains in the ground state Landau energy. The summation is made over all the $\underline{R}$ sites of the impurity potentials.

From the scattering rate expression we may obtain, after the various summations and substitutions have been made,

$$\frac{1}{\tau_H} = \frac{\pi e^4 N_I \varepsilon_z^{-3/2}}{K^2 (2m^*)^{\frac{1}{2}}} \frac{I(\gamma)}{1 + \varepsilon_S/4\varepsilon_z} \qquad (9)$$

where $I(\gamma) = 1 + \gamma\, e^{\gamma}\, Ei(-\gamma)$ and $\gamma = \frac{\epsilon_s}{\hbar\,\omega_c}\left(1 + \frac{4\,\epsilon_z}{\epsilon_s}\right)$.

$\epsilon_s = \frac{\hbar^2}{2m^*}\,\frac{1}{R^2_{HS}}$ R_{HS} being the screening radius with magnetic field (derived in appendix).

Argyres simplifies equation (9) be using the approximation

$$I(\gamma) \sim (1/1 + \gamma)$$

and substituting (5) and (9) into (1) and (2) obtains

$$\frac{\sigma_H}{\sigma_o} = \left(\ln(1 + \bar{x}) - \frac{\bar{x}}{1+\bar{x}}\right)\left(\frac{1}{2} + \frac{3}{4}\frac{1}{\bar{x}} + \frac{3k_BT}{\hbar\,\omega_c}\left(2 + \frac{4}{\bar{x}} + \frac{3}{(\bar{x})2}\right)\right) \qquad (10)$$

for the non-degenerate limit.

The bracket involving the ln term is removed from the integral of σ_o and a value of x chosen such that $\bar{x} = 2\bar{k}R_s$ is the value that maximizes the remaining part of the integral. This is the standard procedure for the evaluation of σ_o, as derived by Brooks and Herring.

Equation (10) is valid only for non-degenerate statistics. We have generalized these expressions for arbitrary statistics, which is a more useful result for indium antimonide at low temperatures.

The general statistics equation is given by,

$$\frac{\sigma_H}{\sigma_o} = \frac{1}{f_2(\partial_o^*)}\,\frac{\hbar\omega_c}{k_BT}\left[\ln(1 + \bar{x}) - \frac{\bar{x}}{1 + \bar{x}}\right]\left[f_1(\partial_H^*) + \frac{3}{2A}\,f_o(\partial_H^*) + \right.$$

$$\left.\frac{6k_BT}{\hbar\omega_c}\left(f_2(\partial_H^*) + \frac{4}{A}\,f_1(\partial_H^*) + \frac{3}{A^2}\,f_o(\partial_H^*)\right)\right] \qquad (11)$$

where, once again $\bar{x}$ is chosen from the value at the maximum of the σ_o integral when the bracket with the ln term is removed. This value is given generally by the expression

$$\bar{x} = \frac{\bar{\partial}\,(k_B T)^{\frac{1}{2}}\ K\ 2\pi\hbar}{e^2\ (2m^*)^{\frac{1}{2}}\ f_{\frac{1}{2}}\ (\partial_o^*)}$$

and $\bar{\partial}$ is the solution of the equation.

$(\bar{\partial} - 3)\ \exp\ (\bar{\partial} - \partial_o^*) = \bar{\partial} + 3$. See Mansfield (1956)

For the non-degenerate case, as used by Argyres in equation (10)

$$\bar{\partial} = 3$$

and $$\bar{x} = \frac{6}{\pi}\left(\frac{m(k_B T)^2}{n_o\ \hbar^2\ e^2}\right)$$

In equation (11) $A = \dfrac{(kT)^{3/2}\ K\ 24\pi}{e^2\ \hbar\omega_c\ f_{-\frac{3}{2}}\ (\partial_H^*)} \left(\dfrac{\hbar^2}{2m^*}\right)^{\frac{1}{2}}$

and $f_n(\partial_o^*)$ and $f_n(\partial_H^*)$ are Fermi Integrals with magnetic field ∂_H^* and without magnetic field ∂_o^*. ∂^* is the reduced Fermi level.

The importance of the finite collision time with the associated uncertainty in electron energy has been discussed in section 3.2. Following the Dubinskaya treatment and using separate relaxation times for the 'Argyres' backward scattering and uncertainty forward scattering, we combine them in the usual way, to give

$$\frac{1}{\tau_{Transport}} = \frac{1}{\tau_B} + \frac{1}{\tau_f}$$

τ_B is given by equation (9).

τ_f is calculated by Dubinskaya and is given by,

$$\frac{1}{\tau_f} = \frac{e^4 N_I}{K^2\ (2m^*)^{\frac{1}{2}}}\ \varepsilon_z^{-3/2} \left[1 + Z_1\ e^{Z_1}\ Ei\ (-Z_1)\right] \frac{R_{HS}}{2\ell_z}\ (2\ k_z R_{HS})\ \ell n\left(\frac{2\ell_z}{R_{HS}}\right)^2 \qquad (12)$$

where $Z_1 = \dfrac{\varepsilon_s}{\hbar\ \omega_c}$

and ℓ_z is the mean free path in the z direction (for all collision processes and not just momentum relaxation interations).

This expression τ_f is derived from a similar expression to equation (8) for the backward scattering case, but the delta function $\delta(\varepsilon_z' - \varepsilon_z)$ is replaced by the Lorentzian

$$\frac{1}{\pi} \quad \frac{\Gamma/2}{(\varepsilon_z - \varepsilon_z')^2 + (\Gamma/2)^2}$$

where Γ is the collision broadening factor $\frac{\hbar}{\tau_c}$.

Using equations (9) and (12) we may write the full transport relaxation time as,

$$\frac{1}{\tau \text{Trans.}} = \frac{\pi e^4 N_I}{K^2 (2m^*)^{\frac{1}{2}}} \left[\frac{\left(1 - \frac{\varepsilon_s}{\hbar \omega_c}\left[1 + \frac{4 k_B T}{\varepsilon_s} y\right]\right) \exp\left(\frac{\varepsilon_s}{\hbar \omega_c}\left(1 + \frac{4 k_B T}{\varepsilon_s} y\right)\right)}{(1 + \varepsilon_s/(4 k_B T y))} \right.$$

$$\times \int_{\left(\frac{\varepsilon_s}{\hbar \omega_c}\left[1 + \frac{4k_B T}{\varepsilon_s} y\right]\right)}^{\infty} \frac{e^{-s}}{s} \, dS + \frac{\left(1 - \frac{\varepsilon_s}{\hbar \omega_c} \exp\left(\frac{\varepsilon_s}{\hbar \omega_c}\right) \int_{(\varepsilon_s/h\omega_c)}^{\infty} \frac{e^{-s}}{s} \, dS\right)}{\Pi} \times \frac{R_{HS}^2}{\ell_z}$$

$$\left. \times \ell_n \left(\frac{2\ell_z}{R_{HS}}\right)^2 \times \left(\frac{2m^*}{h}\right)^{\frac{1}{2}} (k_B T)^{\frac{1}{2}} y^{\frac{1}{2}} \right] y^{-3/2} (k_B T)^{-3/2} \qquad (13)$$

where $y = \frac{\varepsilon_z}{k_B T}$.

Equation (13) is written out in full, to show the detailed dependence on reduced energy, y.

[This expression is given incorrectly in the Dubinskaya reference.]

We can re-write this more conveniently as

$$\frac{1}{\tau_{\text{Trans.}}} = P \left[\frac{(1 - (Fy + C) \exp (Fy + C) \int_{(Fy+C)}^{\infty} \frac{e^{-s}}{s} \, dS)}{(1 + E/y)} + A y^{\frac{1}{2}} \right] y^{-3/2} \qquad (14)$$

Where P, F, C, A and E are all energy independent factors which however, vary with magnetic field and temperature.

The conductivity for arbitrary degeneracy is given by equation (1).

$$\sigma_H = M \int_o^B y^{\frac{1}{2}} \tau_{Trans} \frac{\partial f_o}{\partial y} dy \qquad (15)$$

Where $B = \left(\frac{\hbar \omega_c}{k_B T}\right)$

and $M = \frac{-2e^2}{m^*} \frac{1}{(2\pi)^2} \left(\frac{2m^*}{\hbar^2}\right)^{3/2} (k_B T)^{\frac{1}{2}} \hbar \omega_c$.

Substituting (14) into (15) we obtain the integral for the conductivity

$$\sigma_H \propto \int_o^B \frac{y^2 \exp(y - \partial_H^*)}{[1 + \exp(y - \partial_H^*)]^2} \left[\frac{(1 - (Fy + C) \exp(Fy + C)}{(1 + E/y)} \int_{Fy+C}^{\infty} \frac{e^{-s}}{s} ds) + Ay^{\frac{1}{2}} \right]^{-1} dy$$

There is no analytic solution to this integral and usually approximations are made in its evaluation. e.g.

(1) Forward scattering ignored, so that A = 0.

(2) The Argyres approximation, mentioned previously i.e. $(1 - (F.y + C) \exp(F.y + C) \int_{(Fy+C)}^{\infty} \frac{e^{-s}}{s} dS \sim \frac{1}{(1 + F.y+C)}$.

(3) Calculated for degenerate or non-degenerate limits.

(4) The whole of the [ ] term taken outside the integral and a value of y used which is the value at the maximum of the remainder of the integrand. Dubinskaya uses this approximation in the non-degenerate limit and uses a y value of 2.

These approximations can produce large errors, besides the fact that the evaluation is not valid for intermediate degeneracy. Therefore, the integral has been evaluated by numerical methods without any approximation.

The integral involves another sub-integral (the exponential integral $Ei \equiv \int_{Fy+C}^{\infty} \frac{e^{-s}}{s}\, dS$) which has a function of y as its lower limit. The programme must calculate this sub-integral for each step of the total integral. It is also necessary to limit the exponential integral upper limit to some finite value, as well as to remove the divergence in the main integral for the y = 0 lower limit. An upper limit of 100 is used in the exponential integral and the main integral is given a lower limit of 0.1. Over a wide range the integration was found to be insensitive to the choice of values used in these limits.

B, A, C, E and F along with the reduced fermi energy in a magnetic field ∂_H^*, formed the data for each conductivity to be evaluated.

The reduced fermi energy ∂_H^* is calculated from the expression

$$N_D - N_A = n = \int_0^{\hbar\omega_c} D_H(\varepsilon)\, f\, (\varepsilon, \varepsilon_F)\, d\varepsilon \qquad (16)$$

which for the extreme quantum limit gives

$$n = \frac{(k_B T)^{\frac{1}{2}}}{(2\pi)^2} \left(\frac{2m^*}{\hbar^2}\right)^{3/2} h\, \omega_c \int_0^B y^{-\frac{1}{2}}\, f_o(\partial_H^*)\, dy$$

$$\text{or} \quad F_{-\frac{1}{2}}(\partial_H^*) = \frac{(2\pi)^2 n}{(k_B T)^{\frac{1}{2}}} \left(\frac{\hbar^2}{2m^*}\right)^{3/2} \frac{1}{\hbar\, \omega_o} \qquad (17)$$

$F - \frac{1}{2}(\partial_H^*)$ being a fermi integral (Tabulated in Fistul (1969)) from which we can find ∂_H^*.

The assumptions made in this expression are discussed in section 4.5.

In Graphs (2) we show the experimental results for the three samples S3, S4, and S5 plotted as resistivity ρ versus magnetic field H. On each graph is also shown the theoretical calculations, both with and without the addition of the forward scattering term. The importance of the forward small angle scattering is immediately apparent.

Dubinskaya also gives a treatment for the case of more than just one Landau level being occupied. The second and higher levels only become important for $B < 5$. In this region of magnetic fields it is necessary to solve sets of coupled algebraic equations, the manipulation and evaluation being rather long processes and necessitating involved computer calculations. Therefore, this region of the results has not been analysed and a dotted line shows the supposed theoretical extrapolation when multiple Landau occupancy becomes important. The zero magnetic field resistivity is calculated theoretically, as discussed at the end of this section.

The important parameter, as far as the forward scattering is concerned, is $(R_{HS}/2\ \ell z)$ where R_{HS} is the screening length derived in the appendix and given by

$$R_{HS}^2 = \left(\frac{\hbar^2}{2m^*}\right)^{3/2} \frac{2\pi K\ (k_B T)^{\frac{1}{2}}}{e^2 \hbar\ \omega_c} \frac{1}{F - 3/2\ (\partial_H^*)}$$

where $F_{-3/2}(\partial_H^*)$ is a fermi integral.

Also, $\ell_z = V_z\ \tau_c$ for the collision free path. A proper treatment of this is obviously difficult since all collision processes must be included in τ_c which is not a simple relaxation time. Even if ionized impurities are the only processes involved the relaxation time for the interaction is not equivalent to the collision time and the relaxation time is what the theory is trying to calculate in the first place. There

GRAPHS.(2).

(1). $5.6 \cdot 10^{14}$ ϱ versus H.
(2). $8.0 \cdot 10^{14}$ " " "
(3). $2.23 \cdot 10^{15}$ " " "

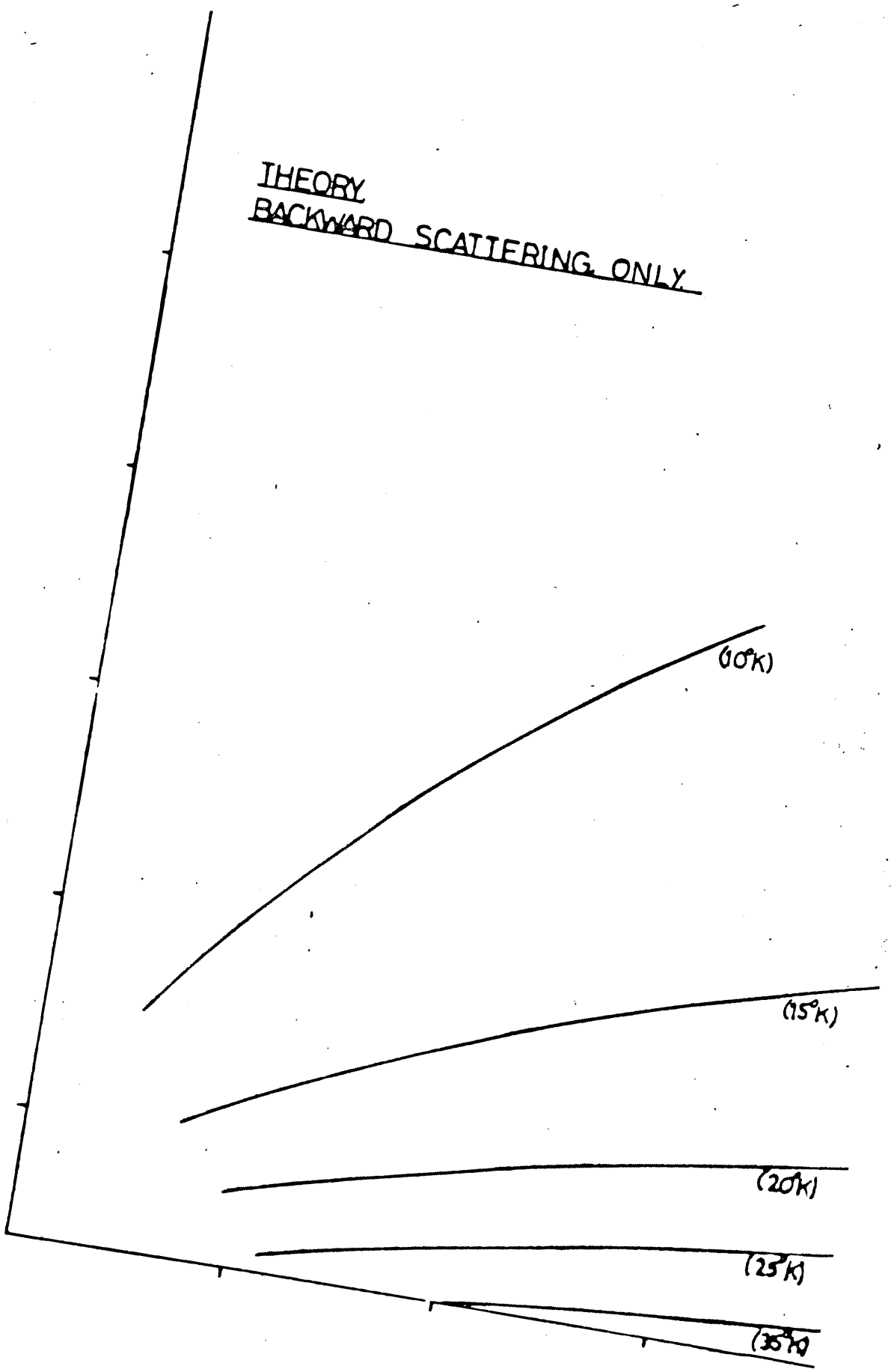
THEORY
BACKWARD SCATTERING ONLY
(10°K)
(15°K)
(20°K)
(25°K)
(35°K)

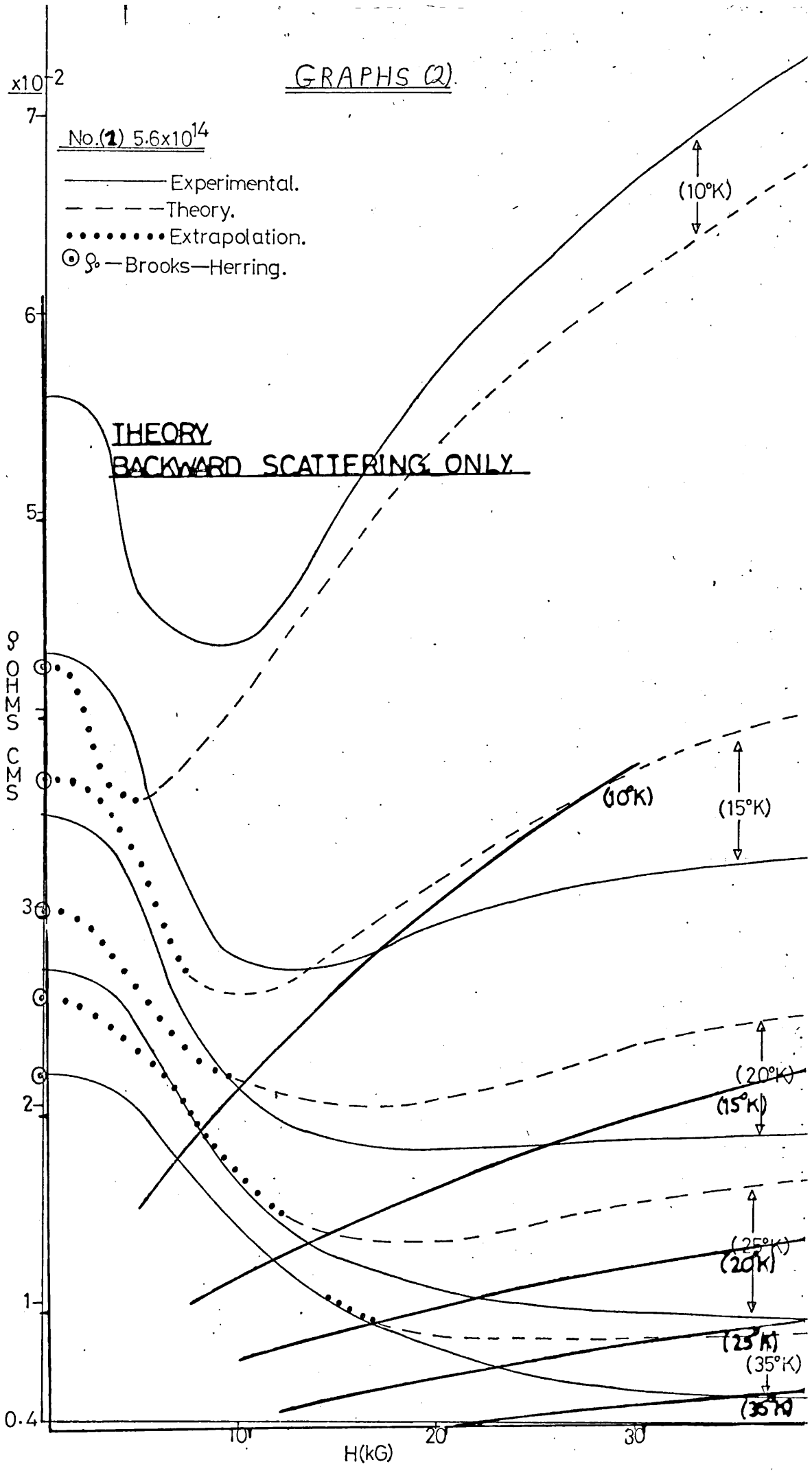
GRAPHS (2).
x10 -2
7
No.(1) 5.6x10^14
Experimental.
Theory.
Extrapolation.
Brooks—Herring.
(10°K)
6
THEORY
BACKWARD SCATTERING ONLY
5
ρ OHMS CMS
(10°K)
(15°K)
3
(20°K)
(15°K)
2
(25°K)
(20°K)
1
(25°K)
(35°K)
(35°K)
0.4
10
20
30
H(kG)

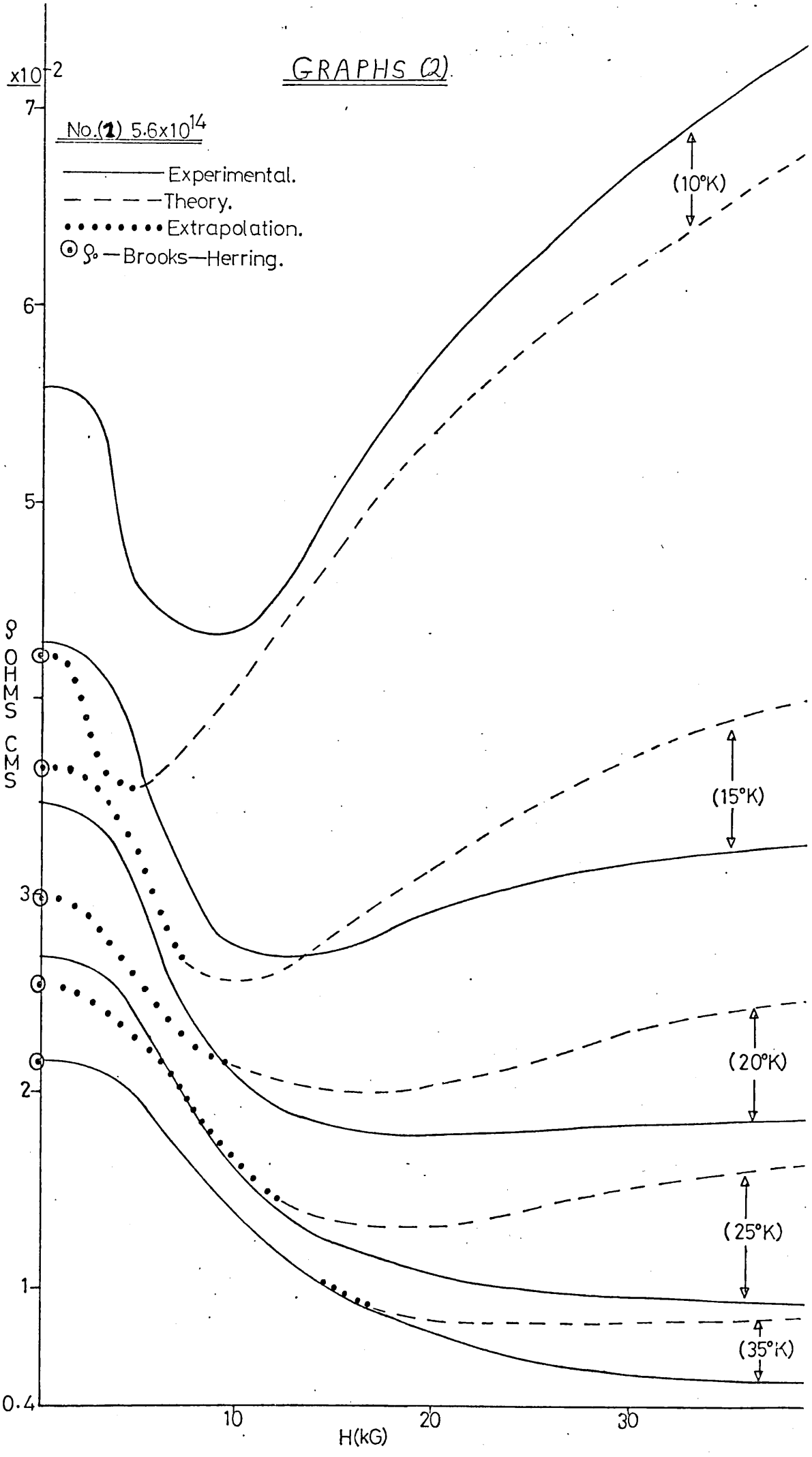
GRAPHS (2)
x10⁻²
No.(1) 5.6x10¹⁴
Experimental.
Theory.
Extrapolation.
Brooks—Herring.
(10°K)
(15°K)
(20°K)
(25°K)
(35°K)
ρ OHMS CMS
H(kG)
7
6
5
3
2
1
0.4
10
20
30

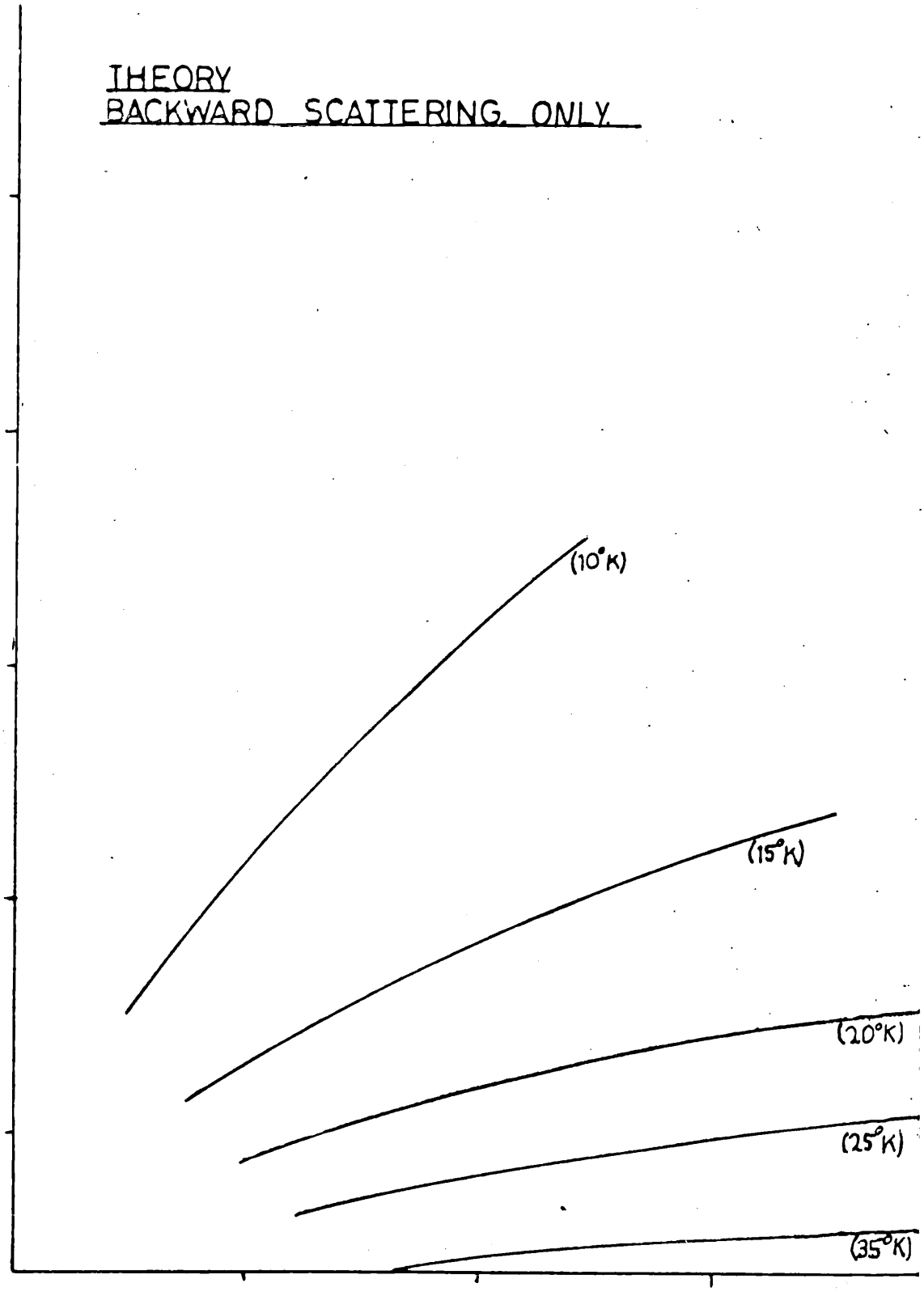
THEORY
BACKWARD SCATTERING ONLY
(10°K)
(15°K)
(20°K)
(25°K)
(35°K)

GRAPHS (2)

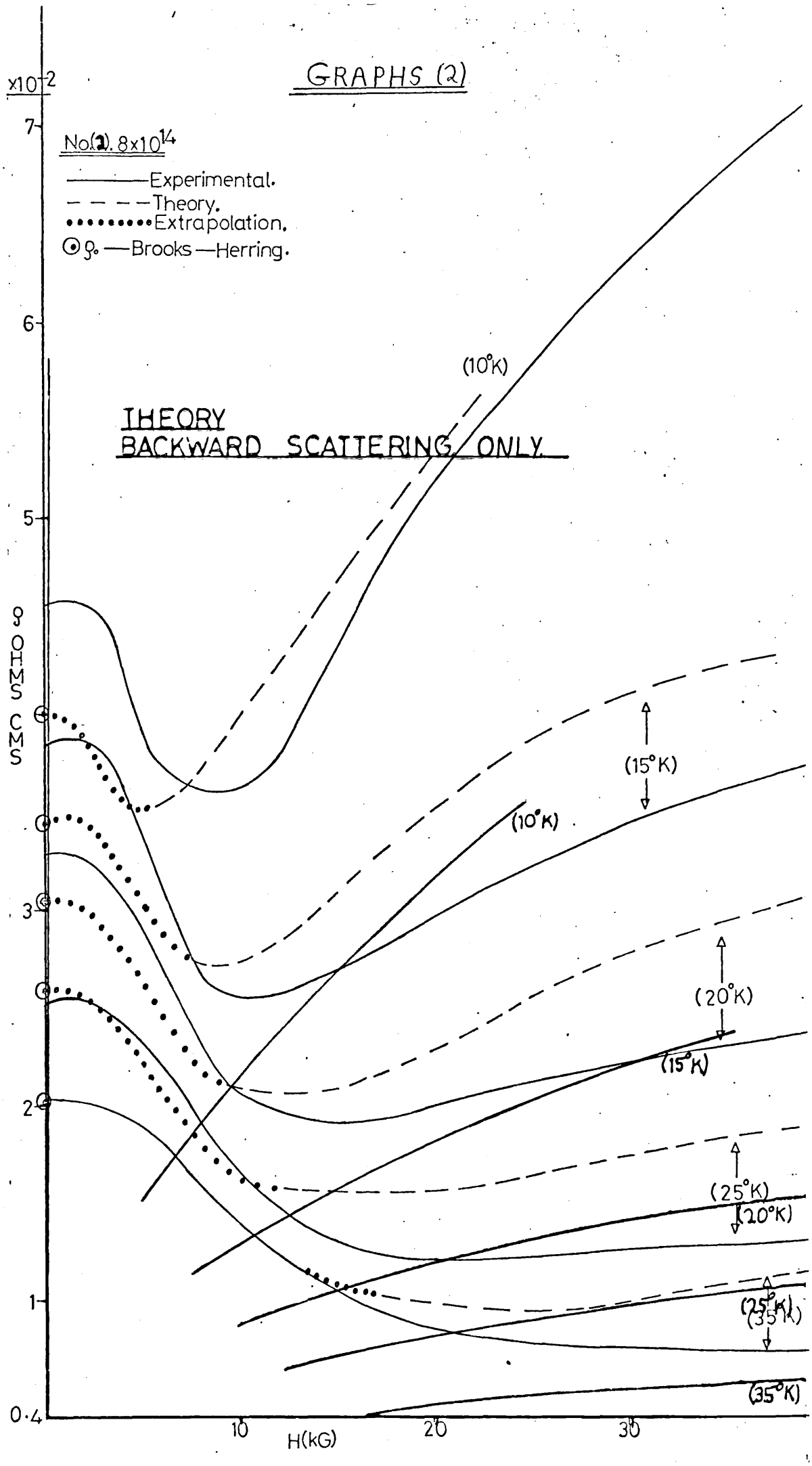
x10⁻²
7
6
5
3
2
1
0·4
No(2). 8x10¹⁴
———Experimental.
– – – –Theory.
•••••••••Extrapolation.
⊙ ρ. —Brooks—Herring.
THEORY
BACKWARD SCATTERING ONLY
ρ OHMS CMS
(10°K)
(15°K)
(10°K)
(20°K)
(15°K)
(25°K)
(20°K)
(25°K)
(35°K)
(35°K)
10
20
30
H(kG)

GRAPHS (2)

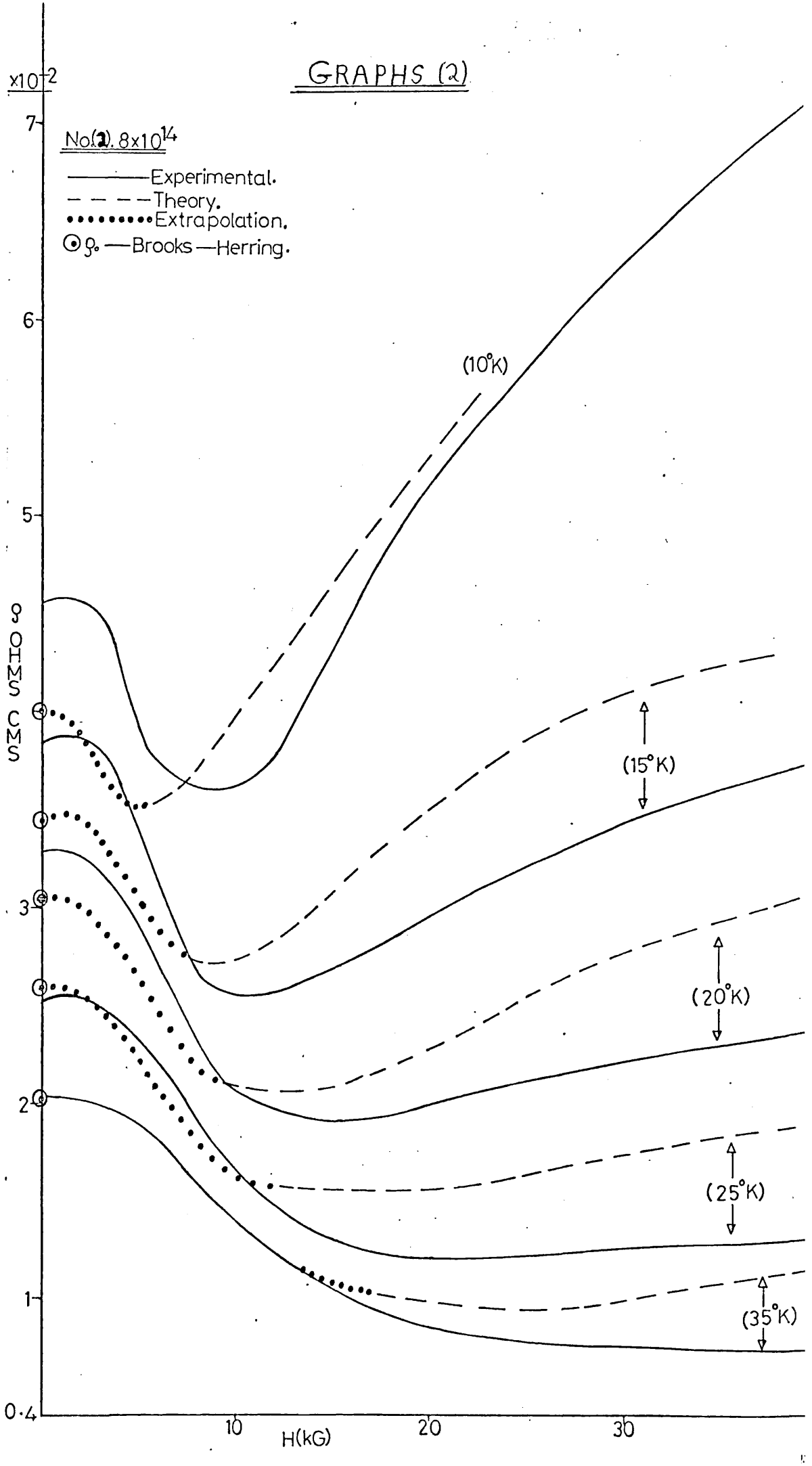
x10⁻²
7
6
5
3
2
1
0·4
ρ OHMS CMS
No(2). 8x10¹⁴
———Experimental.
– – – –Theory.
••••••••Extrapolation.
⊙ ρ₀ —Brooks—Herring.
(10°K)
(15°K)
(20°K)
(25°K)
(35°K)
10
20
30
H(kG)

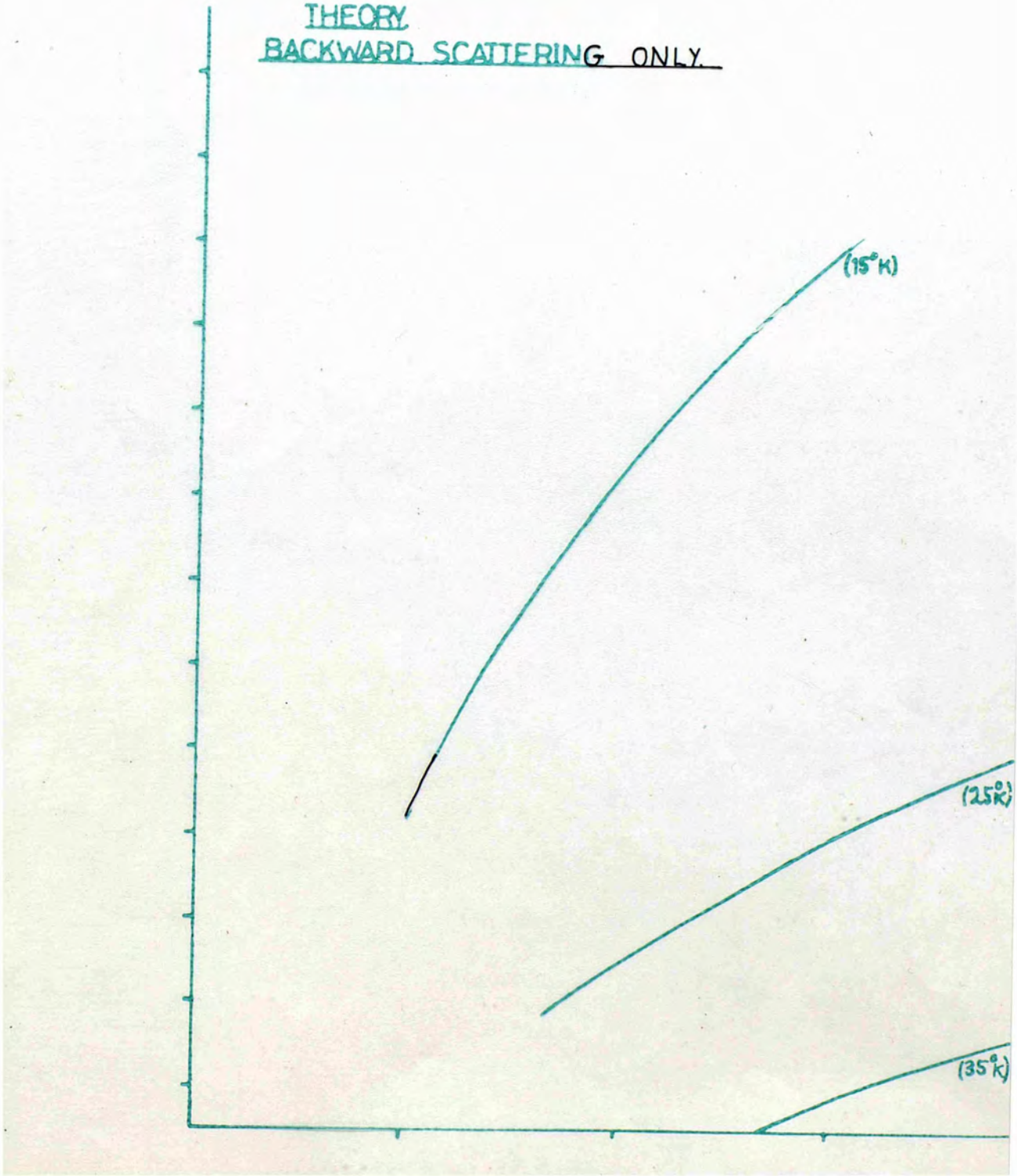
THEORY
BACKWARD SCATTERING ONLY
(15°K)
(25°K)
(35°K)

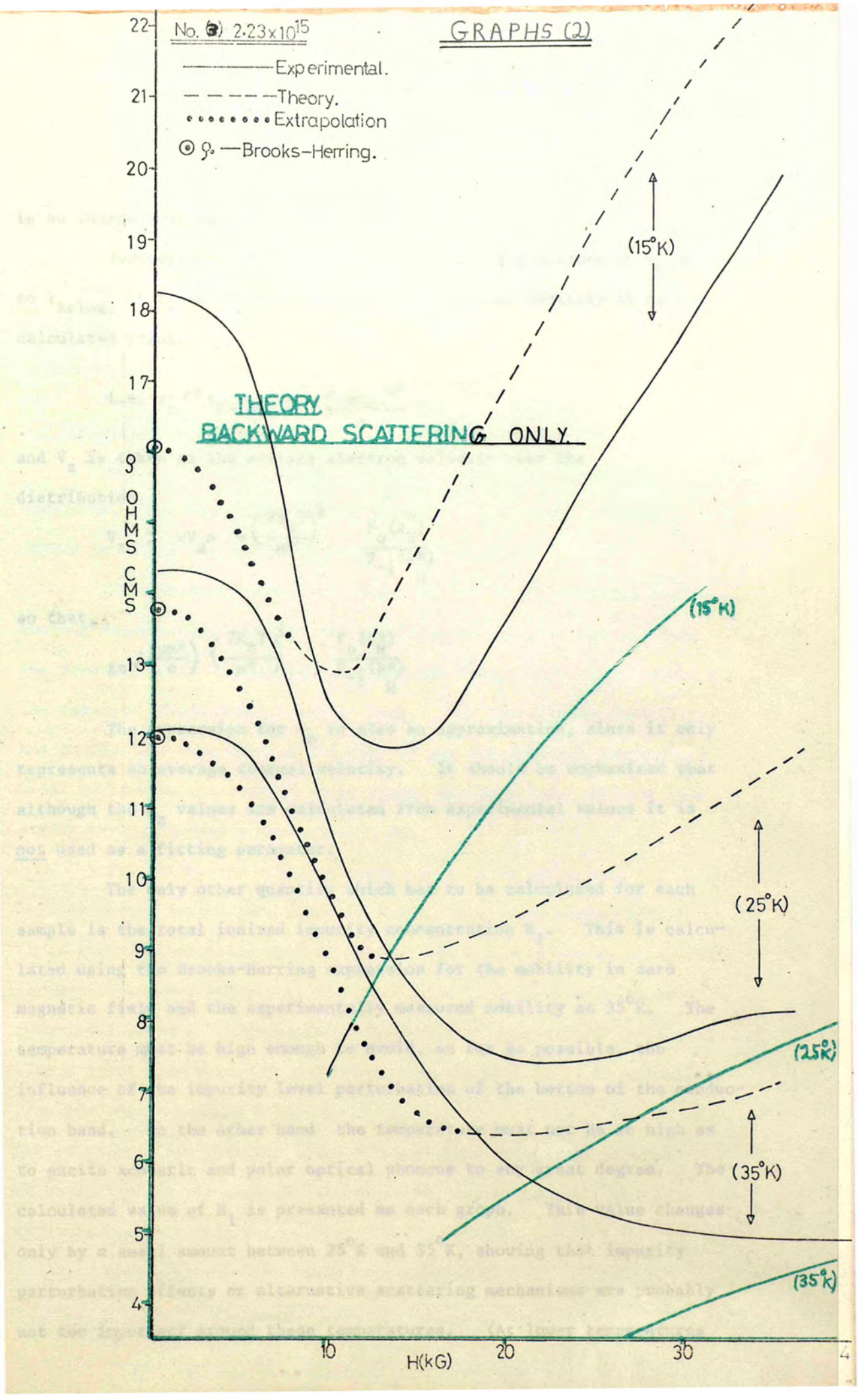
No. 6) 2·23x10^15
GRAPHS (2)
Experimental.
Theory.
Extrapolation
Brooks-Herring.
THEORY
BACKWARD SCATTERING ONLY.
(15°K)
(25°K)
(35°K)
ρ OHMS CMS
H(kG)
22
21
20
19
18
17
13
12
11
10
9
8
7
6
5
4
10
20
30

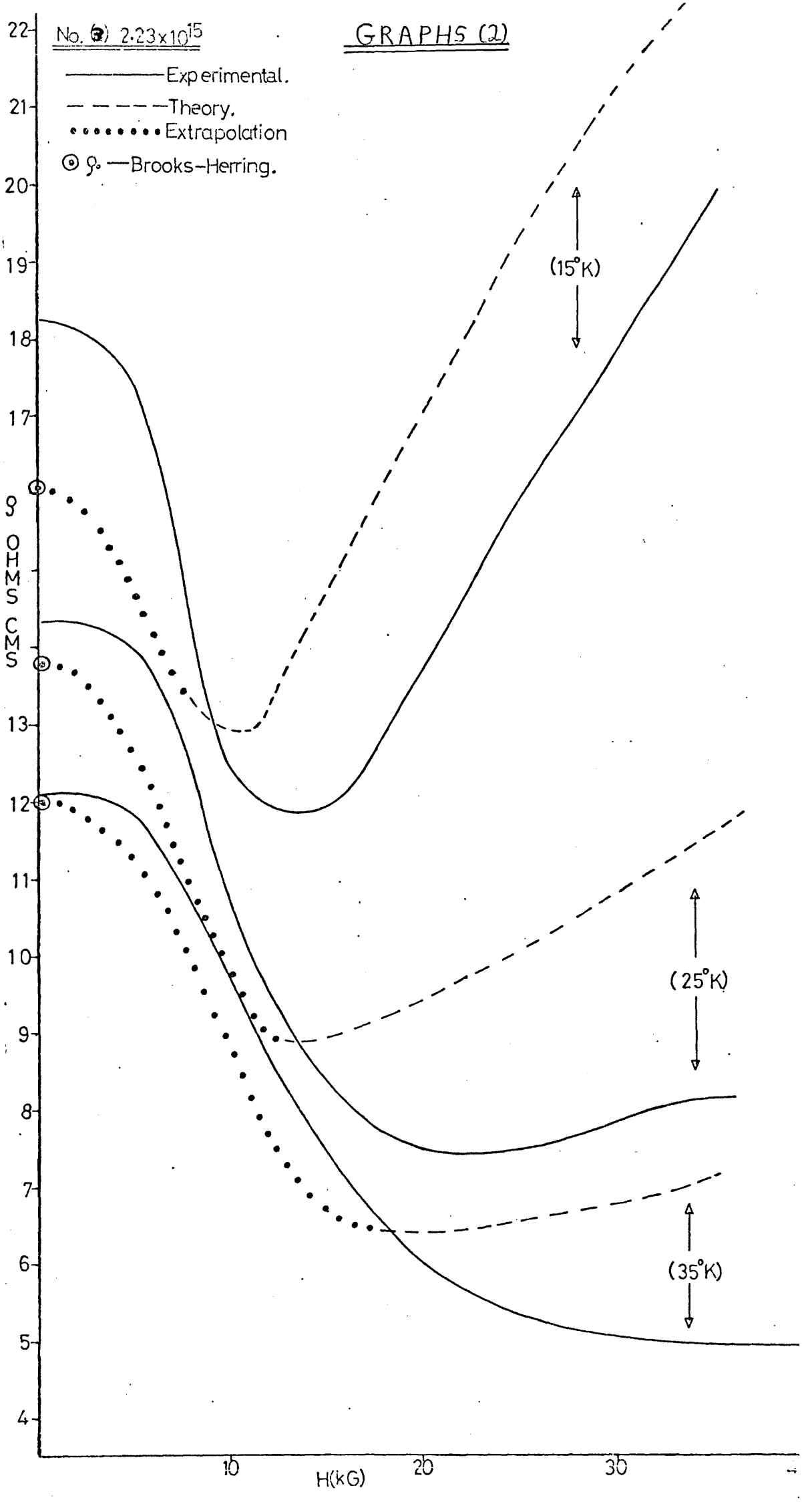
GRAPHS (2)
No. 6) 2·23x10^15
Experimental.
Theory.
Extrapolation
Brooks-Herring.
(15°K)
(25°K)
(35°K)
ρ OHMS CMS
H(kG)
22
21
20
19
18
17
13
12
11
10
9
8
7
6
5
4
10
20
30

is no independent way of arriving at an expression for τ_c.

However, the mobility relaxation time is a measure of τ_c and so $\tau_{Relax.}$ is taken from the experimental value of mobility at each calculated point.

$$\text{i.e. } \tau_c \sim \tau_{Relax} = \frac{\mu_{exp.} m^*}{e}$$

and V_z is taken as the average electron velocity over the distribution.

$$V_z \simeq \langle V_z \rangle = \left(\frac{2k_B T}{m^*}\right)^{\frac{1}{2}} \frac{F_o(\partial_H^*)}{F_{-\frac{1}{2}}(\partial^*)_H}$$

so that,

$$\ell_z \sim \left(\frac{\mu m^*}{e}\right)\left(\frac{2k_B T}{m^*}\right)^{\frac{1}{2}} \frac{F_o(\partial_H^*)}{F_{-\frac{1}{2}}(\partial^*)_H}$$

The expression for v_z is also an approximation, since it only represents an average thermal velocity. It should be emphasized that although the ℓ_z values are calculated from experimental values it is not used as a fitting parameter.

The only other quantity which has to be calculated for each sample is the total ionized impurity concentration N_I. This is calculated using the Brooks-Herring expression for the mobility in zero magnetic field and the experimentally measured mobility at 35°K. The temperature must be high enough to avoid, as far as possible, the influence of the impurity level perturbation of the bottom of the conduction band. On the other hand the temperature must not be so high as to excite acoustic and polar optical phonons to any great degree. The calculated value of N_I is presented on each graph. This value changes only by a small amount between 25°K and 35°K, showing that impurity perturbation effects or alternative scattering mechanisms are probably not too important around these temperatures. (At lower temperatures

the resistivity calculated from the N_I at 35^oK begins to diverge more strongly from the experimental resistivity, underestimating the experimental resistivity to a greater degree as the temperature is lowered. (This can be seen quite clearly on the graphs and is discussed in section 4.5.)

4.4 Non-Ohmic Analysis.

Graph 1 showing the experimental results for non-ohmic behaviour, with resistivity versus electric field, does not lend itself to direct comparison with the ohmic behaviour.

The Kurosawa model calculates the I/V characteristics for various magnetic fields using the distribution function derived from the Brownian motion in energy space and the energy continuity equation. The required computation is rather long. For comparitive simplicity and to test its experimental validity we use the electron temperature model to analyse the results, even though the more exact methods show strong deviation from a Maxwellian form.

Initially, the electron temperature Te is calculated for various points on the zero magnetic field resistivity characteristic. It is assumed that polar optical phonons are the only energy relaxation processes and that the distribution function is Maxwellian with an associated electron temperature. The electron temperature associated with a particular value of resistivity and electric field is calculated from the energy balance equation.

Energy gained from electric field = Energy loss to optical phonons

which applied to the equilibrium situation, where the electrons have attained a stable energy.

Mathematically the above relationship is

$$ne\mu E^2 = neE_o\ No \left(\frac{2k_B\theta}{\pi m^*}\right) \left[\exp(\gamma_o - \gamma) - 1\right] \gamma^{\frac{1}{2}} \exp\left(\frac{\gamma}{2}\right) K_o\left(\frac{\gamma}{2}\right) \qquad (17)$$

where $\gamma_o = \frac{\theta}{To}$ and $\gamma = \frac{\theta}{Te}$, $k\theta$ is the optical phonon energy

To (lattice temperature), Te (electron temperature).

K_o is a modified Bessel function of the second kind.

$$No = \left(\exp(\gamma_o) - 1\right)^{-1}, \qquad Eo = \left(\frac{1}{K_\infty} - \frac{1}{K_o}\right) \frac{m^* e\ k_B\theta}{\hbar^2}$$

K_∞ and K_o being the high frequency and static dielectric constants respectively.

The equation for the rate of energy loss to polar optical phonons was derived by Stratton (1958) and is based upon a Maxwell distribution, applying for To << θ. (In our case To = 4.2°K and θ = 290°K.) The equation should be valid where electron-electron collisions dominate the energy exchange processes. Stratton gives the condition for this as being

$$n_{min.} = 7 \times 10^8\ E_o\ \theta\ K_o^2\ \gamma^{-\frac{1}{2}}\ (-\gamma) \qquad (18)$$

The electron concentration should be greater than this if electron-electron collisions are to predominate. Values for n_{min} versus Te are given below in Table 2.

TABLE 2.

n_{min} cms^{-3}	Te (°K)
7.4×10^{14}	10
6 "	15
5.1 "	20
4.5 "	25
3.6 "	35
3.1 "	45

The conditions become less stringent as Te increases (more e - e collisions take place), but it can be seen that the purest sample having $n = 1.1 \times 10^{14}$ is always below the minimum value, for all temperatures. Table 2 applies to the zero magnetic field resistivity. In the extreme quantum limit no sample should satisfy the conditions for the existence of a Maxwell distribution.

Equation (17) is solved for various points on the ρ_o line, as shown in Graphs (3). From each point we can draw a line with constant$(ne\ E^2)$ (i.e. E^2/ρ) which denotes a constant power input/power loss. If an electron temperature is still valid this line should have a constant T_e, the same as that calculated for the zero magnetic field resistivity.

Besides assuming a Maxwell distribution, we have also only considered polar optical phonons as relaxing electron energy. This is a valid assumption for Te > $18^{o}K$. The lowest input energy rate per electron used in the analysis (the calculated $25^{o}K$ point) is 6.6×10^{-14} watts and comes well into the power range where only polar optical processes need be considered.

It is also assumed that the electron concentration remains constant and that there is no magnetically induced freeze out. (Electron freeze out can be seen to have a very strong effect at lower electric field values.)

The S_1, S_3 and S_5 samples are analysed, two electron temperatures being calculated for each sample. These temperatures are replotted on a resistivity versus magnetic field graph. This is shown on Graphs (4) where ohmic results are also given to enable a direct comparison with non-ohmic results to be made. These results are discussed in the next section.

GRAPHS.(3).

(1). $1.1 \cdot 10^{14}$ ρ versus E , with T_e construction.
(2). $5.6 \cdot 10^{14}$ " " " " " " "
(3). $2.23 \cdot 10^{15}$ " " " " " " "

GRAPHS (3)

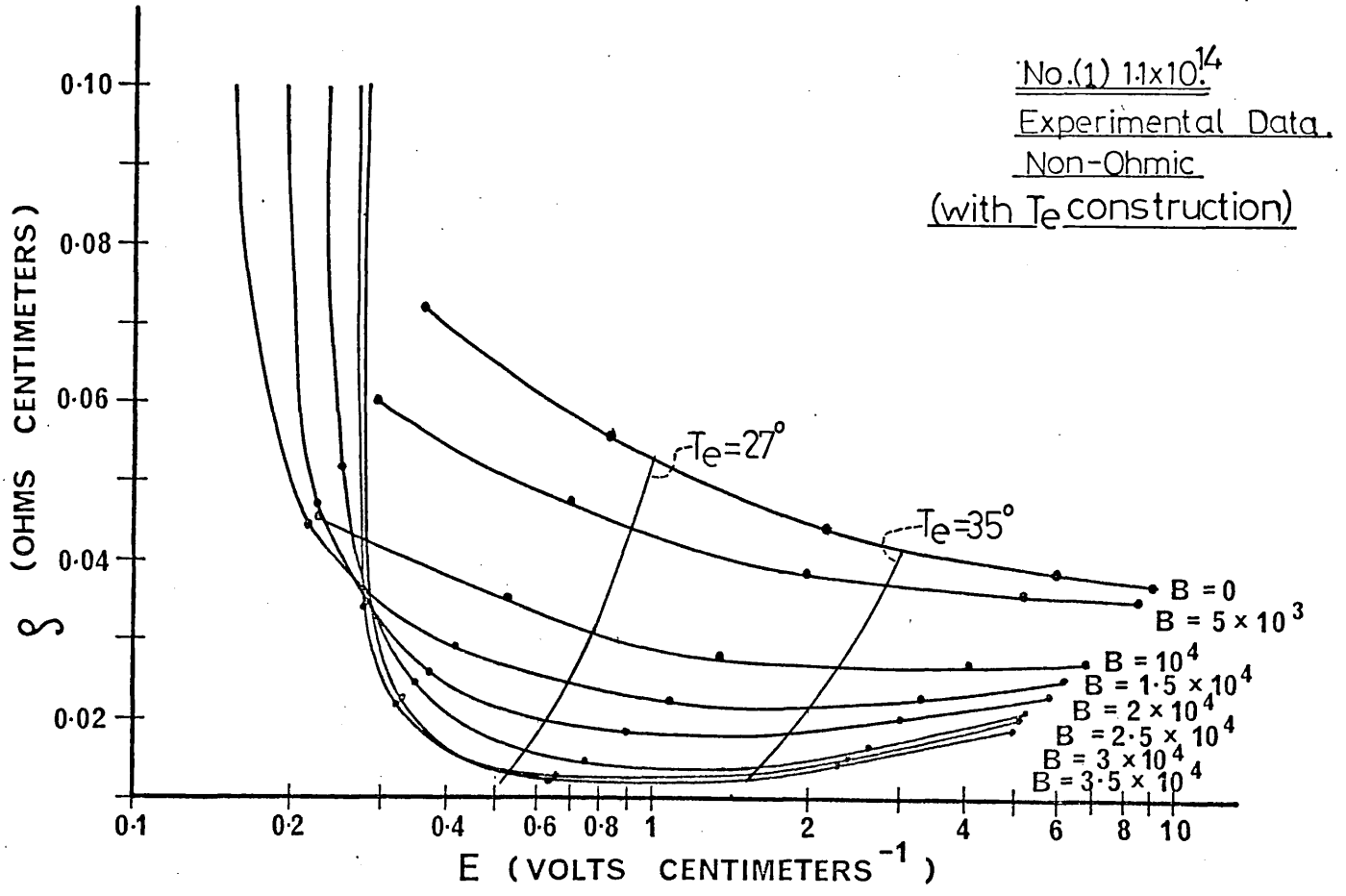
No.(1) 1.1x10^14
Experimental Data.
Non-Ohmic
(with Te construction)
ρ (OHMS CENTIMETERS)
0·10
0·08
0·06
0·04
0·02
Te=27°
Te=35°
B = 0
B = 5 x 10^3
B = 10^4
B = 1·5 x 10^4
B = 2 x 10^4
B = 2·5 x 10^4
B = 3 x 10^4
B = 3·5 x 10^4
0·1
0·2
0·4
0·6
0·8
1
2
4
6
8
10
E (VOLTS CENTIMETERS^-1)

GRAPHS (3)

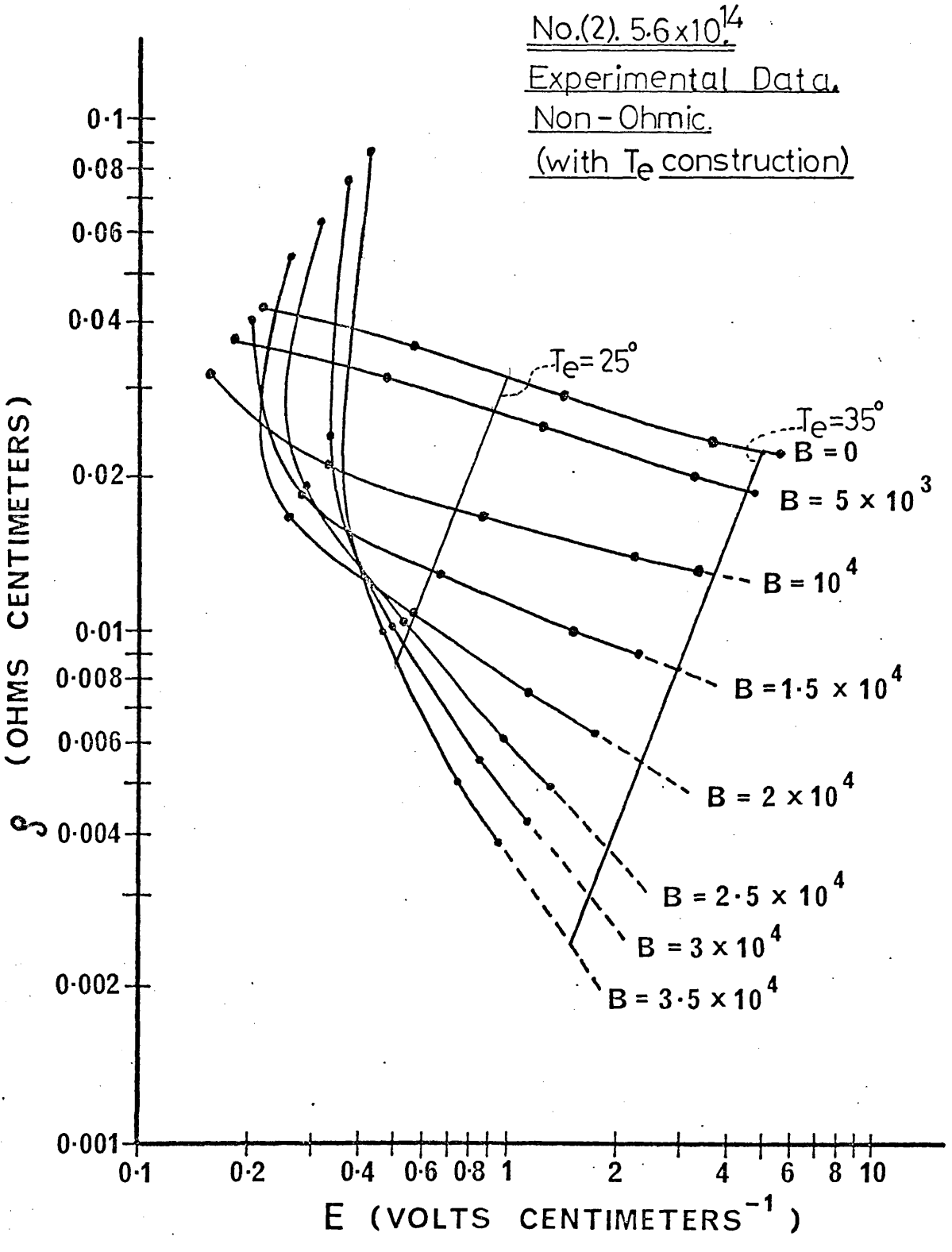
No.(2). 5.6x10^14
Experimental Data.
Non-Ohmic.
(with Te construction)
Te=25°
Te=35°
B = 0
B = 5 x 10^3
B = 10^4
B = 1·5 x 10^4
B = 2 x 10^4
B = 2·5 x 10^4
B = 3 x 10^4
B = 3·5 x 10^4
ρ (OHMS CENTIMETERS)
0·1
0·08
0·06
0·04
0·02
0·01
0·008
0·006
0·004
0·002
0·001
0·1
0·2
0·4
0·6
0·8
1
2
4
6
8
10
E (VOLTS CENTIMETERS^-1)

GRAPHS (3).

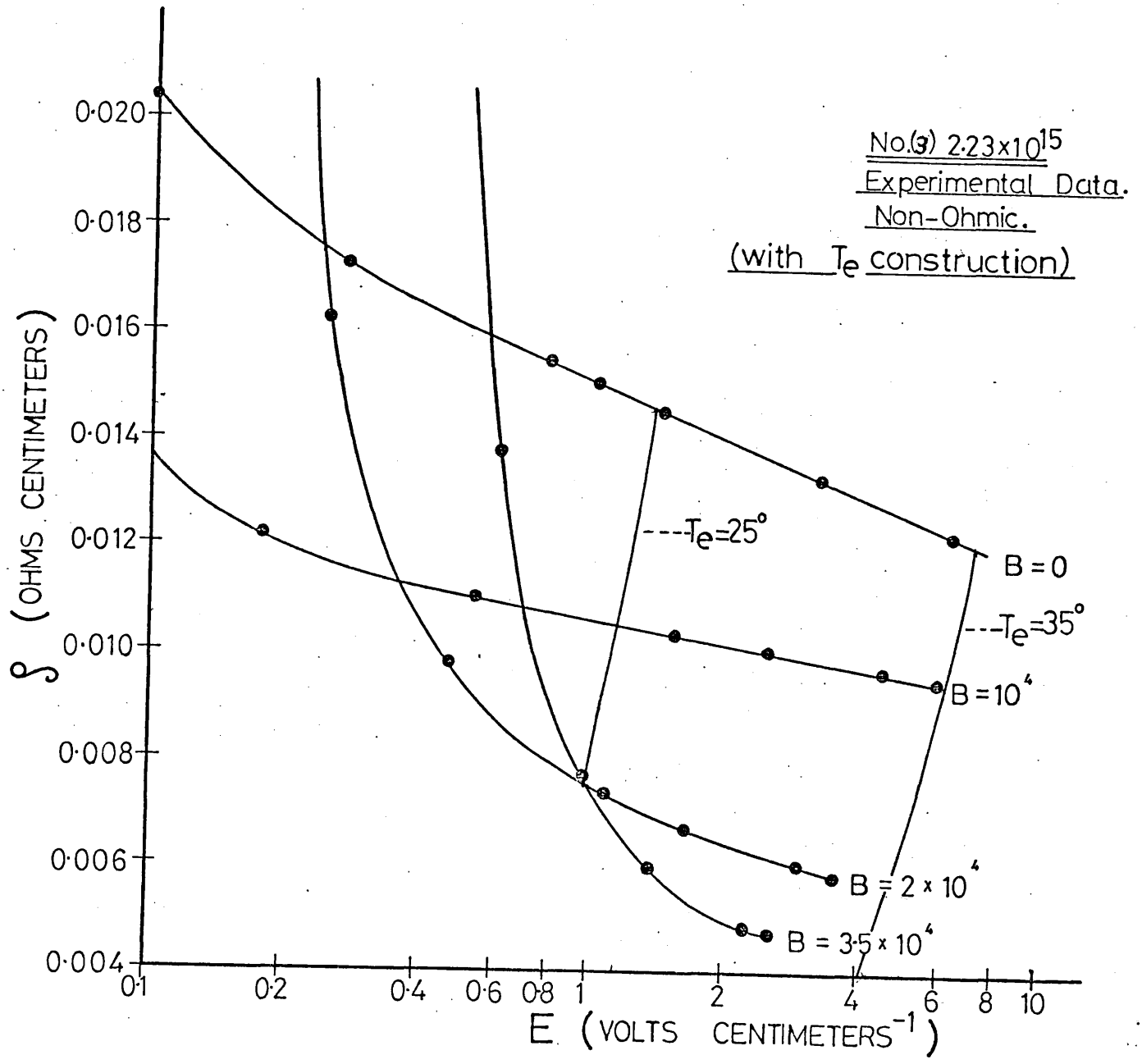
No.(3) 2·23x10^15
Experimental Data.
Non-Ohmic.
(with Te construction)
0·020
0·018
0·016
0·014
0·012
0·010
0·008
0·006
0·004
ρ (OHMS CENTIMETERS)
---Te=25°
B = 0
---Te=35°
B = 10^4
B = 2 x 10^4
B = 3·5 x 10^4
0·1
0·2
0·4
0·6
0·8
1
2
4
6
8
10
E (VOLTS CENTIMETERS^-1)

The S_1, S_3 and S_5 samples were chosen because they scanned the electron concentration from 1×10^{14} to 2.2×10^{15}.

4.5 Discussion.

Graphs (1) show the conventional plot of the magneto-resistance ($\Delta\rho/\rho_o$) ratio versus β, the quantum parameter. This shows very well the overall behaviour and magnitude of the effect. It also has the advantage of having the same axis for all samples. However, for a quantitative analysis it is not so appropriate. We, therefore, replot the experimental results as resistivity versus magnetic field and it is these graphs that are used for analysis. The reasons that this is done are twofold.

Firstly, $\Delta\rho/\rho_o$ contains two parameters with $\Delta\rho$ being the difference $\rho_H - \rho_o$, which for small magnetoresistance values is a small number. Errors in the magnitudes of these quantities (either experimentally or theoretically) give a magnified total inaccuracy, especially for small $\Delta\rho$ values.

Secondly, the calculation of ρ_o using the Brooks-Herring equation (generalized for arbitrary degeneracy) can be a rather inaccurate evaluation. Along with the increasing inaccuracy of the Born approximation as the temperature decreases and the possibility of multiple scattering from two, or more, centres (a second order perturbation calculation by Moore (1969) gives corrections to the Brooks-Herring equation from these effects) we also have the possibility of the impurity states perturbing the bottom of the conduction band.

In indium antimonide, down to low concentrations, the impurity levels merge with the conduction band and there is no distinct activation energy. When calculating the position of the Fermi energy the impurity sites are ignored and the standard unperturbed conduction band density of states are used. This evaluation ignores the perturbation of the

GRAPHS.(4).

(1). $1.1 \cdot 10^{14}$ Ohmic and Non-Ohmic Comparison.
(2). $5.6 \cdot 10^{14}$ " " " " "
(3). $2.23 \cdot 10^{15}$ " " " " "

GRAPHS (4).

Ohmic and Non-Ohmic Comparison.

No(1). 1.1×10^{14}

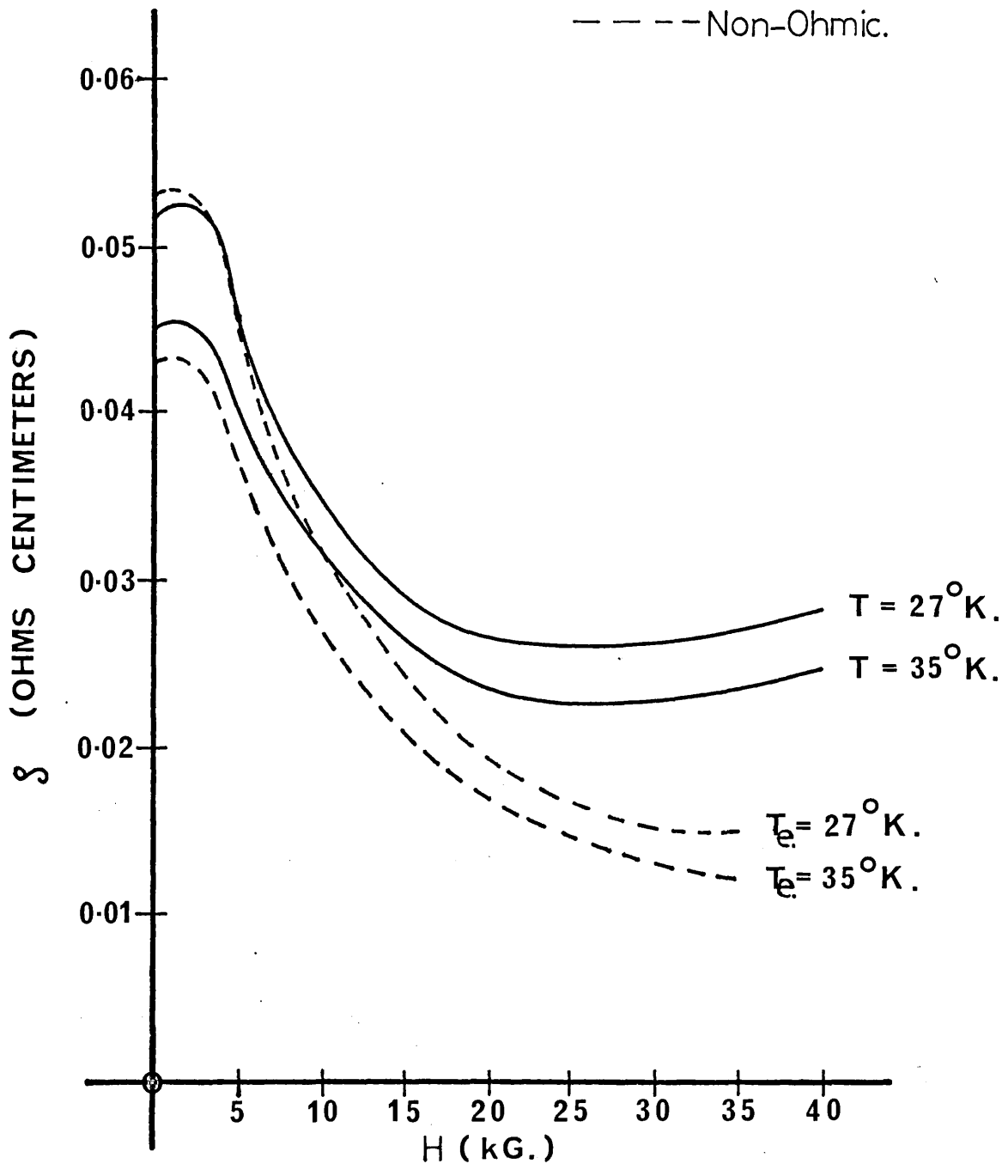

GRAPHS (4)

Ohmic and Non-Ohmic Comparison.

No.(2). 5.6×10^{14}

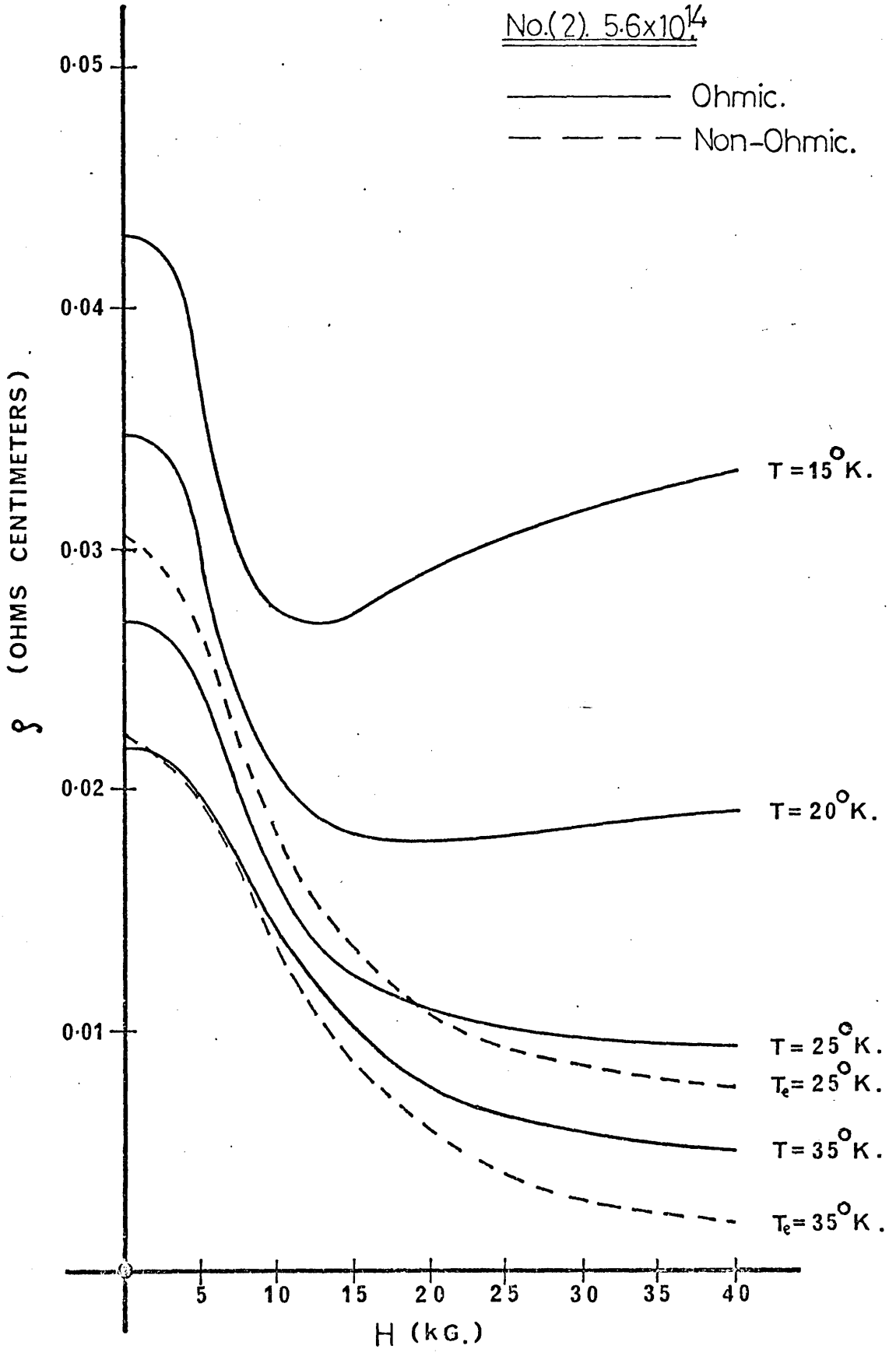

GRAPHS (4).

Ohmic and Non-Ohmic Comparison.

No.(3). 2.23×10^{15}

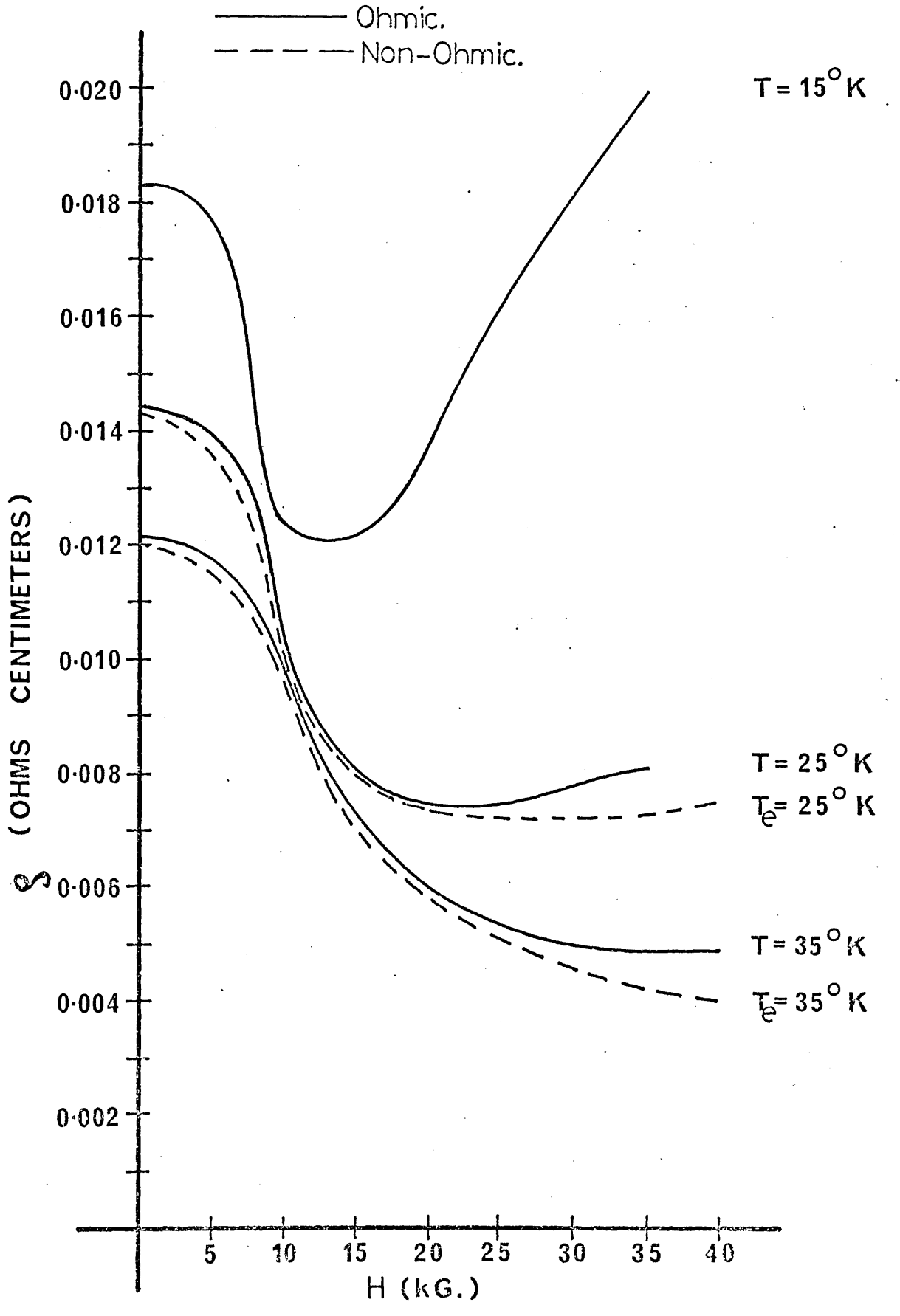

conduction band by the N_I impurities. It should be noted that this may be particularly important in indium antimonide, where the small effective mass m* gives a low density of states around the bottom of the conduction band. There is no simple treatment to arrive at a proper state density and the problem has to be solved in a self-consistent form using combinations of free electron and localized wavefunctions.

In the extreme quantum limit the density of states in the conduction band is radically transformed by the magnetic field, and the conduction band state density at low energies is far greater than the zero magnetic field state density. It is therefore plausible to assume that the perturbation by the impurities should have less percentage effect on the total state density. It is also true that in a quantizing magnetic field the electron wavefunction takes on a cigar type shape, with a shrinking cross-section for increasing magnetic field. Multiple scattering events and deviations from the Born approximation may be reduced:- Reduced multiple scattering events because of the decreasing wave size and greater Born approximation accuracy resulting from the importance of the back scattering events in the extreme quantum limit, which arise from close penetration "unscreened" interactions for which the Born approximation is an exact solution.

For these reasons we use a direct plot of ρ_H for the quantitative ohmic analysis. The ohmic analysis was applied to three samples S_3, S_4 and S_5. The S_1 sample was not analysed, even though theoretically this should give the largest effect. In the purer samples, such as S_1, the effect of acoustic phonons becomes important at lower temperatures, limiting the temperature range of present interest. The results also seem rather low (small negative magnetoresistance) for this sample and inhomogeneities would appear to have a significant effect in reducing the magnitude of the negativity.

The importance of the Dubinskaya forward scattering is illustrated in Graphs (2) by showing both the backward scattering alone and the backward and forward combined scattering. Not only is the resistive magnitude strongly increased, the qualitative behaviour is also modified, especially for low B values. The resulting fit is quite good, although somewhat too high (negativity smaller) for the S_5 sample. The theoretical calculations extend down to $\beta = 5$, and show a turning point (minima) at approximately the same value of β as the experimental results, i.e. $\beta \sim 9$. [This refers to GRAPHS(1)] The turning point is normally explained as arising from electrons beginning to occupy the second Landau level, with associated inter-Landau scattering and a relaxation on the "back flip only" condition. This is calculated as giving a turning value around $B \sim 4$ or 5. It would seem, therefore, that forward scattering events are the determining factor for the turning value as well as the magnitude of the magnetoresistance.

Calculations to include second and higher Landau levels are very tedious and can only be evaluated numerically. The considerable extra computational work would not extend the range of the theory very greatly, and at lower magnetic fields we very quickly arrive at the situation where multiple Landau occupancy becomes important and the computational components rise exponentially.

At higher temperatures ($35^{\circ}K$), but where ionized impurities still provide the dominant scattering mechanism, experimental results show a tendency not to saturate and exhibit greater negativity than the theoretical prediction. In fact, except for the lowest temperatures, the experimental results are always more negative, with smaller resistance values than theory.

At temperatures greater than $35^{\circ}K$ (results shown on Graphs (1) for the S_3 sample extend up to $130^{\circ}K$) the negative magnetoresistance shows a gradual decline. The analysis cannot be extended into this

region because acoustic and polar optical phonons become important electron scatterers. We also begin to see the oscillatory magneto-phonon effect (see Stradling (1970)) in which electrons are resonantly scattered whenever a Landau level coincides with the optical phonon energy. An expanded view of this behaviour is shown with the graph of the S_3 results.

It should be possible to analyse the magnetoresistance at these temperatures using Magnussons solution of the Boltzmann equation in the extreme quantum limit. The theory could be computed incorporating acoustic and polar optical phonons, as well as ionized impurity scatterers. However, no additional treatment for forward scattering events is given by this theory. The negative magneto-resistance associated with polar optical phonons should be particularly important as this interaction shows a strong angular dependence similar to the ionized impurity case. The acoustical processes give rise to positive magnetoresistance for $B > 2$ and tend to blanket out the negative magnetoresistance from the polar processes.

Although ρ_H is plotted against H so as to avoid the use of ρ_o and its associated inaccuracies, it is still necessary to use ρ_o to find N_I from the Brooks-Herring equation. This is done using the ρ_o value at $T = 35^oK$. for all the samples considered.

This value of N_I is used to calculate ρ_o from the Brooks-Herring equation for all the experimental temperatures used, as well as being used for all ρ_H calculations. From Graphs (2) it can be seen that starting from the forced fit at 35^oK the ρ_o experimental resistivity soon begins to exceed the theoretical value. The discrepancy rapidly increases for decreasing temperatures, showing the inaccurancy of the Brooks equation for analysing the ρ_o data. The ρ_H curves on the other hand do not display such a marked change, especially considering the

greatly increased complexity of the quantum limit theory. The N_I values calculated from the ρ_o (35^oK) value give a reasonable fit for the ρ_H theory in the S_3 and S_4 samples. For the S_5 sample, which has the highest impurity concentration, the theory gives resistivity values which are too high and this may well be due to an overestimation of N_I calculated from Brooks-Herring. Reducing N_I by 20% gives a better quantitative match. Changing N_I shifts all the theoretical lines by an equal amount and does not alter the relative behaviour or magnitudes.

In view of the importance of forward scattering the approximations used in its incorporation into the present analysis should be noted. The main problem is the treatment of the collision free path, ℓ_z. As previously pointed out this is not a mobility free path as used in the present calculations. Also, using the expression $\ell_z = \langle V_z \rangle \tau$ is not strictly accurate when $\langle V_z \rangle$ is taken as the average thermal energy. Some idea of the importance of the ℓ_z and the sensitivity of the theory to this parameter can be seen on Graph (5). This graph shows the results of the S_3 sample along with the theory incorporating the combined backwards and forwards scattering. However, the theory for the 15^oK characteristic shows the sensitivity to ℓ_z by multiplying and dividing ℓ_z by factors of 2, 3 or 5. By dividing ℓ_z (increasing the collisions) the forward scattering achieves greater preponderance and increases the resistance. By multiplying ℓ_z (decreasing collisions) the forward scattering has a smaller effect and the characteristics start to approach the backward only form. It is interesting to note how a strongly defined turning point appears to emerge with increased forward scattering. We see from these characteristics that by changing ℓ_z by a factor of 2 makes a fairly substantial difference - enough to cover the difference between theory and experiment. In view of this and the

aforementioned approximations in ℓ_z, it may be possible to improve the agreement by endeavouring to calculate ℓ_z with greater precision.

The Argyres and Dubinskaya theories used in the present analsysis are semi-classical equations and do not come from a rigorous quantum mechanical formulation. Dubinskaya introduces the forward scattering by relaxing the delta function condition on the ionized impurity matrix elements. This is a fair first order approximation, but may lead to certain inaccuracies. The standard conduction band density of states is used in the theory with the associated discontinuity (infinity) at the bottom of the band. This singularity should be rounded off by various broadening processes. As well as the collision broadening mechanisms there is also the possibility of broadening resulting from the random impurity distribution, with the fluctuating impurity potential perturbing the bottom of the conduction band.

However, it should be emphasized that improvements in the theoretical analysis are limited by the experimental inaccuracies resulting from the presence of sample inhomogeneities. These can modify the qualitative behaviour as well as the magnitude of the negative magnetoresistance. Inhomogeneous samples cannot necessarily be pinpointed by a low mobility value, because high mobility samples can exhibit strong variations. (Very pure samples can exhibit inhomogeneity by producing anomalously high mobilities.) Unfortunately, magnetoresistive behaviour seems to be the most sensitive probe of the irregularities. The inhomogeneities are presumed to introduce transverse components of current with an associated positive magnetoresistance. We may view any sample giving anomalously low negativity as being subject to inhomogeneities and therefore not analizable on a quantitative basis.

GRAPH (5).

Effect of Forward Scattering Parameter (l_z).

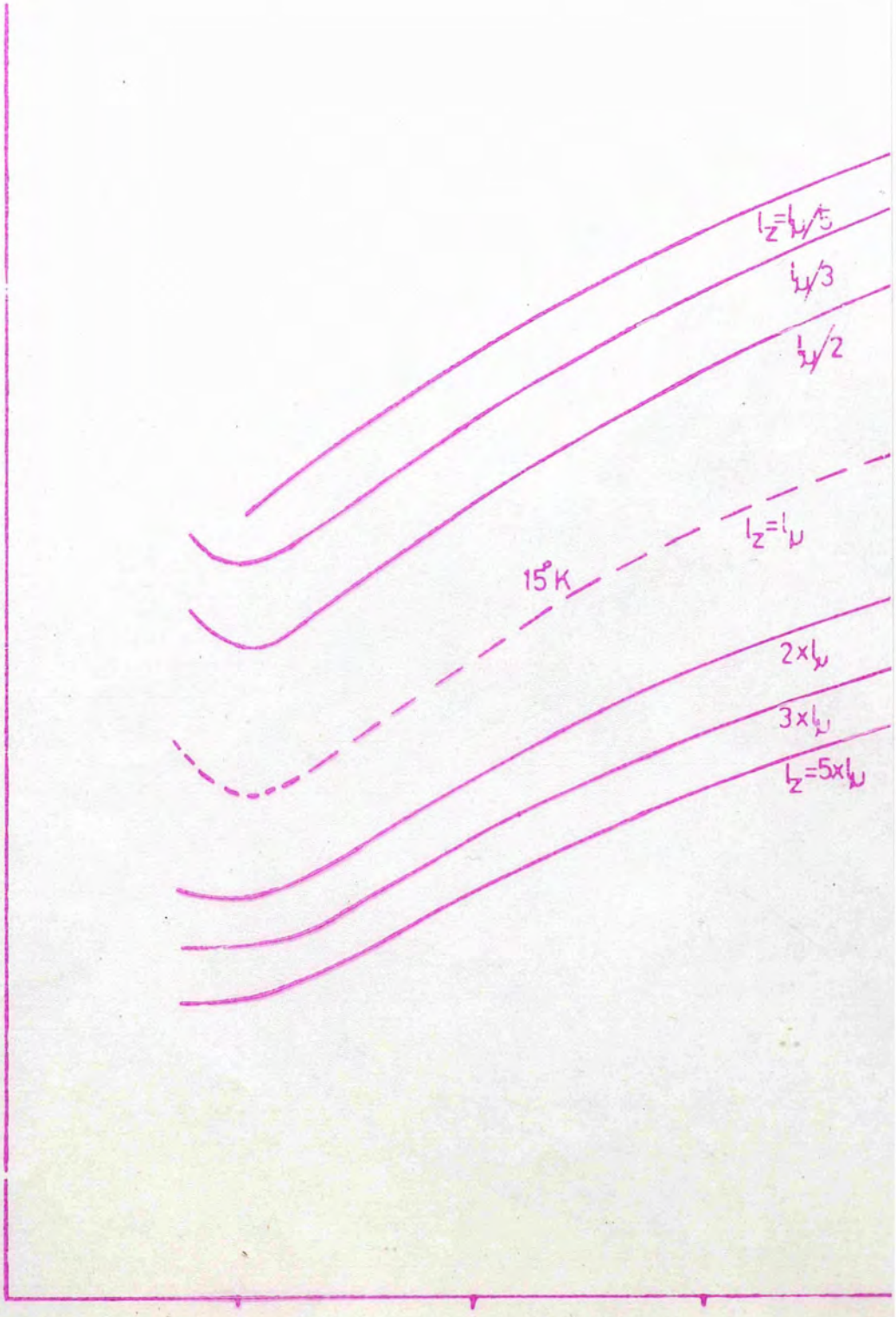

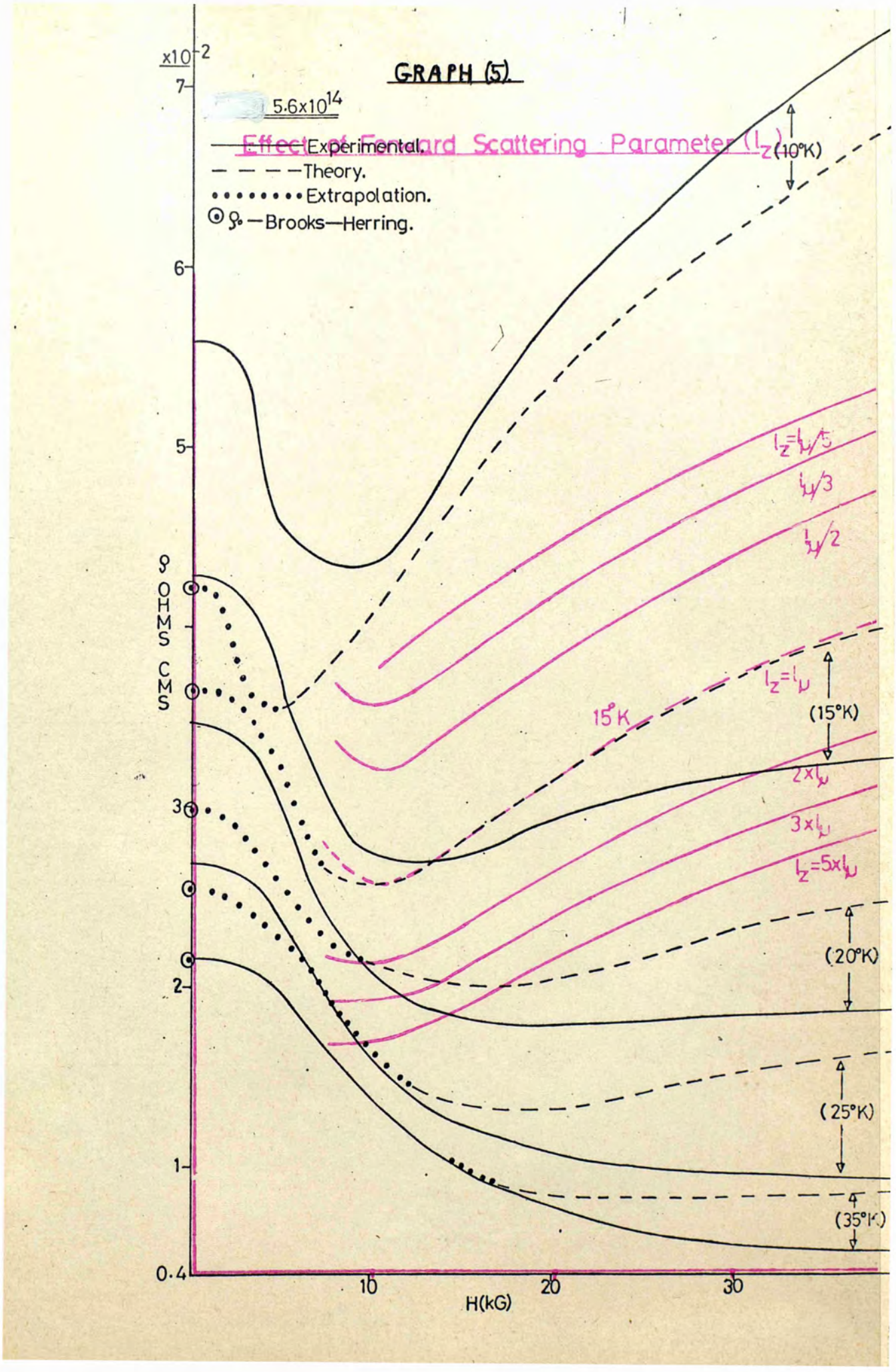
GRAPH (5).
5.6x10^14
Effect of Forward Scattering Parameter (l_z)
Experimental.
Theory.
Extrapolation.
Brooks—Herring.
x10^-2
7
6
5
3
2
1
0.4
ρ OHMS CMS
10
20
30
H(kG)
(10°K)
l_z=l_μ/5
l_μ/3
l_μ/2
15°K
l_z=l_μ
(15°K)
2xl_μ
3xl_μ
l_z=5xl_μ
(20°K)
(25°K)
(35°K)

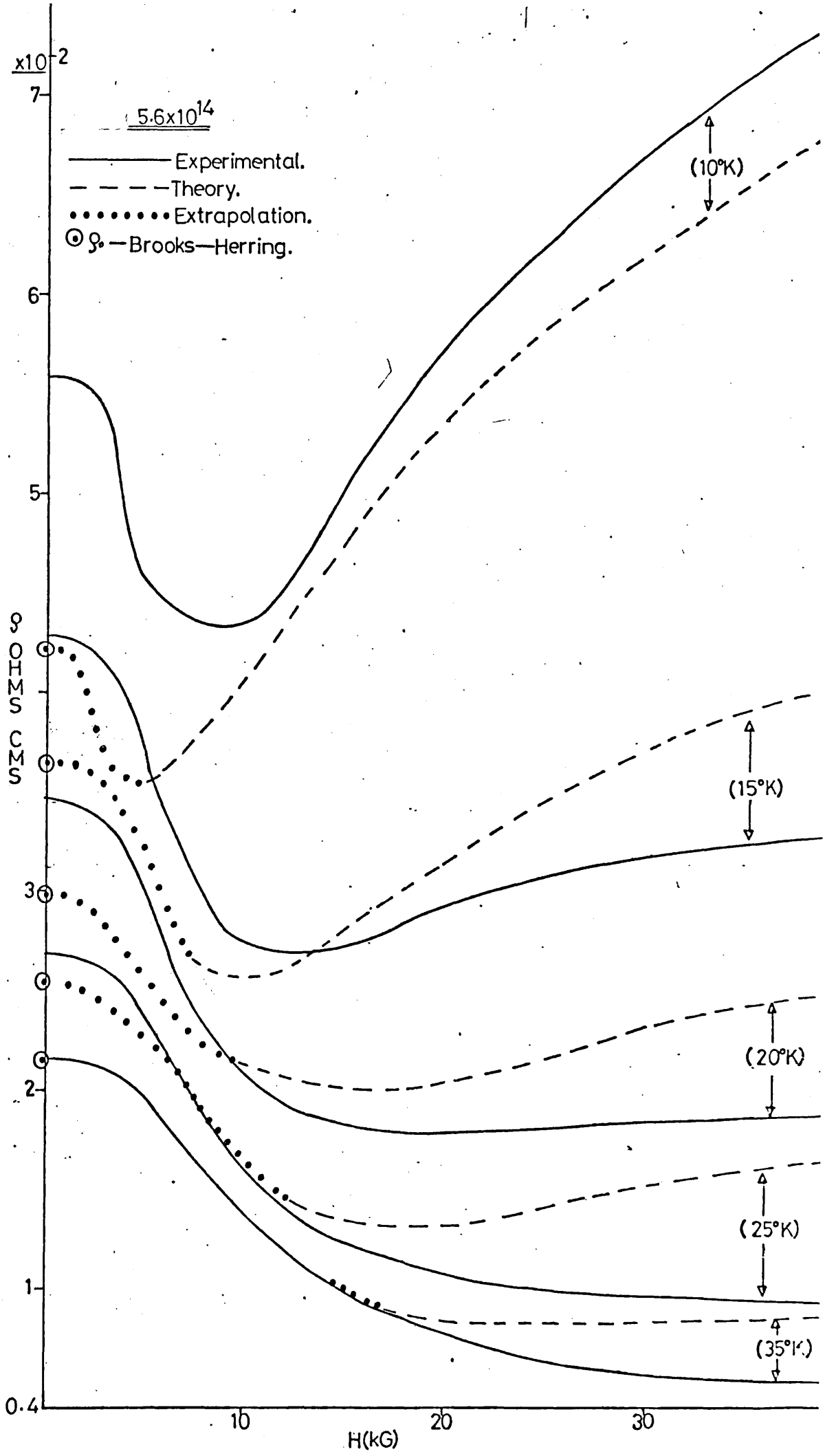
x10-2
7
6
5
2
1
0.4
5.6x10^14
Experimental.
Theory.
Extrapolation.
ρo—Brooks—Herring.
ρ OHMS CMS
(10°K)
(15°K)
(20°K)
(25°K)
(35°K)
10
20
30
H(kG)

A possible way of prior testing for inhomogeneities is by looking at the behaviour of the Hall coefficient factor, r as the magnetic field is increased from a classically weak $\omega_c\tau<<1$ to a classically strong $\omega_c\tau>>1$ regime. For a known scattering mechanism r should follow a well defined variation, going to unity as the strong regime is approached.

The non-ohmic results are shown for the S_1, S_3 and S_5 samples. Ohmic and non-ohmic results were always taken during the same experimental run for each sample, in order that no relative errors from inhomogeneity effects could result in spurious differences between the two. This makes a straight comparison unambiguous, except for a slightly greater error in the non-ohmic results because voltage and current were measured as pulses.

A general observation, applicable to all the samples, is that the non-ohmic characteristics show greater negativity than the ohmic. This is particularly noticeable for the purest sample S_1. It can also be said that the negative magnetoresistance for the ohmic and non-ohmic cases clearly arises from the same basic mechanism.

Unfortunately, the electron temperature can only be calculated over a narrow range. When the electric field is too low we see magnetic freeze out of conduction electrons and when the field is too high the optical phonons beging to limit the electron mobility. Temperatures of $25^{o}K$ and $35^{o}K$ are used as the most convenient comparision temperatures. These are also pretty much at either end of the above mentioned limiting processes. It is these two temperatures which are used for the ohmic comparison in Graphs (4). It would have been desirable to view electron temperatures less than $25^{o}K$, but electron freeze out and the need to incorporate acoustic phonons in the energy relaxation processes preclude

this comparison. (The two phonon relaxation process can become important around 20°K as well as the standard single phonon interactions.)

Viewing the comparison in Graphs (4) we see that it is fairly good, except for the pure S_1 sample. The agreement would seem to improve with greater sample impurity. In the purest sample the non-ohmic results only agree well with the ohmic for the low magnetic field region. For high magnetic fields the non-ohmic characteristics display a much greater negativity. This applies, but to a lesser extent, to the more impure samples. The only exception to this is the rather anomalous result for the 25°K line in the S_3 sample, where the calculated non-ohmic zero magnetic field resistivity is rather too high. Even in this case for higher magnetic fields the non-ohmic resistivity drops to a lower value than the ohmic resistivity.

The difference between the ohmic and non-ohmic characteristics probably arises from the role of acoustic phonons which begin to have some effect, reducing the negative magnetoresistance, around these temperatures in the ohmic conditions. This certainly would appear to explain the large discrepancy in the S_1 sample, where acoustic phonons become more effective because of the sample purity. However, there does not appear to be a great deal of difference between the relative behaviours for the 25°K and 35°K characteristics, i.e. there should be greater divergence for the 35°K line because of the increasing presence of acoustic phonons. Secondly, the non-ohmic is in excess (greater negativity) of the ohmic, even for the 25°K line in the most impure sample S_5. A further investigation on samples with greater impurity concentration would clarify this behaviour.

We should also note that for high magnetic fields where we enter the extreme quantum limit regime the distribution function is rather distorted and the "electron temperature" distribution could be inaccurate. This also could explain the divergence of the ohmic and

non-ohmic lines at high magnetic fields.

In view of this last point the simple electron temperature model gives rather good agreement. The far more complicated calculations based on the Kurosawa formulation would hardly appear to be worthwhile. This is particularly the case for the most impure sample S_5, where the agreement is very good over the whole range, except for a slight divergence at the highest magnetic fields. It would be interesting to extend the magnetic fields above the present limits to see if this behaviour continued.

Finally, this work would benefit from a more comprehensive and extended study on the experimental side. Samples of greater impurity would be a useful extension, as well as increased facilities for high magnetic fields. Neutron bombardment as a means of increasing the electron concentration (and impurity concentration) in a controlled fashion also offers potential interest. Rather than using samples of increased conduction band electron concentration, it would be desirable to view more compensated samples. This would avoid the increasing degeneracy of the conduction band, with the associated de-Haas Shubnikov oscillations. Similar investigations could also be made on otherIII-V compounds such as indium arsenide and gallium arsenide, although higher magnetic fields are more of a necessity here, and for any substance where the effective mass is large. The effects of sample inhomogeneities can exert substantial limitations on the various investigations and means of controlling or investigating their range should be given further study.

CONCLUSION.

In spite of difficulties in obtaining accurate results, without spurious size and inhomogeneity effects, a reasonably good quantitative analysis has been achieved. The magnetic field reduction of the collision cross-section from ionized impurity scattering sites has been identified as the mechanism giving the negative magnetoresistance in both the ohmic and the non-ohmic cases. The inclusion of scattering events allowed by the uncertainty of the electron energy is found to be of strong significance in the analysis. The electron temperature model has been investigated in a situation where it has doubtful validity, but it has been found to give a reasonable analysis, especially for the more impure samples. Possible extensions of the investigations, both theoretically and experimentally, have been discussed.

ACKNOWLEDGEMENTS

Grateful acknowledgements to my supervisor, Dr. R.A. Mansfield, for his constant guidance throughout the work. Thanks to Mr. A.K. Betts for the design and construction of a versatile pulse generator, used for the non-ohmic research. Thanks also to all the technical staff at Bedford College, and the workshop in particular for their help on a variety of technical matters. Thanks to L. Kusztelan for many interesting and even instructive conversations, and to Mrs. Pearson for the typing of the thesis. I also gratefully acknowledge the financial support of the Science Research Council.

APPENDIX.

Screening Length R_s^H for Arbitrary Degeneracy and Extreme Quantum Limit.

The theory used for scattering from ionized impurities uses a screened coulomb potential, of the form

$$V(r) = \frac{e}{Kr} \exp \frac{-r}{R_s}$$

where R_s is a screening length indicative of how effectively the impurity charge is shielded by the free conduction band electrons.

We must calculate R_s in the extreme quantum limit for the analysis (R_s^H).

This is done by solving Poisson's equation

$$\nabla^2 V(r) = \frac{-4\pi e}{K} (n_o - n(r)) \qquad (1)$$

where n_o is the concentration of electrons in the unperturbed lattice and n(r) the concentration in the perturbed lattice, i.e. with an ionized impurity present.

If $n_o = F(\emptyset)$ (some function of potential)

and $n(r) = F(\emptyset + V)$

we use the approximation

$$F(\emptyset + V) = F(\emptyset) + V F'(\emptyset) = n(r)$$

Therefore, $n_o - n(r) = - V F'(\emptyset)$ (2)

Now

$$n_o = F(\emptyset) = \int_o^\infty f(\varepsilon_z \varepsilon_F) D_H(\varepsilon_z) d\varepsilon_z$$

So $$F(\emptyset) = \frac{(k_B T)^{\frac{1}{2}}}{(2\pi)^2} \left(\frac{2m^*}{\hbar^2}\right)^{3/2} \hbar \omega_c f_{-\frac{1}{2}}(\partial_H^*) \qquad (3)$$

where $f_{-\frac{1}{2}}(\partial_H^*)$ is a tabulated fermi function for the reduced fermi-energy in a magnetic field

and $e\phi = \partial_H^* kT$

Therefore, $F'(\phi) = \frac{(k_B T)^{\frac{1}{2}}}{(2\pi)^2} \left(\frac{2m^*}{\hbar^2}\right)^{3/2} \hbar\omega_c \, f'_{-\frac{1}{2}}(\partial_H^*) \frac{e}{(kT)}$

and using the relationship $f'_{-\frac{1}{2}}(\partial_H^*) = -\frac{1}{2} f_{-3/2}(\partial_H^*)$

we have

$$F'(\phi) = \frac{-e}{2(2\pi)^2 (k_B T)^{\frac{1}{2}}} \left(\frac{2m^*}{\hbar^2}\right)^{3/2} \hbar\omega_c \, f_{-3/2}(\partial_H^*) \qquad (4)$$

substituting (2) and (4) into equation (1)

$$\nabla^2 V(r) = \frac{-4\pi e}{K} \times \frac{e}{2(2\pi)^2 (k_B T)^{\frac{1}{2}}} \left(\frac{2m^*}{\hbar^2}\right)^{3/2} \hbar\omega_c \, f_{-3/2}(\partial_H^*) \times V(r)$$

or $$\nabla^2 V(r) = \frac{1}{(R_s^H)^2} V(r)$$

where $$V(r) = \frac{e}{Kr} \exp\left(\frac{-r}{R_s^H}\right)$$

so that the screening length

$$(R_s^H)^2 = \frac{2\pi K (k_B T)^{\frac{1}{2}}}{e^2 \hbar \omega_c} \left(\frac{\hbar^2}{2m^*}\right)^{3/2} \frac{1}{f_{-3/2}(\partial_H^*)}$$

==========

For the case of non-degenerate statistics

$$\partial_H^* << 0.$$

$$f_{-3/2}(\partial_H^*) \longrightarrow -2(\pi)^{\frac{1}{2}} \exp(\partial_H^*)$$

so $$(R_s^H)^2 = \frac{-2\pi K (k_B T)^{\frac{1}{2}}}{e^2 \hbar \omega_c} \left(\frac{\hbar^2}{2m^*}\right)^{3/2} \frac{1}{2\sqrt{\pi} \exp(\partial_H^*)}$$

Using the standard expression for n_o in the extreme quantum limit

$$n_o = \frac{(k_B T)^{\frac{1}{2}}}{(2\pi)^2} \left(\frac{2m^*}{\hbar^2}\right)^{3/2} \hbar\omega_c \sqrt{\pi} \exp(\partial_H^*)$$

We can write

$$(R_s^H)^2 = \frac{K k_B T}{4\pi e^2 n_o}$$

==========

Thus, for nondegenerate statistics the screening length reduces to the standard zero magnetic field expression and the magnetic field has no effect.

==========

For completely degenerate statistics

$$\partial_H^* >> 0$$

and $f_{-3/2}(\partial_H^*) \rightarrow -2(\partial_H^*)^{-\frac{1}{2}}$

so $$(R_s^H)^2 = -\frac{2\pi K (k_B T)^{\frac{1}{2}}}{e^2 \hbar\omega_c} \left(\frac{\hbar^2}{2m^*}\right)^{3/2} \frac{1}{2(\partial_H^*)^{-\frac{1}{2}}}$$

and

$$n_o = \frac{(k_B T)^{\frac{1}{2}}}{(2\pi)^2} \left(\frac{2m^*}{\hbar^2}\right)^{3/2} \hbar\omega_c \, 2(\partial_H^*)^{+\frac{1}{2}}$$

Using this expression in $(R_s^H)^2$ gives

$$(R_s^H)^2 = \frac{2\pi^3 K}{e^2 (\hbar\omega_c)^2} \left(\frac{\hbar^2}{2m^*}\right)^3 n_o.$$

==========

Thus, in the degenerate case the screening length decreases as H^2, i.e. the magnetic field increases the screening.

For no magnetic field present, a similar procedure to the one previously outlined yields

$$R_s^2 = \frac{K \hbar^3 \pi}{2 e^2 (2m^*)^{3/2} (k_B T)^{\frac{1}{2}}} \qquad \frac{1}{f'_{\frac{1}{2}}(\partial_o^*)}$$

==========

It should be noted that these derivations are simple semi-classical derivations of the screening parameter. The magnetic field expression also uses an unbroadened density of states equation, which may have an important effect in the degenerate case. Other more involved vigorous treatments have been given. See Wallace (1974). However, although some of the sample are degenerate in zero magnetic field, they all go to non-degenerate statistics with increasing magnetic field where the general expression for R_s^H has greatest validity.

REFERENCES.

Aas and Bløtekjaer, J.Phys. Chem. Solids, 35 1053 (1974)

Agaeva, Askerov and Gashimzade, Sov.Phys. - Semicond. 7.8.1085 (1974)

Alexander and Holcomb, Rev.Mod.Phys. 40.4.815 (1969)

Alier, Askerov, Agaeva and Daibov, Sov.Phys. - Semicond. 9.3.377 (1975)

Alier, Daibov and Ismailov, Sov.Phys. - Semicond. 9 3 375 (1975)

Amikhanov and Bashirov, Sov. Phys. Solid State 8 2482 (1967)

Ancker-Johnson and Dick, App.Phys.Letts. 15 5 141 (1969)

Andrianov, Lazarera, Sarder and Fistul, Sov.Phys.Semic. 9 2 141 (1975)

Argyres and Adams, Phys.Rev. 104 4 900 (1956)

Baranski, Glushkov and Televanaya, Sov.Phys. - Semicond. 3 9 1401 (1970)

Barker, J.Phys.C. 5 1657 (1972)

Bastard and Rigaux, 12th Int.Conf.Phys.Semic. 239 (1974)

Bate, Bell and Beer, J. of Appl.Phys. 32 5 806 (1961)

Berchenko and Pashkovskii, Sov.Phys. - Solid State 15 12 2479 (1974)

Blatt, J.Phys.Chem.Solids 1 262 (1957)

Bløtekjaer, Physics Letters 24A 1 15 (1967)

Bowers and Steele, Proc. I.E.E.E. 52 1105 (1964)

Buchsbaum, Chynoweth and Feldmann, App.Phys.Lett. 6 4 67 (1965)

Crandall, Phys.Rev.B. 1 2 730 (1970)

Chusov and Yaramenko, Sov.Phys,Semicond. 7 6 830 (1973).

Chynoweth and Murray, Phys.Rev. 123 2 515 (1961)

Conwell, Solid State Physics, Suppl. 9

Delhaes, Gasparaux and Ulrich, Carbon (G.B.) 10 3 354 (1972)

Delhaes, Kepper and Ulrich, Philos.Mag. (G.B.) 29 6 1301 (1974)

Dubinskaya, Sov.Phys. - Solid State, 7 2280 (1966)

Dubinskaya, Sov. Phys. J.E.T.P. 29 3 436 (1969)

Dutta, Chattopadhyay and Nag, J.Phys.C. Solid St. 7 1854 (1974)

Dyakonov, Efros and Mitchell, Phys.Rev. 180 3 813 (1969)

Dyanonov, Efros and Mitchell, Phys. Rev. 180 3 819 (1969)

Eisele and Dorda, Phys.Rev.Lett. 32 24 1360 (1974)

Ehrenreich, J.Phys.Chem.Solids, 9 129 (1959)

Fawcett, Boardman and Swain, J.Phys.Chem.Solids, 31 1963 (1970)

Felsch and Ulinzer, Solid State Commun. 13 5 569 (1973)

Fistul, Monographs in Semiconductor Physics, P lenum Press (1969)

Frederikse and Hosler, Phys.Rev. 108 5 1136 (1957)

Frohlich, Proc.Royal.Soc. A 188 532.

Fujita, Carbon (G.B.) 6 5 746 (1968)

Garyagdyer, Zotova, Emelyanenko, Lagunova and Nasledov, Sov.Phys. Semicond. 7 4 487 (1973)

Gerhardts and Hajdu, Z.Phys. 245 2 126 (1971)

Gerhardts and Hajdu, Solid State Commun. 9 1607 (1971)

Gershenzon, Kurilenko, Litrak-Gorskaya and Rabinovich, Sov.Phys - Semicond. 7 8 1005

Gershenzon, Ilin, Litrak-Gorskaya, Rabinovich and Shapiro, Sov.Phys. Semicond. 6 10 1626 (1973)

Glicksman and Steele, Phys.Rev.Letts. 2 11 461 (1959)

Gurevich, Yakovlev, Karpovich, Vinnik and Rubolskaya, Sov.Phys.Semicond. 9 1 1 (1975)

Hammar, J.Phys.C. (G.B.) 6 1 70 (1973)

Hedgcock and Giovannini, Solid State Commun. 11 2 367 (1972)

Hedgcock and Raudorf, Solid State Commun. 8 1819 (1970)

Hughes and Tree, J.Phys.C. Solid St. 3 1943 (1970)

Il'in, Litvak-Gorskaya, Rabinovich and Shapiro, Sov.Phys. Semicond. 7 8 1089 (1974)

Il'in and Shapiro, Sov.Phys. Semicond. 7 2 281 (1973)

Iwai, Endo and Irie, J.Phys.Soc.(Jap) 36 1 307 (1974)

Kabakaddi, Kahlert and Bauer, Phys.Rev. B 7 6 2670 (1973)

Kane, J.Phys.Chem.Solids 1 249 (1957)

Katayama and Tanaka, Phys.Rev. 153 873 (1967)

Kazarinov and Skobov, Sov.Phys. JET.P. 15 4 726 (1962)

Keldysh and Proshko, Sov.Phys.Solid State 5 12 2481 (1964)

Keyes and Sladek, J.Phys.Chem.Solids 1 143 (1956)

Khosla and Fischer, Phys.Lett.A. Vol 32 2 96 (1970)

Khosla and Fischer, Phys.Rev.B. 2 10 4084 (1970)

Kinch, Proc. Phys.Soc. London, 90 819 (1967)

Komatsubara and Yamada, Phys.Rev. 144 2 702 (1965)

Kotera, Komatsubara and Yamada, J.Phys.Soc.Jap. 21 Supplement p. 411 (1966)

Kotera, Yamad and Komatsubara, J.Phys.Chem.Solids, 33 1311 (1972)

Krotkus and Repas, Phys.Stat.Solidi, 50 1 K31 (1972)

Kubo, Solid State Physocs Vol. 17 1965

Kurosawa, J.Phys.Soc.Japan, Vol. 20 No. 6 937 (1965)

Kurosawa, Maeda and Sugimoto, J.Phys.Soc.Jap. 36 2 491 (1974)

Kurosawa, J.Phys.Soc. (Jap), Suppl. 21 424 (1966)

Larsen and Voermans, J.Phs.Chem.Solids 34 4 645 (1973)

Levinson and Mazhuolite, Sov.Phys.JET.P. 23 4 697 (1966)

Löschner, J.Appl.Phys. 44 11 5041 (1973)

Magnusson, Phys.Stat.Solidi, 52 361 (1972)

Magnusson, Phys.Stat.Solidi(b), 56 269 (1973)

Mansfield and Ahmad, J.Phys.C.SolidSt. 3 423 (1970)

Matveenko and Shender, Fiz.Tekh.Poluprov (U.S.S.R.) 5 2 349 (1971)

Mell and Stuke, J.Non-Cryst.Solids (Netherlands) 4 304 (1970)

Moore, Phys.Rev. 160 3 618 (1969)

Mott, Philos.Mag.(G.B.) 29 1 59 (1974)

Newhouse and Ferguson, Appl.Phys.Letts. 14 10 308 (1969)

Nozières, Proc.14thInt. Conf. on Low Temp. Phys., Finland, 5 339 (1975)

Oliver, Phys.Rev. 127 4 1045 (1962)

Phadke and Sharma, J.Phys.Chem.Solids 36 1 (1975)

Podor, Acta.Phys.Hungary, 27 1-4 449 (1969)

Polyanskaya and Saidashov, Sov.Phys.Semic. 9 1 102 (1975)

Price, I.B.M. J. Res.Develop. p.12 Jan 1970.

Putley Proc. 7th. Int. Conf. 1964.

Rabinovich, Sov.Phys. Solid State 12 2 440 (1970)

Ridley, Proc.Phys.Soc. 82 954 (1963)

Rosenbaum, Rev.Sci.Instruments 39 6 890 (1968)

Sasaki, Yamanouchi and Hotoyama, Int.Conf. on Phys.Semic. Prague, (1961)

Sasaki, De Bruyn Oubater Physica, 27 877 (1961)

Serre and Leroux-Hugon, 12th Int.Conf. on Phys.Semic. 244 (1974)

Shapira, Foner and Oliveira, Phys.Lett.A. 37A 5 323 1971

Sladek, Phys.Rev. 120 1589 (1960)

Sladek, J.Phys.Chem.Solids, 5 157 (1958)

Szymánska and Maneval, Sol.State Commun. 8 879 (1970)

Stradling and Wood, J.Phys.C. 3 2425 (1970)

Stratton, Proc.Roy.Soc.London A 242 355 (1957)

Takita, Hagiwara and Tanaka, J.Phys.Soc.(Jap) 34 6 1548 (1973)

Tokumoto, Yamanouchi and Yoshihiro, J.Phys.Soc. (Jap.) 37 878 (1974)

Toyozawa, J.Phys.Soc.(Japan) 17 579 (1962)

Vositius and Levinson, Sov.Phys.JET.P. (23) 6 1104 (1966)

Wallace, J.Phys.C., 7 1136 (1974)

Weiss, J.Appl.Phys. Suppl to Vol. 32 10 2064 (1961)

Yamada and Kurosawa, Int.Conf.Phys.Semic.Mowcow 805 (1968)

Yamada, Solid St.Commun. 13 503 (1973)

Yazawa, J.Chem½Phys.(France) 149, 1969

Yosida, Phys.Rev. 107 396 (1957)

Zaitser, Zvezdin and Osipov, Sov.Phys.Semicond. 4 12 1941 (1971)

Zavaritskaya, Voronova and Rozhdestvenskaya, Sov.Phys.Semic. 6 10 1668 (1973)

Zlobin and Zyryanov, Sov.Phys.Uspekhi, 14 4 379 1972

Zotova, Lagunova and Nasledov, Translated from Fiz.Tverd.Tela 5 11 3329 (1963)